Hepatocellular lipid metabolism in Hepatitis C Virus infection

By

Melanie Beer

Christ Church, Oxford

Submitted in partial fulfillment of the requirements for the degree of

Doctor of Philosophy at the University of Oxford

Trinity Term 2013

Supervised By

Prof. Nicole Zitzmann

To those who believed in me.

Gewidmet all denen, die an mich geglaubt haben.

Acknowledgements

First of all I would like to specially thank my supervisor, Prof. Nicole Zitzmann, for guiding and supporting me in those 4 years of my DPhil. Her support helped me push through tough times and made good times even better.
I would like to distinctively thank Prof. Raymond Dwek, for giving me the opportunity to work on those projects as a member of the Glycobiology Institute. It is a very special place and I am very grateful for having spent those exciting years there and nowhere else.
Furthermore, I would like to express my gratitude for receiving the Baruch Blumberg Scholarship. It has been a great honour to me and I would like to thank my funding body and the Blumberg family for their support.

My special thank extends to all Zitzmanns and Zitzmannins who have grown on me immensely and made every day at work special. Providing scientific, culinary, health, and personal advise at any time of the day, or sometimes night; Dr. Stephanie Pollock for even providing a project.

I would also like to thank my family, for being excited with me when my bacteria or viruses were doing well, and words of encouragement when they did not.

I would like to thank friends who have been there for me when I needed them. Thank you, to those who have accompanied me in my Oxford years. It has been the time of my life. For now.

Hepatocellular lipid metabolism in Hepatitis C Virus infection

Melanie Beer, Christ Church, D.Phil. Thesis, Trinity Term, 2013

Abstract

The work described in this thesis investigates the lipid metabolism of human hepatocytes in the context of Hepatitis C Virus (HCV) infection. This includes lipoprotein signalling and cholesterol metabolism targeted analysis of gene expression as well as the influence of polyunsaturated ER targeting liposomes (PERLs) on infection.

These analyses indicate that HCV suppresses the expression of key regulators throughout the cholesterol biosynthesis pathway. This effect was quantified and the influence of liposome treatment evaluated. The latter resulted in the formulation of the hypothesis that PERL treatment interfers with virus-induced abberations of the cholesterol biosynthesis pathway and normalises the expression of four genes directly involved in cholesterol regulation. In addition, the lipidome of isolated lipid droplet was analysed by mass spectrometry. These data, combined with microscopy data suggest that PERLs interfere with S-palmitoylation of the HCV core protein resulting in dissociation of core from lipid droplets. This is likely to interrupt the viral assembly process, leading to inhibition of the production of infectious viral particles.

Further described here are two different yet unsuccessful approaches to fluorescently label HCV RNA for live cell microscopy studies, namely an MS2 coat protein mediated approach, and Alexa®UTP labelling.

Table of contents

List of figures and tables

1. Hepatitis C Virus

1.1 Hepatitis C Virus epidemiology

A non-A, non-B form of hepatitis was noticed to be transmitted via blood transfusions in the 1970s. However, it took until 1989 for two papers to be published describing the discovery of Hepatitis C Virus (HCV) [1, 2].

Today, HCV is recognised as a major health concern. It affects about 3% of the world's population of which 170 million are chronically infected [3]. In the United States of America (USA) alone there are 3.2 million people infected with HCV, counting 17 000 new infections each year [4]. HCV is a member of the *Hepacivirus* genus within the family of the *Flaviviridae*. There are 7 different genotypes, which share about 30% nucleotide sequence analogy and can be further divided into several subtypes (Figure 1) [5].

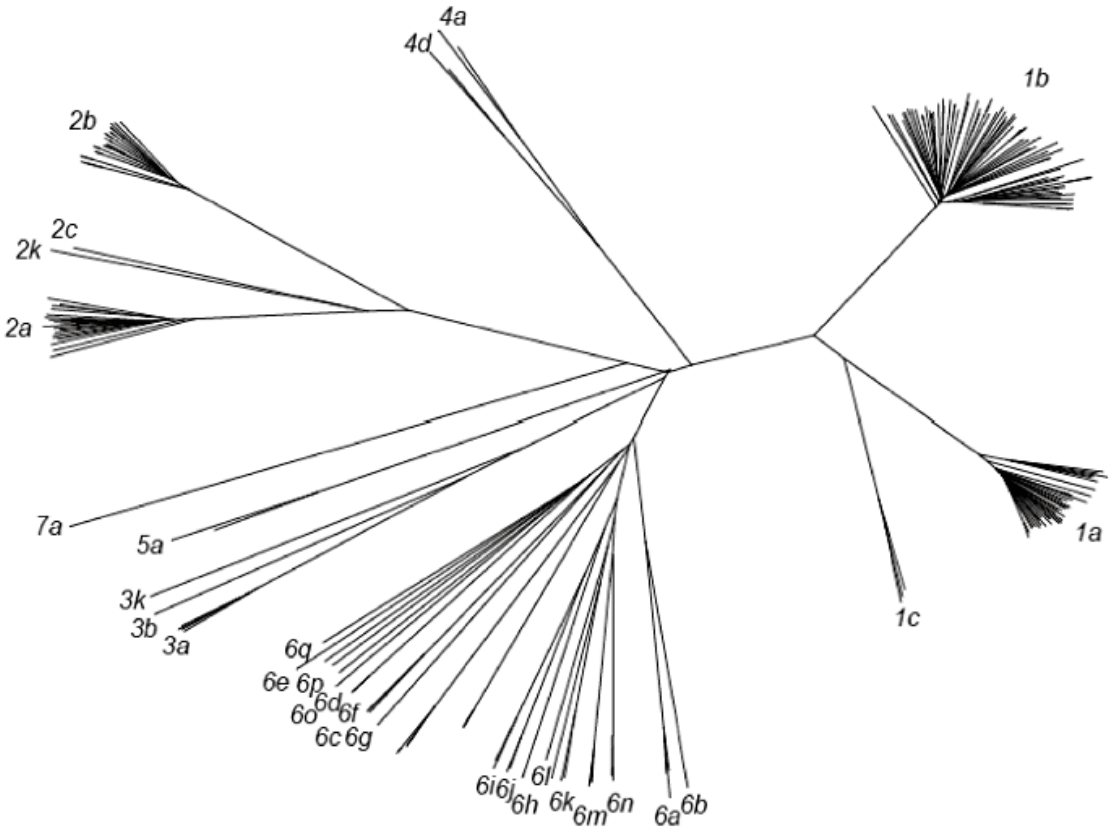

Figure 1: Phylogenetic tree of the seven HCV genotypes based on nucleotide sequence. The nucleotide sequence analogy between genotypes is about 30%. The 7 genotypes split up into numerous sub-groups designated by a letter. (source: [5]).

The worldwide distribution of these genotypes shows distinct patterns (Figure 2). The most prominent genotypes worldwide are genotypes 1b, 2a and 3. Genotype 5 is the predominant genotype in southern Africa, genotype 4 in Egypt and genotype 3 in Pakistan [3, 6, 7].

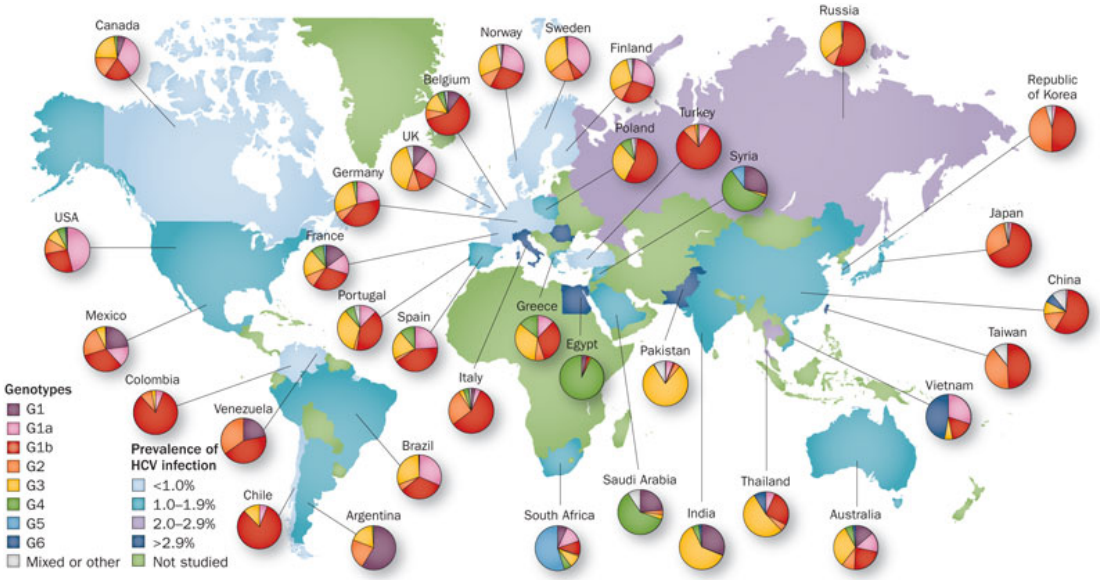

Figure 2: Global distribution and prevalence of HCV genotypes. Clear differences in genotype distribution can be seen between regions. Genotype 1 is the most widely spread genotype in the northern hemisphere and South America (source: [7]).

HCV is a blood-borne virus, primarily transmitted through contaminated needles or blood products. Infection rates of up to 90% can be accounted for by intravenous drug abuse, but also non-intravenous drug abuse through nasal mucosa can occur. Accidental needle sticks account for 0.2 to 10% of infections, contaminated healthcare equipment, and sexual transmission have also been reported. Mother to child transmission during birth is described with a 3 to 10% risk (reviewed in [8]). Up to 75-90% of the 15 million of HCV-positive individuals in Europe are not aware of their infection, and only a fraction undergoes treatment despite recent advances in this field [9]. Without treatment, 20-30% of acutely infected patients spontaneously clear the virus, the remaining 70-80% will develop a chronic infection [10]. An infection can ultimately lead to liver cirrhosis and eventually hepatocellular carcinoma

(HCC) and thereby accounts for approximately 350 000 deaths per year in the USA and 350 000 in Europe [11, 12]. Furthermore , HCV is the leading cause of liver transplantations in the USA and Europe [13]. However, liver transplants are inevitably re-infected, and are not a cure, or sufficient to clear the virus [14]. In 2007, HCV related mortality has surpassed Human Immunodeficiency Virus (HIV) mortality in the USA and about 10-times more people are living with chronic HCV infection than HIV in Europe [12, 15]. Due to the common routes of transmission, co-infections with HIV are very common counting 50-90% amongst intravenous drug users in the USA, impacting antiviral treatment [16].

1.2 HCV genome

HCV is a positive stranded RNA virus with a 9.6 kb genome, which encodes an approximately 3011 amino acid (aa) long polyprotein [1]. The genome is densely packed and both the 3'-untranslated region, and the 5'-untranslated region (UTR) fold into complex secondary structures. These are essential for genome replication and present binding regions for regulatory factors e.g. host proteins, viral proteins or short RNAs (details in 1.4.2). Instead of a 5'-polyA cap, HCV translation is initiated at an internal ribosomal entry site (IRES), which is extensively folded, structured and highly conserved between isolates [17-19]. Both UTRs interact physically during replication and form the so called kissing complex [20].

1.3 HCV proteins

One large open reading frame encodes a polyprotein, which is subsequently cleaved into at least 10 viral proteins (Figure 3). These can be categorised into structural (core, E1, E2), and non-structural proteins (NS2, NS3, NS4A, NS4B, NS5A, and NS5B). Situated between those two groups is the hexa- and heptamer forming protein p7, for which it not yet clear whether it is part of the virion or not [21]. These days p7 is more commonly named amongst the non-structural protein [22].

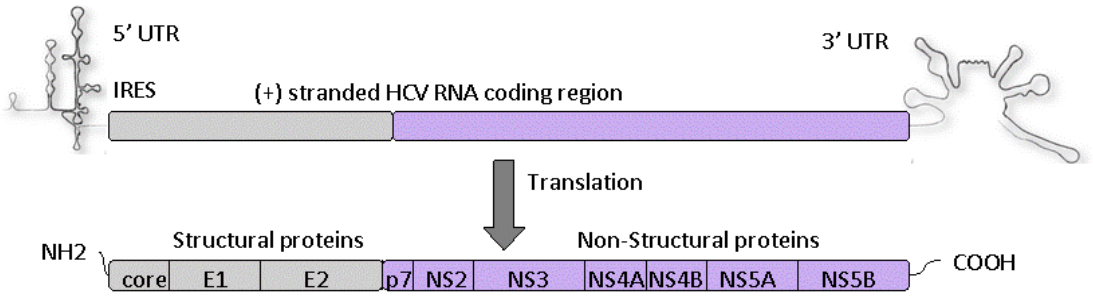

Figure 3: The HCV polyprotein is translated from a single open reading frame. The open reading frame is flanked by highly structured UTRs. The polyprotein can be readily translated in an IRES-mediated manner from the viral genome and is cleaved into structural and non-structural viral proteins.

1.3.1 Frameshift protein

The F protein (14-15 kDa) arises from a +1 ribosomal frameshift at the N-terminal region of the core protein within the polyprotein. F protein specific antibodies have been found in patient sera [23, 24]. The exact role of the F-protein within the viral lifecycle remains to be elucidated but some functions have already been linked to it [25]. Those include interaction with the NF-κB pathway and thereby apoptosis, as well as interaction with tubulin and the

rearrangement of the cytoskeleton [26, 27]. It is hypothesised, that the F protein may also contribute to viral persistence similar to the L* protein in Theiler's murine encephalomyelitis virus [24].

1.3.2 Core protein

The core protein is the capsid forming protein of the virus. It is cleaved from the polyprotein by the host signal peptidase, resulting in an immature form (p23) comprising 3 domains. Domain 1 spans the residues 1-117 and is involved in RNA-binding and oligomerisation [28]. This domain contains a nuclear localisation sequence (NLS), however, the presence of core in the nucleus has not yet been convincingly demonstrated [29]. Core domain 2 (aa 118-177) is formed by two amphipathic helices that interact with membranes and thereby anchors the protein and allows association with the endoplasmic reticulum (ER) membrane, mitochondria and lipid droplets (LDs) [30-34]. Domain 3 is a signal peptide comprising amino acids 178-191 [34]. It aids the translocation of E1 to the ER and is cleaved off by a signal peptide peptidase to reveal the mature core protein. Following this cleavage, core oligomerises into homodimers through interaction of uncharged residues at the N-terminus. This induces the interaction of core with NS3 and further assembly into capsids [34-36]. Besides its structural function, core interacts with a number of host proteins, like DEAD (Asp-Glu-Ala-Asp) Box Polypeptide 3, X-Linked **(**DDX3), microsomal triglyceride transfer protein (MTP), and the innate immune system [37-39]. Its interaction with p7 facilitates core loading onto lipid droplets as a crucial step in virus assembly [40].

1.3.3 E1/E2 envelope proteins

The envelope proteins E1 (33-35 kDa) and E2 (72-77 kDa) are glycoproteins, essential for cell entry and fusion with the host membrane [41-43]. Both are heavily glycosylated with 4-5 and 11 glycosylation sites respectively, some of which are highly conserved [44]. Each has a single transmembrane domain that anchors the protein in membranes but is also essential for heterodimerisation and retention in the ER [45, 46]. In addition, E2 contains a hypervariable region (HVR1), which varies in amino acid sequence by up to 80% between genotypes, but physical properties of those residues remain similar. This HVR1 plays major roles in viral infectivity, cell entry, and recognition by neutralising antibodies [47-50].

1.3.4 p7

This hexa- and heptameric viroporin is a 7 kDa, highly hydrophobic protein, essential for viral infectivity [51, 52]. Its hydrophobicity is based on its two transmembrane domains, which are connected through a cytoplasmic loop [53]. P7 is a multifunctional protein, involved in assembly, interacting with NS2, and core, and it may protect E2 from degradation [40, 52, 54-56]. It is unlikely to be part of the virion and its physiological role as a cation-selective ion-channel is still debated [21, 22, 57-59]. The p7 sequence is heterogeneous amongst different genotypes and interchanging p7 between, as well as within genotypes has a major impact on the infectivity of viral particles. This may reflect interactions with other viral proteins [60, 61].

1.3.5 NS2

The 23 kDa, dimeric, zinc-dependent metalloprotease NS2 has a short half-life, after facilitating its own cleavage from NS3, thereby losing its protease activity [62-64]. The unglycosylated, hydrophobic protein contains 3 trans-membrane domains, which keep it anchored in the ER membrane and facilitate direct interactions with NS3 and E2 [65-67]. It interacts with host proteins, like p53, interferes with cell cycle regulation, and inhibits apoptosis, contributing to HCV pathogenesis [68-70]. Furthermore, NS2 is an interferon antagonist and together with NS3/4 modulates the host immune response [71]. Like p7, NS2 is indispensible for viral particle assembly and directly interacts with E2 and p7 to promote the assembly process. The exact mechanism of this involvement is not fully understood [52, 54].

1.3.6 NS3-NS4A

The NS3 (68 kDa) protein possesses both, protease and helicase-/NTPase activity [72, 73]. The NS3 serine protease cleaves the polyprotein, with NS4A (6 kDa) acting as a co-factor, releasing NS4A, NS4B, NS5A and NS5B [74, 75]. In addition to its role in replication, it plays a major part in HCV persistence. The protease complex inhibits the innate immune response by cleaving signalling factors, inhibiting downstream activation of immune response elements, such as the adaptor protein Cardif, which links the double strand RNA (dsRNA) sensor RIG-I to the interferon response [76]. It further prevents oligomerisation of mitochondrial antiviral signaling (MAVS) and thereby subsequent antiviral signaling, and cleaves TRIF, the TLR3-signalling adaptor molecule, thus preventing chemokine production which leads to T-cell

activation [77, 78]. NS3-NS4A protease presents a potent drug target due to its diverse roles in RNA replication and suppression of antiviral immune response. Despite its very shallow binding site, the first HCV specific inhibitors Telaprevir and Boceprevir have been developed against this protease, and after successful clinical trials were approved in 2011 [79, 80].

1.3.7 NS4B

The 29 kDa NS4B protein contains 4 trans-membrane domains spanning the ER membrane [81, 82]. It interacts with an extensive range of cellular proteins involved, amongst others, in the immune response, lipid metabolism, cellular stress, and autophagy (reviewed in [83]). The formation of the membranous web, a distinct microenvironment for HCV replication formed through the redistribution of cellular membranes, is initiated by NS4B [84]. Furthermore, it physically interacts with NS5B and the replication complex and together with NS4A it acts as an inhibitor of IRES-mediated translation, which appears to be a self-regulatory mechanism [85, 86]. The localisation of NS4B to LDs is crucial for viral replication and a loss of this association with LDs results in critical replication defects [86-88].

1.3.8 NS5A

The NS5A phosphoprotein exists in a 56 kDa basally phosphorylated (p56) and a 58 kDa hyperphosphorylated (p58) full-length form, which acts as a regulatory switch. Phosphorylation of NS5A is controlled by phosphatidylinositol 4-kinase III alpha (PI4KIIIα), increasing levels of PI4P within the replication area. However, PI4KIIIα levels are tied to membranous web morphology and replication in a yet undefined mechanism [89, 90] (see

chapter 2). Furthermore, as opposed to p56, the p58 form of NS5A does not interact with the cellular factor human vesicle-associated membrane protein-associated protein A (hVAP-A), thereby having a suppressive effect on viral replication [91]. The first 30 aa of this protein are essential for ER-association and conserved amongst different genotypes [92]. NS5A further contains 3 domains of which domain I (aa 33-202), the zinc-binding domain, is the most conserved amongst the different genotypes [93, 94]. Domain I and II (aa 251-342) facilitate specific RNA binding with the poly(U/UC) tract of the HCV 3'UTR and localise NS5A to LDs, suggesting a role of NS5A in assembly [95-97]. Further, NS5A plays an additional regulatory role in replication by binding directly to the viral polymerase NS5B [98]. Domain III (aa 359-447) of NS5A is not essential for replication, however, especially the last 30 aa are crucial for virus production. This domain appears to be involved in protein-protein interactions, which also extend to cellular proteins, e.g. for cell cycle control and apoptosis, involving p53 and Bax having an inhibitory effect, or antiviral signalling through inhibition of PKR which is activated by dsRNA [99-101]. These are only a few examples and the interaction network is rather extended (reviewed in [102]). However, its interplay with the host interferon response has been subject of several studies with respect to drug resistance and NS5A has become a prominent target of small molecule inhibitors itself [103, 104].

1.3.9 NS5B

NS5B is an RNA-dependent RNA polymerase (RdRp) consisting of a thumb, finger, and palm domain, engulfing the template RNA [105]. Enzymatic activity is 4 to 20-fold increased by Mn^{2+} compared to Mg^{2+} but inhibited by

other divalent metal ions [106, 107]. Protein kinase C-related kinase 2 (PRK2) phosphorylates NS5B and thereby enhances its activity [108]. For full-length genome replication, 3 non-structural proteins are essential: NS2 (for NS2/NS3 cleavage), NS3, and NS5B. However, under normal circumstances the replication complex also comprises the other non-structural proteins, NS4A, NS4B, and NS5A [109]. The complex assembles shielded from host nucleases and proteases in spherules from rearranged cellular membranes [110].

1.4 HCV lifecycle

1.4.1 HCV cellular attachment and entry

Cellular tropism of HCV is still not fully understood. The virus primarily infects hepatocytes of either human or chimpanzee origin. However, RNA has been found in hematopoietic derived cells and HCV can infect neuronal cells *in vitro* [111-113]. This phenomenon is likely due to the virus utilising numerous cellular receptors for cell entry. However, entry alone does not necessarily lead to a successful replication cycle and virion release.

HCV cell entry is a complex, multistep process. 14 host-cell surface factors have been identified that are involved in the HCV cell entry process (Table 1). However, not all of these need to present on the cell surface for the virus to enter. The main entry receptors are CD81, SR-B1, occludin, and the tight-junction protein CLDN1.

Abbreviation	Receptor	Reference
Tetraspanin CD81	**C**luster of **D**ifferentiation-81	[114-116]
SR-B1	**S**cavenger **R**eceptor class **B-1**	[117]
LDLR	**L**ow **D**ensity **L**ipid **R**eceptor	[118, 119]
CLDN1	Claudin 1	[120, 121]
CLDN6	Claudin 6	[121, 122]
CLDN9	Claudin 9	[121, 122]
OCLN	Occludin	[123, 124]
EGFR	**E**pidermal **G**rowth **F**actor **R**eceptor	[125]
NPC1L1	**N**iemann-**P**ick **C**1-**L**ike-**1**	[126]
TfR1	**T**rans**f**errin **R**eceptor-**1**	[127]
GAGs	**G**lycos**a**mino**g**lycans	[128-130]
EphA2	**E**phrin **R**eceptor **A2**	[125]
L-SIGN	**L**iver/lymph node-**S**pecific **I**ntercellular adhesion molecule-3-**G**rabbing **N**on-integrin	[131]
DC-SIGN	**D**endritic **C**ell-**S**pecific **I**ntercellular adhesion molecule-3-**G**rabbing **N**on-integrin	[132]

Table 1: HCV entry factors.

Upon attachment to the cell, a yet undefined sequence of interactions between the virus and cellular receptors initiates cell entry via clathrin-mediated endocytosis [116, 121, 133, 134]. Interaction with the host cell is mediated by the viral envelope glycoproteins E1/E2 and lipoproteins that are incorporated in the viral particle [135]. The importance of lipoproteins in the context of viral entry is explained in more detail in chapter 2. After fusion with

the cellular membrane, the virus-containing vesicle follows the endosomal maturation pathway during which the endosomal pH is decreased to 5-6. The drop in pH causes the viral envelope to fuse with the endosomal membrane leading to the release of the capsid into the cytoplasm [43].

This route of transmission applies to mature virus particles. However, HCV can also transmit from cell-to-cell independently of the cell-free mechanism [136]. This route of transmission is not well characterised. Several entry receptors that are part of cell-free transmission are also involved in cell-to-cell transmission, such as NPC1L1, EphA2, EGFR, and CLDN1 [125, 126, 136, 137]. Cell-to-cell transmission has been discovered and originally described after transmission of the virus had occurred in the presence of neutralising anti-CD81 antibodies. However, very recently the same group described a new monoclonal CD81, which blocks cell-to-cell transmission [138]. It is also not known what the viral particle looks like for this route of transmission. With regards to the development of antivirals and treatment of infections it is crucial to investigate this area further.

1.4.2 HCV replication

Upon clathrin-mediated endocytosis, acidification of the endosome facilitates fusion of the viral particle with the endosomal membrane. The HCV capsid and RNA are released into the cytosol and transported in a microtubule-dependent manner towards the ER [139-141]. In close proximity to the ER, HCV induces the formation of a detergent-resistant microdomain, called the membranous web, through the reorganisation of cellular membranes. This specialised region is the actual site of replication and assembly [84, 142]. Its

formation involves viral and host proteins. NS4B initiates the recruitment of ER- and other cellular membranes [84, 143, 144]. NS5A, functioning as an adapter protein, interacts with cellular factors like phosphatidylinositol-4-kinase III (PI4KIIIα) to stabilise the web and ensure local phosphatidylinositol (PI) synthesis for viral replication. LDs, which accumulate in close proximity to the ER, play an essential part of the replication and assembly process [145]. The viral core protein and NS5A are loaded onto LDs by the cellular diacylglycerol glycerol acetyltransferase-1 (DGAT1) [96, 146, 147]. The association of core with LDs is essential for virus replication and its disruption leads to a decrease of formation of infectious particles [147, 148]. NS5A interacts with the LD binding protein tail-interacting protein of 47 kDa (TIP47), further mediating the association of the viral replication complex, which includes NS3, NS5B, and viral RNA, with LDs [149]. The involvement of host factors and the replication process itself are not fully understood.

HCV is a single strand, positive-sense RNA virus. This allows viral genomes to either be transcribed or translated into protein straight away. However, the translation process is dependent on an active transcription process [150]. Both processes are thought to happen in close proximity to each other, which would allow fast adaptation and regulation of either one. With the release of the viral genome, the host-cell translation machinery synthesizes the first polypeptide. Translation is initiated at the IRES, which constitutes domains II-IV of the 5'UTR where a complex of 40S ribosome and eukaryotic initiation factor binds to the start codon [151]. The ribosome binds to domain II, and partly III and the eukaryotic initiation factor-3 (eIF3) recruits the 60S ribosome to form an active ribosomal complex [152].

The 5'UTR interacts with the 3'UTR, forming a circularised RNA structure, the kissing complex [153]. Both UTRs are highly structured with numerous regulatory stem loop structures (Figure 4).

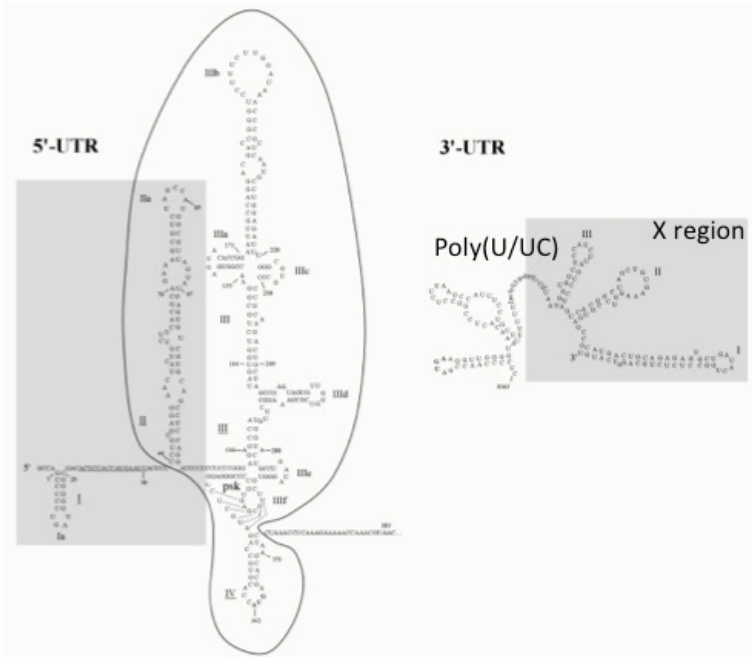

Figure 4: The HCV untranslated regions (UTRs). Both UTRs are highly structured and divided into several domains. The IRES interaction occurs with the circled sequence comprising domains II-IV, whereas grey shaded sequences represent those parts of the UTRs that are involved in RNA replication (Figure adapted from [154]).

The poly(U/UC) variable region in the 3'UTR plays a significant regulatory role in the replication process as its length is tied to replication efficiency [155]. The complex interplay of several interactions also comprises host factors binding to short sequences within the UTRs thereby influencing the efficiency of viral replication. Prominent examples are synaptotagmin binding cytoplasmic RNA interacting protein (SYNCRIP), polypyrimidine tract-binding protein (PTB) or the liver specific micro RNA miR-122. Some of these interact

with the two UTRs, or are involved in both, transcription and translation [156-159]. For genome replication the positive-strand RNA is transcribed into negative-strand RNA by NS5B, most likely resulting in a dsRNA intermediate [160]. Transcription requires domain I and II within the 5'UTR as well as in the 3'UTR the X-region with a NS5B binding domain, and the poly(U/UC) region [161, 162]. NS5B initiates transcription of the negative strand in a primer-independent manner just upstream of the X-region [163]. The continuation of the transcription of the 3'end by NS5B results in a positive-strand product [164]. However, NS5B is also able to initiate the transcription *de novo* [107]. The positive-strand product is then used for translation or is packaged into progeny viruses. Therefore, the abundance of positive-strand RNA in an established infection is about 10-times higher than the abundance of negative-strand RNA [165]. The amount of protein translation is regulated by the amount of progeny RNA released from the site of replication [166]. Binding of regulatory small RNAs to the viral genome, for example miR-122, stimulates translation due to a conformational change of the 5'UTR, which activates the translation process [167, 168]. The viral protease NS3 contributes to regulating the switch by competing for binding to the IRES-HCV complex with the host La-protein, thereby promoting the shift from translation to replication [169]. The level of protein synthesis in turn regulates the rate of particle formation upon polyprotein processing.

The HCV polyprotein is translocated into the ER lumen, where a host signal peptide peptidase cleaves and releases the immature p23 core protein, which is further processed by a host ER-signal peptidase into the mature p21 [170]. The same signal peptide that released core, facilitates the E1-E2 cleavage.

Partial cleavage between E2-p7 and p7-NS2 occurs through ER signal peptidases, leading to an E2-p7-NS2, and E2-p7 intermediates, delaying the release of p7 [171]. Autolytic cleavage of the non-structural proteins occurs through viral proteases NS2/3 and subsequently NS3/4A [172, 173]. The cleavage of NS2/3 and NS3/4A is facilitated rapidly, whereas the cleavage of NS4-NS5A by NS3/4A is delayed [174]. NS4B/5A cleavage is also delayed in contrast to a rapid NS5A/5B cleavage. This leads to NS4B/5A intermediates with yet unknown function [175]. Variable efficiency of cleavage sites thereby regulates and times the abundance of viral proteins, which contributes to the regulation of replication and transcription.

1.4.3 HCV assembly and release

HCV assembly and release are both parts of the viral lifecycle that are not yet entirely understood. How viral RNA is packaged into the capsid and how the capsid forms is unclear. Based on *in vitro* RNA selection experiments, Stewart et *al.* presented evidence for the presence of packaging signals within the HCV genome. These signals are recognised by the core protein, however, this finding has yet to be published in a peer-reviewed journal [176].

The core protein and NS5A recruit viral proteins and RNA for assembly to LDs, where core interacts with the viral RNA to form nuclear capsids [145, 177, 178]. NS2 is a major regulator in the assembly process by facilitating interactions between non-structural and structural viral proteins, E2, p7, and NS3 on LDs [54, 179].

Many host proteins are also involved in assembly such as phospholipase A2, DGAT1, and clathrin adaptor AP2M1 [145, 147, 180-183]. Lipoproteins,

involved in the very low density lipoprotein (VLDL) synthesis pathway like ApoB and ApoE, are required for effective particle formation and are also incorporated into the viral particle [184]. The viral particle and its association with lipoproteins are discussed in detail in chapter 2. Release of progeny viruses occurs through an unknown mechanism.

1.4.4 HCV antivirals

Currently, there is no vaccine available. Several vaccination studies have been conducted and more vaccine candidates are being trialed ([185-187], Inovio INO-8000 HCV, ClinicalTrials.gov Identifier: NCT01701336). At the same time, a growing number of antivirals are being developed. Ribavirin in conjunction with pegylated interferon-α (PEG-INF-α) has been the standard of care (SOC) therapy for many years. However, the efficacy of interferon-based treatment regimes is genotype-dependent and interferon treatment is accompanied by major side effects, often leading to poor compliance. Because of this, and advances in drug development in the recent years, SOC is aimed to become interferon-free [188]. The efficiency of SOC treatment is increased by the addition of direct acting antivirals (DAA). DAAs target the non-structural protein NS5A, the viral polymerase NS5B, the NS3/NS4A protease, or p7 and are only given in combination therapy to minimise the likelihood of treatment failure due to escape mutants [189, 190]. Currently, only the protease inhibitors Telaprevir and Boceprevir are administered in combination with SOC treatment for treatment of genotype 1 infections [191, 192]. The addition of Telaprevir increases the sustained virological response (SVR) rate from 44% with SOC alone to 75% [192]. However, the

combinational approach comprising the polymerase inhibitor Sofosbuvir results in an up to 100% SVR in clinical trials [193]. Many more DAAs and drug combinations are in clinical trials or are awaiting approval (reviewed in [194]).

Besides DAAs, there are a number of host-targeting molecules in development and under investigation. Some of those target viral entry through the inhibition of entry receptors like SR-B1, CD81, NPC1L1, and EGFR [125, 126, 195-197]. Erlotinib and Ezetimibe are already approved drugs and are currently tested as NPC1L1 and EGFR inhibitors, respectively for HCV treatment (ClinicalTrials.gov Identifier: NCT01835938, [198]). Other studies focus on replication co-factors that promote viral replication, like the liver-specific small inhibitory RNA miR-122, cyclosporinA, PI4KIIIα, or the assembly process exploiting ER α-glucosidase inhibitory iminosugars [199-202]. The administration of any drug comes with the risk of mild to severe side effects and efficient drug targeting in order to minimise the amount of drug administered is desirable.

1.5 *In vitro* models for HCV propagation

Initial attempts to cultivate HCV *in vitro* involved primary human foetal hepatocytes, which were infected with patient sera [203]. The limiting factors with this HCV infection system were cytotoxic effects due to interferon production, contamination issues, and a low level infection, which only lasted for up to 2 months [204].

The first stable and reproducible *in vitro* system was the replicon system. In 1999 a sub-genomic replicon (only encoding non-structural proteins for RNA

replication) was developed, followed by the full-length replicon in 2000. Both are based on genotype 1b and are propagated in a human hepatocyte cell line (Huh-7) [205, 206]. However, those replicon-infected cells did not release mature viral particles [207].

In 2003, HCV pseudotype particles (HCVpp) were developed and used to study viral entry. Those particles are produced in human embryo kidney cells (293T) by transfecting three vectors encoding i) the retroviral packaging construct CMV-Gag-Pol, ii) fluorescent reporter, and iii) HCV glycoproteins E1 and E2 [41]. Released pseudotype particles are able to infect Huh-7 cells but do not replicate and are only suitable for studying early infection events, like viral entry.

In 2005 a full-length replicon, derived from a Japanese patient with fulminant hepatitis genotype 2a, hence termed JFH-1, was successfully propagated, resulting in the release of viral particles from Huh-7 cells *in vitro* [208]. This JFH-1 cell culture system was further refined by the construction of a chimera, based on JFH-1 for the structural proteins and a J6 genotype 2a isolate, providing the non-structural proteins, resulting in the Jc-1 HCV cell-culture (HCVcc) system [209, 210]. Additional improvements were made concerning the Huh-7 cell line resulting in Huh7.5.1 and Huh-7.5 [211]. These cells are derived from replicon-harboring Huh-7 cells that were treated with INF-α and subsequently cured of the replicon infection. Thereby, the permissiveness for HCV infection was increased from 10% to 30-75%, depending on the replicon system used [212]. Huh7.5 cells also carry a non-functional copy of RIG-I, leading to suppressed INF-β activation [213]. However, those cells also do not support the production of lipoviral particles (LVPs, described in chapter 2),

as found in patient sera. This is due to a defect in VLDL production, a crucial component of HCV maturation (detailed information in chapter 2) [214]. Despite recent advances in the development of cell culture with human induced pluripotent stem cells (iPSCs) derived hepatocytes, micropatterned co-culture (MPCC), or human fetal liver cell (HFLC) cultures, it is not yet possible to simulate the complexity of the liver with its different cell types and 3-dimensional structure [215-217]. As of today, there is no complete cell culture system modeling HCV infection as it occurs in human patients.

1.5.1 *In vivo* models for HCV

HCV tropism is restricted to humans and chimpanzees. As far as it is known, those are the only two species that are fully permissive and can support the viral lifecycle with a competent immune system in place. The chimpanzee is most valuable in vaccine studies that require a fully competent immune system in order to give accurate results [218]. However, the use of chimpanzees for experimental studies is strongly limited due to ethical, financial and practical reasons. SCID (severe compromised immunodeficiency) mice are T-cell and B-cell deficient but can, if engrafted with human hepatocytes, sustain HCV infection [219]. Most humanised mouse models were developed to mirror specific pathological aspects of HCV infection and only very recently a mouse model has been described, which supports the entire lifecycle of HCV [220-222]. However, in the context of inflammation, mouse models very poorly reflect human responses and might therefore be questionable models for human disease studies [223].

Other animal models have been tested, including other primates and rats but those require further characterisation [224, 225].

Viruses closely related to HCV are also studied, used or tested as surrogate models. Those models include GBV-B, and recently discovered bat and small rodent hepaciviruses, as well as hepaciviruses in dogs [226-228]. These discoveries may open up the possibility to use small animal models in the future.

2. Analysis of lipoprotein- and cholesterol pathway gene expression in Huh7.5 cells

2.1 Objective

The work described in this chapter as well as the following chapter, is based on an antiviral liposome treatment, developed in our lab [229]. Experiments outlined in both chapters are an extension of early characterisation experiments of the antiviral polyunsaturated ER-targeting liposome (PERL) treatment of HCV infected cells. These early experiments revealed a decrease in secreted cholesterol from PERL-treated, HCV Jc1-infected Huh7.5 cells, which was thought to be the main mechanism of action leading to the antiviral activity of PERLs [230]. To contribute to the understanding of the antiviral mechanism of action of fully synthetically optimised (SO)-PERLs in the context of HCV infection, a lipoprotein signalling and cholesterol metabolism targeted microarray experiment was performed (chapter 2). The analysis of these data reveals changes in the regulation of genes involved in host lipid metabolism that occur due to HCV Jc1 infection as well as changes introduced by SO-PERL treatment in naïve and infected cells. These results prompted the lipidomics study discussed in chapter 3. The aim for chapter 3 was to analyse if lipid droplets, cellular organelles, essential to viral infectivity, are altered in their lipid composition due to the changes in cholesterol and lipid metabolism observed in chapter 2. To introduce the data presented in both chapters, the beginning of chapter 2 briefly outlines lipid metabolism and the involvement of HCV.

2.2 Fatty acids and triacylglycerols

Fatty acids (FAs) are esterified carbon chains that can either be unsaturated, or saturated to various degrees. The most commonly found FAs in lipids from mammalian tissue are long, straight chain FAs with 14, 16 or 18 carbon atoms. FA biosynthesis primarily takes place in the liver. Acetyl-CoA, derived from pyruvate in mitochondria, is converted into malonyl-CoA by acetyl-CoA carboxylase (ACC) in the cytoplasm of hepatocytes. This is the substrate for fatty acid synthase, a complex enzyme, catalysing a series of reactions resulting in 16:0 palmitic acid. Fatty acid synthase is regulated by sterol regulatory element binding protein 1 (SREBP-1), which is induced by insulin and inhibited by polyunsaturated fatty acids (PUFAs). To extend from the C16 carbon chain product and form longer chain FAs, C2-malonyl-CoA molecules are repeatedly ligated to the growing carbon chain by numerous elongases at the ER. Desaturases introduce double bonds at specific positions resulting in polyunsaturated FA species (Figure 5).

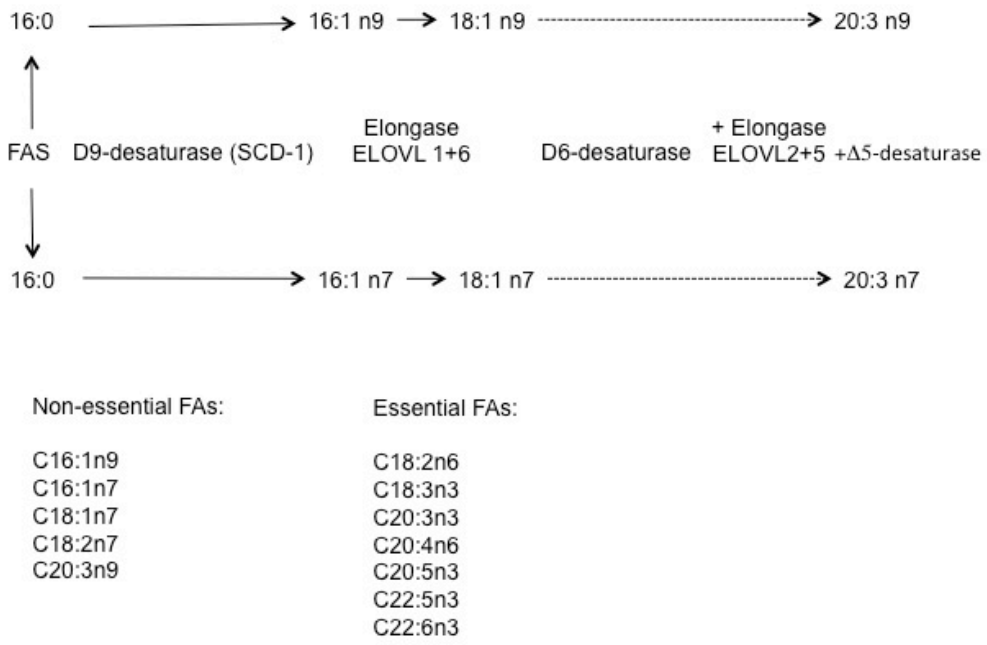

Figure 5: Elongation of fatty acids. Fatty acids are elongated by elongases and double bonds are introduced by desaturases, resulting in long chain fatty acids with different saturation status. These fatty acids are classified into non-essential and essential FAs, depending on whether they can be *de novo* synthesised or need to be taken up through the diet. C represents the number of carbon atoms in the chain and n the number of double bonds.

Fatty acids can be esterified to glycerol, forming triacylglycerol (TAG), a simple lipid (Figure 6).

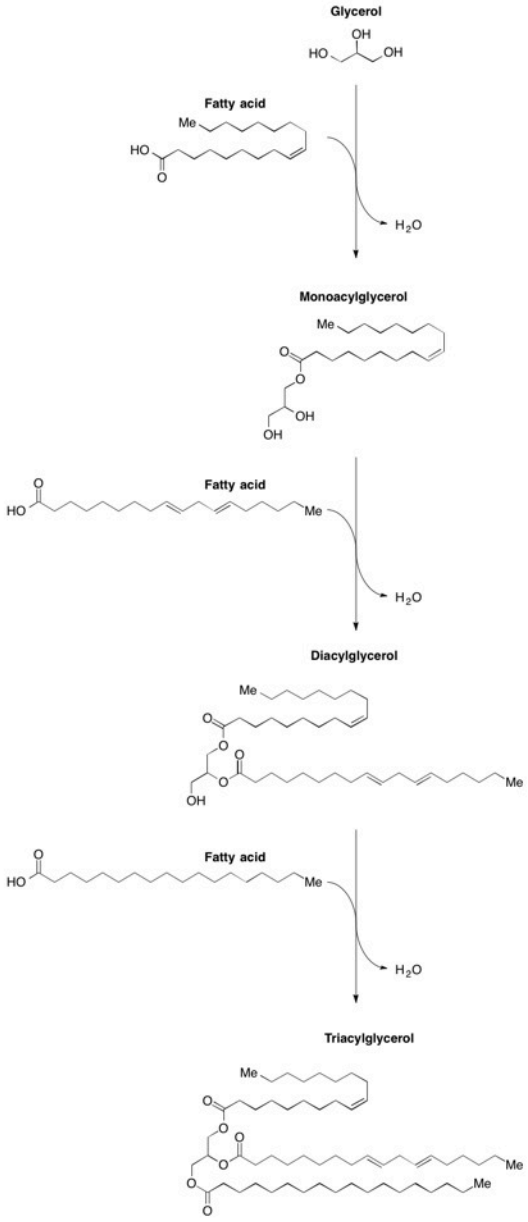

Figure 6: Free fatty acids and glycerol are esterified to form triacylglycerol. A mixture of different fatty acids results in various different triacyglycerol molecules. Shown here is a triacylglycyerol consisting of palmitoleic acid and linoleic acid.

TAGs contain essential FAs from the diet, and non-essential FAs from *de novo* biosynthesis. Various types of FAs are preferentially linked to either position of the glycerol molecule. *Sn*-1, *sn*-2, and *sn*-3 are predominantly linked to saturated, unsaturated and long FAs, respectively. TAG

biosynthesis in the liver and adipose tissue is described by the Kennedy pathway, which provides the substrates for phospholipid biosynthesis (Figure 7).

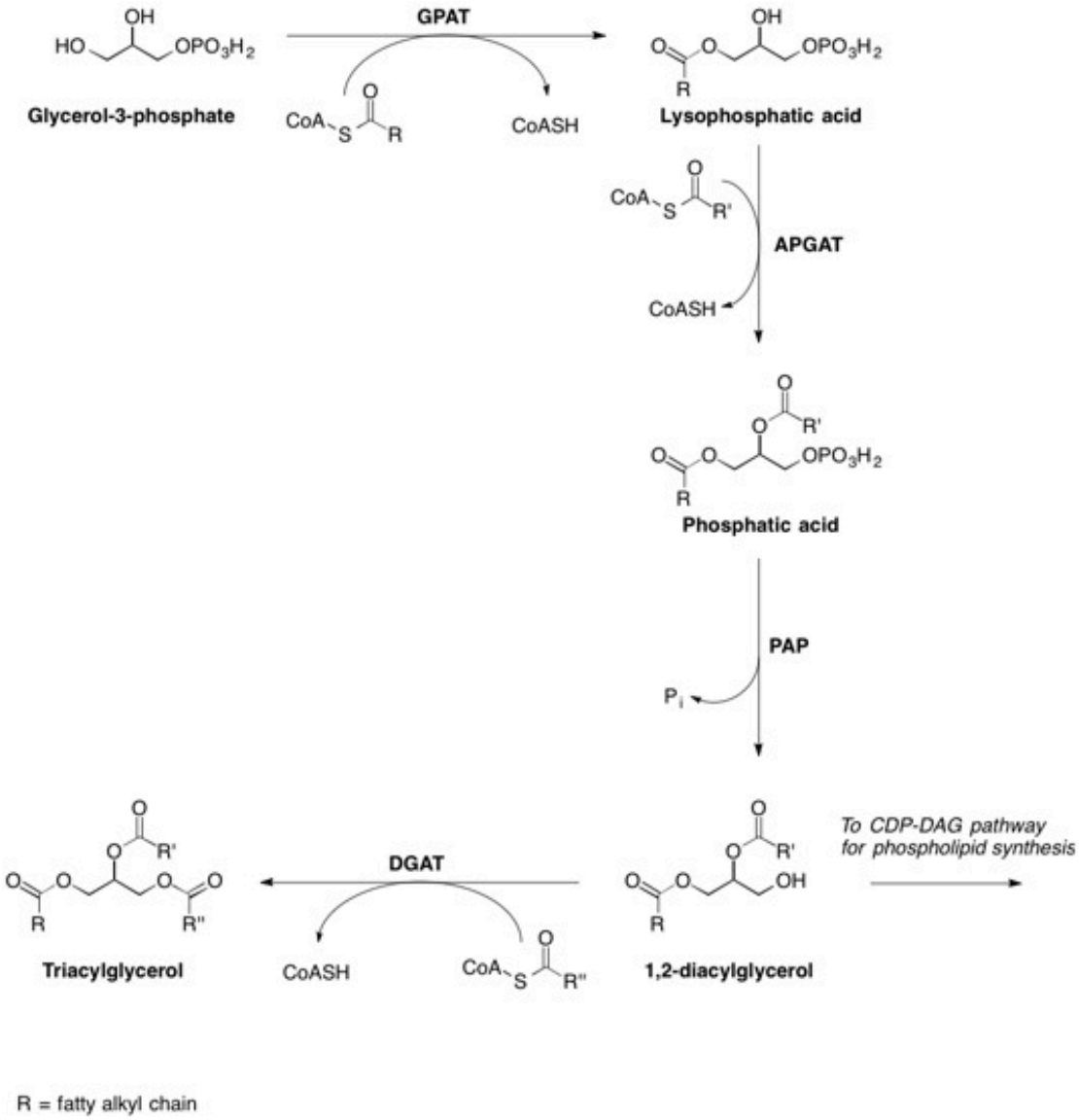

Figure 7: The Kennedy pathway. The synthesis of diacylglycerol and triacylglycerol forming the substrates for further processing to phospholipids via the cytidine diphosphate - diacylglycerol (CDP-DAG) pathway and from there phospholipid conversion through the phosphatidylethanolamine *N*-methyltransferase **(**PEMT) pathway.

GPAT: glycerol-3-phosphate acyltransferase, AGPAT: acylglycerolphosphate acyltransferase, PAP: phosphatic acid phosphohydrolase, DGAT: diacyglycerol acyltransferase

2.2.1 Phospholipids

Phospholipids are the main constituents of mammalian membranes. Besides their structural function, phospholipids and their metabolites play a major role in cell signalling and transduction.

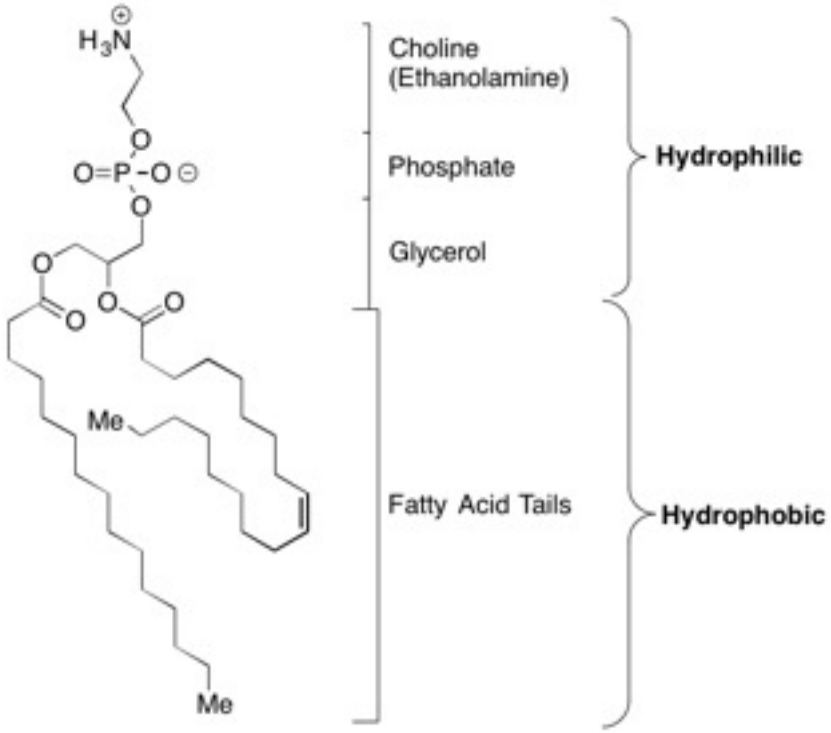

Figure 8: Phospholipids. Phospholipids are characterised by a hydrophilic glycerol – phosphate – choline head group with hydrophobic alkyl chains from usually two linked fatty acids. The example shown here is phosphatidylethanolamine.

Phosphatidylcholine (PC) is the most common phospholipid in mammalian membranes, constituting 50% or more of total lipids. *De novo* biosynthesis of PC starts with the phosphorylation of choline to phosphocholine by choline kinase; the first reaction in the CDP-choline pathway (Figure 9). Phosphocholine reacts to cytidine diphosphocholine, which becomes a substrate for CTP-phosphocholine cytidylyltransferase (CPT). This enzyme is active once it is anchored in the ER membrane. There, it catalyses the formation of PC in a final step by transferring the cytidine diphosphocholine onto diacylglycerol [231]. In an alternative pathway, PC can be synthesised from phosphatidylethanolamine (PE) in the ER (Figure 10) (reviewed in [232]). The phosphatidylethanolamine *N*-methyltransferase (PEMT) pathway is mainly active in the liver where PC is additionally required for the formation of VLDL particles and bile secretion [233]. This pathway accounts for approximately 30% of the PC synthesised in the liver.

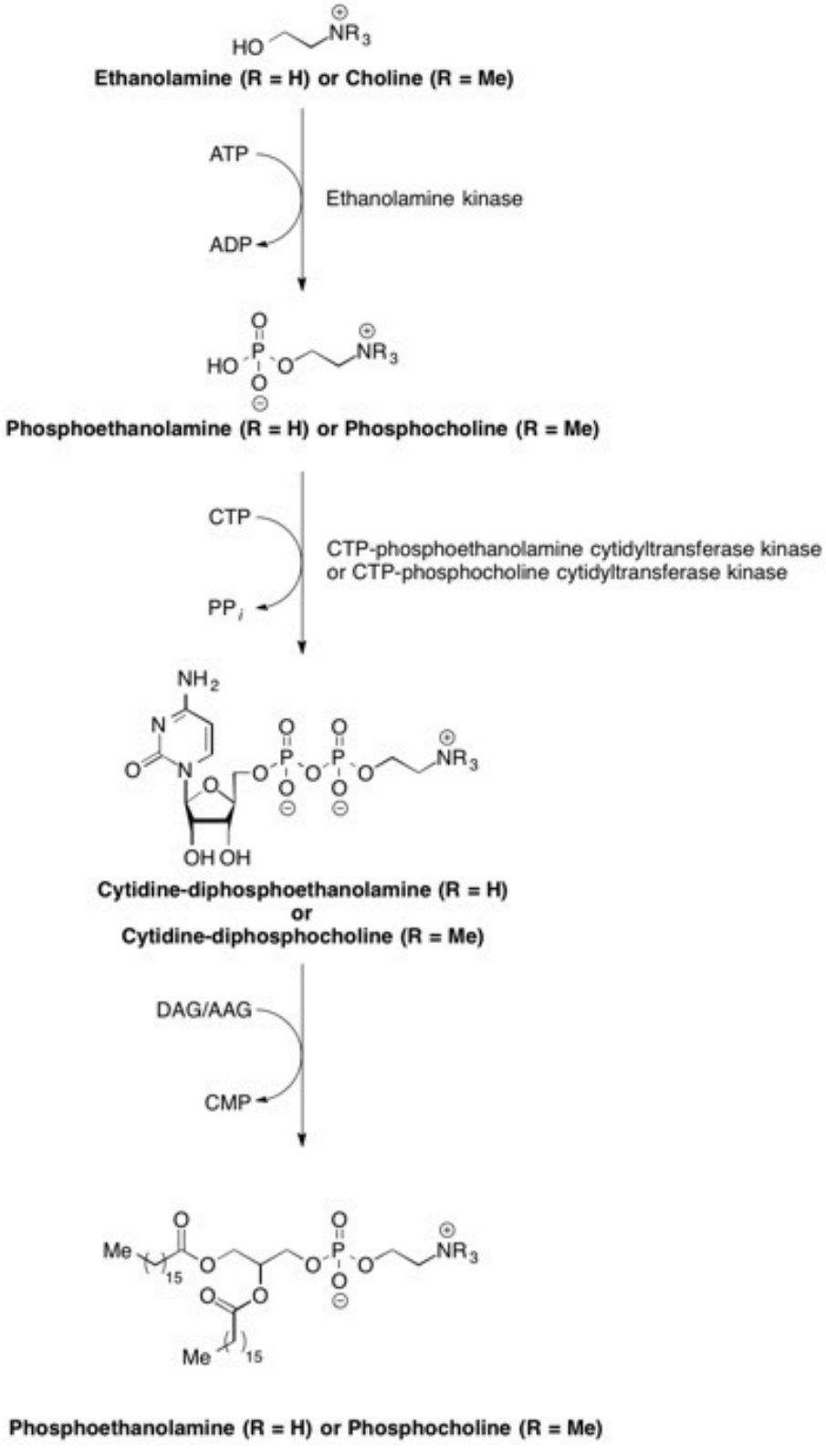

Figure 9: The CTP-DAG pathway. The synthesis of PE and PC from DAG and ethanolamine or choline, respectively.

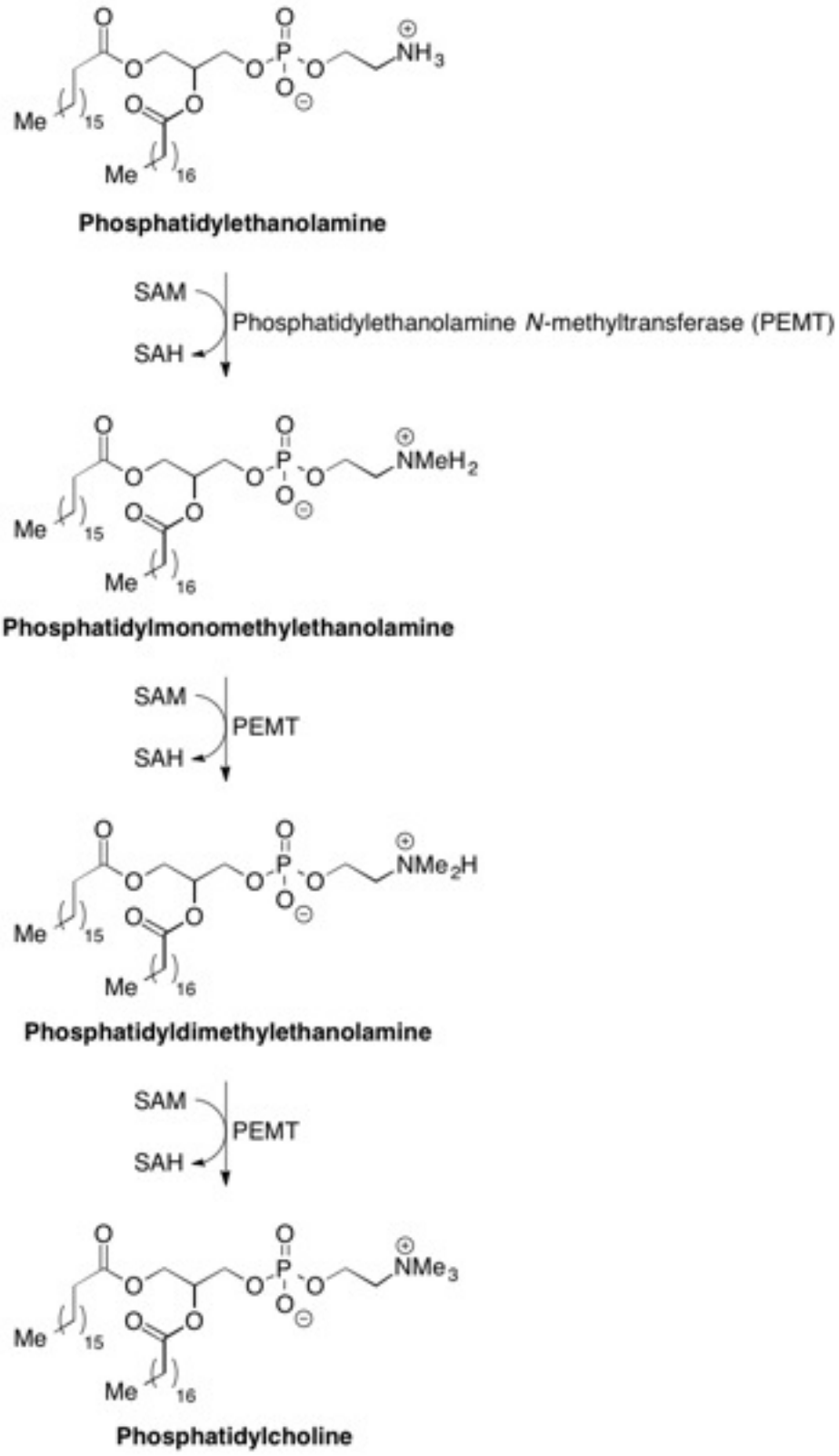

Figure 10: Pathway for the alternative synthesis of PC from PE. The synthesis of PC from PE occurs through a 3-step reaction by the enzyme phosphatidyl ethanolamine methyl transferase (PEMT).

PE is the second most common phospholipid in cellular membranes, constituting 20 to 30% of total lipids. It is characterised by a small headgroup in comparison to the other phospholipids. This results in strong interlipid connections due to hydrogen bond formation between lipids rather than binding of water molecules [234]. PE, like PC, is synthesised following the Kennedy pathway and the CDP-ethanolamine pathway. The alternative synthesis pathway for PE is through decarboxylation of phosphatidylserine by phosphatidylserine decarboxylase in the inner mitochondrial membrane. From there, PE becomes distributed to other organelles.

Phosphatidylserine (PS) accounts for less than 10% of total phospholipids in mammalian cells. It is a major signaling molecule for apoptosis, by flipping, in a calcium-dependent mechanism, from the inner to the outer plasma membrane leaflet. PS is thereby presented to immune cells, activating phagocytosis. PS is also synthesised through the CDP-DAG pathway, or alternatively from PC or PE. If synthesis is based on PC or PE as substrates, serine is conjugated by PS-synthase I and II, respectively, in exchange for the respective headgroup.

Phosphatidylinositol (PI) is the fourth of the main phospholipids accounting for the smallest fraction of total phospholipids with less than 8%. It is derived from a diacylglycerol (DAG) precursor, cytidine diphosphate DAG, and inositol, catalysed by CDP-diacylglycerol inositol phosphatidyltransferase (or phosphatidylinositol synthase). PI is the precursor of phosphoinositides, which are signaling molecules involved in cell cycle, and insulin regulation.

Phospholipases of the A_2 family hydrolyse the *sn*-2 position of phospholipids, releasing free FAs, and the lyso-form of the phospholipid [235]. However, lyso-phosphatidylcholine (lysoPC) can also be synthesised by lecithin-cholesterol acyltransferase (LCAT) in the liver [236]. LCAT catalyses the transfer of the *sn*-2 linked FA of PC onto free cholesterol releasing lysoPC and cholesterol ester. LysoPC affects membrane fusion events due to its contribution to membrane curvature similar to cholesterol. In addition, lysoPC influences soluble NSF attachment protein receptor (SNARE)-mediated fusion by delaying the disassembly of the SNARE-complex. This results in a prolonged fusion process, which may partly contribute to its role in cancer development [237]. LysoPC is further involved in proinflammatory, G-protein coupled receptor (GPCR)-mediated signaling [238].

2.2.2 Ceramides

Ceramides are long-chain sphingoids with a fatty acid linked through an amide bond. The long acyl chains are mainly saturated or monosaturated (Figure 11). Due to variation in length and saturation, there are almost 200 different ceramide species. With sphingosine being the simplest sphingolipid without any head group, ceramide, with only one head group is considered a simple sphingolipid.

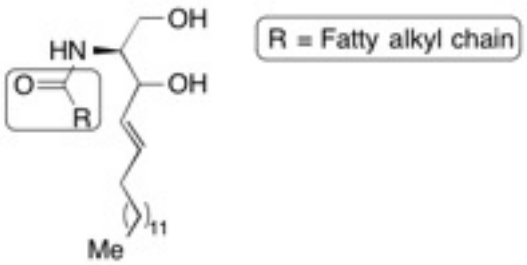

Figure 11: Ceramide structure. Ceramide is a sphingosine, linked through an amide bond to a fatty acid (boxed), which is commonly 16-26 carbons long. Compared to complex sphingolipids, ceramide does not carry any other head groups besides the FA.

De novo biosynthesis of ceramides is initiated at the ER through the condensation of serine to palmitoyl-CoA by serine palmitoyltransferase. The product, 3-keto-sphinganine, is reduced under NADPH consumption to sphinganine, which is rapidly *N*-acytylated to dihydroceramide by dehydroceramide synthase. In the last step, dihydroceramide-desaturase converts dihydrocaeramide to ceramide through the introduction of a C4 *trans*-double bond.

Catabolism of ceramide is controlled by ceramidases, which catalyse the hydrolysation of the molecule, releasing free FAs and sphingoid bases. Depending on the cell organelle, different ceramidases operate under different pH optima and can be categorised into acid (ASAH1), neutral (ASAH2) or basic (ACER1-3). Free FAs can be utilised in various ways, whereas sphingoid bases are likely to be recycled to synthesise new sphingolipids.

Ceramides are constituents of lipid membranes in the form of lipid domains. Those are sphingolipid and cholesterol rich regions 50 nm in diameter and mainly localised to the outer leaflet of plasma membranes [239, 240]. Interactions between sphingolipids occur through the hydrophilic head groups.

Cholesterol inserts between sphingolipids and thereby stabilises this region's structure [241]. Ceramides promote the fluid state and spontaneously form those rafts, which serve to organise various receptors for cell signalling [242]. Ceramides have a major impact on the regulation of metabolic pathways through the regulation of the Akt pathway. They regulate the phosphorylation state of Akt, which, in case of dephosphorylation, decreases the expression of the glucose transporter GLUT-4. Glucosylceramide is a negative regulator of insulin-mediated glucose uptake and therefore a major contributory factor for insulin resistance [243].

2.2.3 Sphingomyelin

Sphingomyelin (SM) is the most abundant sphingolipid, and the analogue to the phospholipid PC. It consists of a ceramide bound to a phosphorylcholine headgroup with two long chain fatty acids (Figure 12). The FAs are generally saturated or mono-unsaturated, most commonly 16:0 [244].

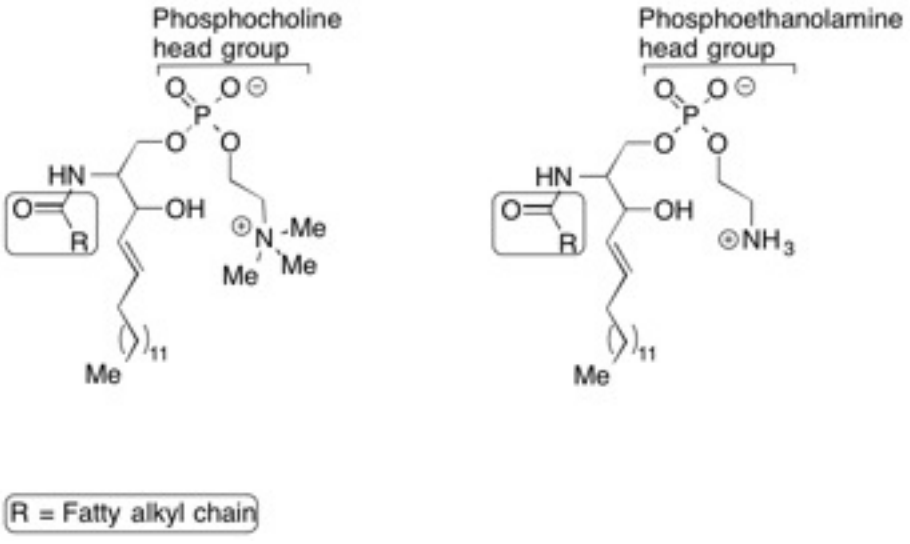

Figure 12: Sphingomyelin structures. Sphingomyelin is a complex sphingolipid with two head groups. It contains ceramide with a phosphocholine or phosphoethanolamine head group.

De novo biosynthesis of sphingomyelin occurs in the Golgi, and to a minor extent in the plasma membrane. However, synthesis is initiated in the ER with the production of ceramide. Ceramide is then transported to the Golgi by the ceramide transport-molecule (CERT). PC derived phosphorylcholine is transferred onto ceramide by sphingomyelin synthase-1, releasing DAG, and SM [245]. Newly synthesised SM is transported in vesicles to the plasma membrane where it is inserted into the outer leaflet of the bilayer. Small amounts of sphingomyelin can be directly synthesised at the plasma membrane by sphingomyelin synthase-2. SM is essential for membrane stability and as a second-messenger molecule. Together with cholesterol it forms lipid domains within the plasma membrane, making up 70% of the region's molecular composition. Lipid domain formation is driven by the interaction of saturated, long chain FAs and cholesterol. Other constituents besides SM and cholesterol are PE, PS, arachidonic acid, ceramide, lactoceramide, phosphatidylglucoside, and glycerolphospholipids. Lipid domains are dynamic and carry cell-signaling proteins to a high density. These include glycosyl phosphatidylinositol (GPI) anchored proteins, G proteins, mitogen-activated protein kinase (MAPK), protein kinase C, and other kinases [246]. Despite the fact that ATP-Binding Cassette Transporter (ABCA)-1, a cholesterol transporter, is not located to lipid domains, its levels and therefore cholesterol efflux are regulated by the amount of SM present in those rafts. This is because SM is a binding partner of cholesterol and low SM in lipid domains leads to decreased cholesterol binding to SM, and increases ABCA-1- dependent cholesterol efflux [247].

SM is degraded by sphingomyelinases releasing ceramide. Ceramide in turn is a versatile second-messenger regulating various cellular processes, e.g. metabolic pathways including insulin- and glucose regulation. There exists a range of different sphingomyelinases with varying pH optima and metal ions, depending on the cell organelle they reside in. In addition, sphingomyelinases differ in their affinity for cholesterol, contributing to the regulation of cholesterol levels in different membranes [248].

2.2.4 Cholesterol

Cholesterol is a sterol, and important membrane component. It is able to intercalate between phospholipids due to its amphiphilic character. It disrupts electrostatic interactions between phospholipid head groups. The tetracyclic structure of cholesterol further interferes with van der Waals interactions between phospholipid carbon chains and is also able to form hydrogen bonds with membrane lipids. Increasing cholesterol levels limit the mobility of lipid, thereby resulting in a reduction in membrane permeability, inhibiting passive transport [249]. However, cholesterol can also increase membrane fluidity by breaking up lipid-lipid interactions upon intercalation, maintaining membrane fluidity at low temperatures. Both effects are possible because cholesterol broadens the transition state of membrane lipids, e.g. the temperature range, determining when a transition occurs between the gel and fluid phase, becomes larger.

Cholesterol is stored and trafficked in its esterified form since this is less hydrophilic and therefore less reactive. Cholesterol esters are preferably formed with C18, polyunsaturated FAs.

Biosynthesis is localised to the ER and tightly regulated (Figure 13).

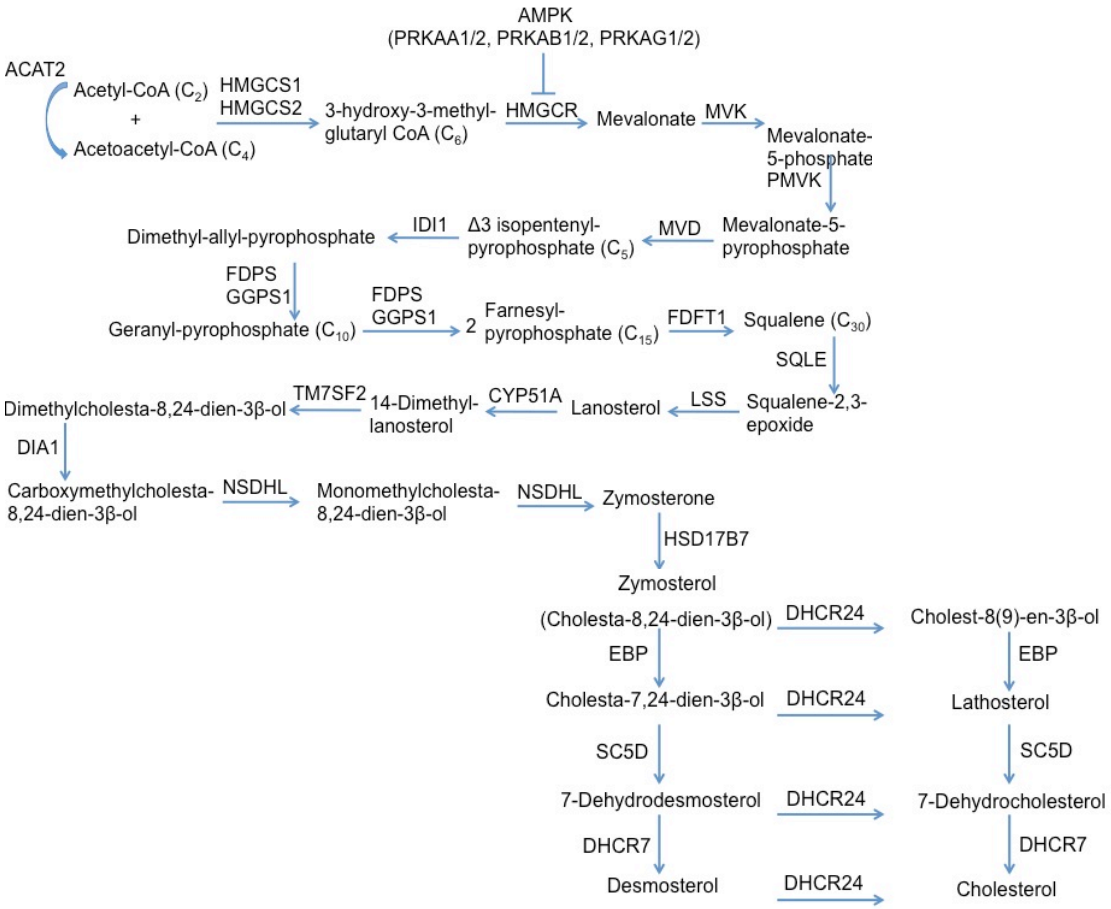

Figure 13: Cholesterol biosynthesis in the ER. AMPK/PRKAA: protein Kinase, AMP-Activated; ACAT: acetyl-CoA acetyltransferase; HMGCS: 3-hydroxy-3-methylglutaryl-CoA synthase; HMGCR: 3-hydroxy-3-methylglutaryl-CoA reductase; MVK: mevalonate kinase; PMVK: phosphomevalonate kinase, MVD mevalonate (diphospho) decarboxylase, IDI: isopentenyl-diphosphate delta isomerase; FDPS: farnesyl diphosphate synthase; GGPS1: geranylgeranyl diphosphate synthase 1; SQLE: squalene epoxidase; CYP: cytochrome P450; TM7SF2: transmembrane 7 superfamily member 2; NSDHL: NAD(P) dependent steroid dehydrogenase-like, DHCR24 24-dehydrocholesterol reductase; EBP: emopamil binding protein (sterol

isomerase); SC5D: sterol-C5-desaturase; DHCR7: 7-dehydrocholesterol reductase

Cholesterol sensing occurs at the ER membrane where SREBP-1a/c and 2, the three isoforms found in mammalian cells, are anchored with the SCAP present [250]. The SREBP-SCAP complex is bound by INSIG-1 and retained in the ER-membrane in a cholesterol-dependent manner. Low cholesterol levels lead to destabilisation of the triple complex and trafficking of the SREBP-SCAP complex in a COPII vesicle-dependent manner to the Golgi (Figure 14).

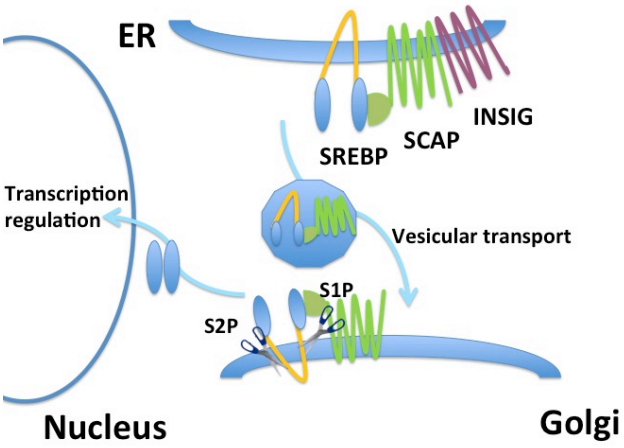

Figure 14: SREBP-mediated regulation of cholesterol synthesis gene expression. The sterol regulatory element-binding protein (SREBP) bound to the cleavage-activating protein (SCAP) is anchored in the ER membrane. Low cholesterol levels destabilise this complex's association with INSIG-1, the protein, which is encoded by the insulin-induced gene 1, and release it. The complex is then transported in COPII vesicles to the Golgi where it inserts into the membrane. There, Site-1 and Site-2 Proteases (S1P, S2P) cleave off the N-terminus of SREBP, which translocates into the nucleus to activate sterol synthesis gene transcription.

At the Golgi, the membrane proteases S1P and S2P cleave off the N-terminus of SREBP, releasing it to enter the nucleus and positively regulate the transcription of sterol synthesis genes. SREBP-1a induces the transcription of cholesterol and fatty acid synthesis, SREBP-1c fatty acid synthesis, and SREBP-2 cholesterol synthesis and uptake. Cholesterol synthesis is further regulated by a feedback mechanism, whereby SREBP regulates its own expression levels. SREBP expression is additionally coupled to the expression of miR-33a/b. This mechanism regulates β-oxidation and lipid export. Furthermore, miR-122 and miR-370 are involved in the cholesterol homeostasis though regulation of fatty acid biosynthesis and β-oxidation. Those factors also regulate each other, resulting in a cascade of miR-370 activating miR-122, which in turn up-regulates SREBP in the event of low cholesterol levels.

Cholesterol homeostasis beyond synthesis control is facilitated through the regulation of cholesterol import and export via ATP-binding cassette transporters and lipoproteins. High intracellular cholesterol levels activate the liver X-receptor (LXR), which regulates cholesterol efflux control [251]. SREBP-2 is further co-transcribed with LXR and miR-33a leading to up-regulation of the cholesterol exporters ABCA1, ABCG1, and endosomal NPC1 [252, 253].

2.2.5 Human lipoproteins

Lipoproteins serve as lipid transporters in the human body and are synthesised as chylomicrons mainly in the intestines from where they are transported as precursors of other lipoproteins to other organs via the blood

stream and the lymphatic system. Cholesterol esters and triglycerides form the hydrophobic core of lipoproteins, apolipoproteins (Apo) on their outside allow transport in a hydrophilic environment, receptor mediated transfer across membranes, and signalling. Lipoproteins are categorised into 4 different subsets. High-, low-, very low density lipoproteins and chylomicrons (Figure 15).

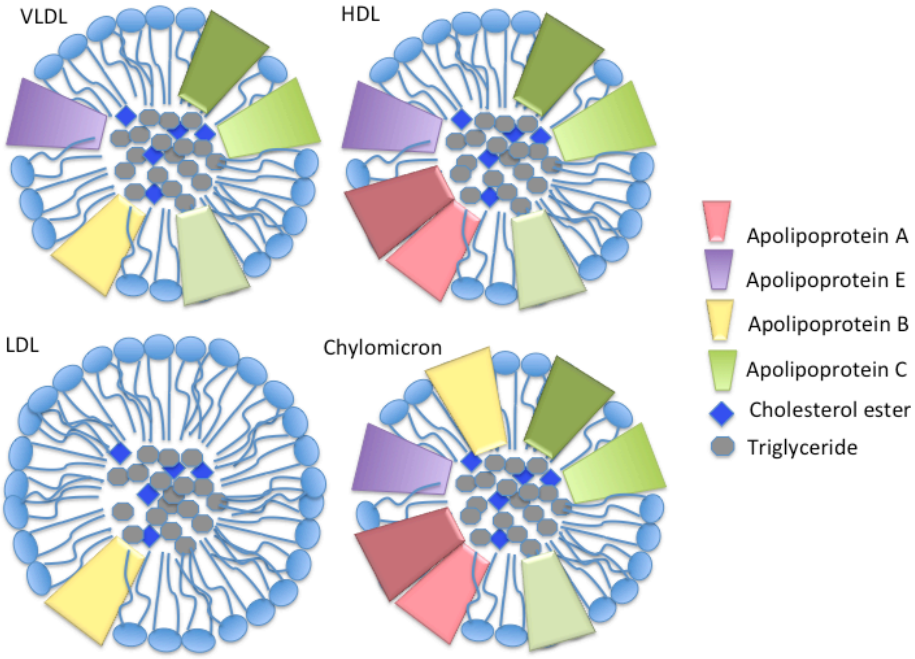

Figure 15: Human lipoproteins are divided into 4 classes. These 4 classes are VLDL, LDL, HDL, and chylomicron. The differences in their protein composition are depicted above. Various members of one apolipoprotein family are represented in different shades of the same colour of this particular protein. It should be noted that human lipoproteins differ in size, which is not represented in this figure.

Chylomicrons serve as transporters for dietary triglycerides and cholesterol around the body. After passing the lymphatic system, ApoC-II, and ApoE are acquired in the blood stream from HDL. In muscle and adipose tissue,

lipoprotein lipase releases free FAs from the triglycerides. In addition, ApoA, and ApoC are transferred onto HDL. Resulting chylomicron remains are recycled or taken up by hepatocytes through an ApoE-LDLR interaction.

VLDL derives from endogenously produced triglycerides from carbohydrate and fat metabolism. ApoC-I, II, II and ApoE are acquired from HDL in the blood stream. VLDL follows the same process of FA unloading as chylomicrons. The resulting VLDL remnants predominantly contain ApoB-100 and ApoE. VLDL remnants are converted into LDL through further loss of triglycerides or taken up by the liver through LDLR. VLDL assembly and association with ApoB-100 is defective in Huh7.5 cells [214, 254].

LDL is the primary, system wide transporter for dietary cholesterol. It contains exactly one ApoB-100 molecule, which interacts with LDLR leading to endocytosis. The lysosomal pH of 5.5 results in denaturation of ApoB-100 and hydrolysation of cholesterol.

HDL transports cholesterol from the periphery to the liver, where it is converted into bile acid. It contains multiple copies of Apo-CI, II, III, ApoA-I and ApoE. HDL also carries multiple enzymes for complement activation, acute phase response, proteinase inhibitors, and lipid metabolism [255].

2.3 Lipid droplets

Lipid droplets are cell organelles that are found in many cell types, predominantly in adipocytes and hepatocytes. They consist of a neutral lipid core of triglycerides and cholesterol esters, surrounded by a phospholipid monolayer, associated with a defined set of proteins. Lipid droplets function as a lipid storage or energy reservoir and are variable in size, ranging between 20 and 100 nm. Biosynthesis is thought to occur between the two ER leaflets where neutral lipid biosynthesis takes place [256]. Upon accumulation of lipids, the droplets are believed to bud from the ER, acquiring the cytosolic ER lipid monolayer. The LD monolayer in mammalian cells consists of mainly PC (60%), followed by PE (24%), PI (8%), lysoPC and sphingomyelin [257] (reviewed in [258]). The phospholipid composition can be altered by *de novo* biosynthesis or conversion of phospholipids as described at the beginning of this chapter. Analysis of LDs in adipocytes has shown that the FA composition of PC and PE significantly changes during the process of LD differentiation. Over time, saturated FAs decrease in abundance and monounsaturated FAs and PUFAs increase. The authors speculate that this change may result in a more fluid phospholipid monolayer in mature LDs compared to newly synthesised LDs [259].

There are two distinct classes of LDs. A static subset of small LDs, whose formation is dependent on DGAT-1 and growth can only occur through fusion of LDs. In contrast, large LDs that carry enzymes for *de novo* lipid biosynthesis and grow by active lipid biosynthesis [260]. Cells grown in the presence of excess lipids rapidly form lipid droplets. Wilfing *et al.* suggested

that LD associated proteins may be loaded onto LDs at the ER or later across an ER-LD bridge.

Furthermore, there is a distinct heterogeneity amongst hepatocytes with regards to lipid storage and number of LDs in the cytosol. Herms *et al.* describe how hepatocytes are divided into either high- or low- lipid cells, but are rarely equalised [261]. They further demonstrate a positive correlation between accumulation of reactive oxygen species (ROS) and cellular lipid content, concluding that this division into high- and low- lipid cells is advantageous for the cell population as a whole, in that it protects the majority of cells from relatively high ROS overall. Employing labelled FAs Herms *et al.* show that high-lipid cells function as FA donors for low-lipid cells, similar to adipose tissue. This kind of heterogeneity is most pronounced in a lipid-deprived environment.

There are many LD associated proteins. The most abundant ones are the PAT-proteins, which count 5 family members: Perilipin, Adipose differentiation-related protein (ADRP), Tail-interacting protein of 47 kDa (TIP47), S3‑12, and OXPAT [262-264]. They all share sequence homology, are present across species and have the ability to enter LDs. TIP47 is thought to stabilise the LD structure in an apolipoprotein-like manner, and is involved in the incorporation of TAG, thereby contributing to the maturation process of LDs [265]. Its expression levels negatively correlate to those of ADRP. Knock-down of TIP47 results in a 2 to 4-fold increase in ADRP expression. ADRP expression reduces TIP47 and adipose triglyceride lipase (ATGL) association with LDs [266]. Apart from the PAT proteins, there are more protein subsets that can be found associated with LDs. They include

proteins involved in phospholipid metabolism, N-glycan biosynthesis, triacylglyceride biosynthesis, lipolysis, ER-organisation, and protein degradation [267]. It is hypothesised that the association of proteins is regulated through hydrophobic interactions. LD surface hydrophobicity in turn is manipulated by protein incorporation. Proteins with strong hydrophobic binding properties will associate with LDs first, regulating the association of proteins with a lower affinity for hydrophobic regions.

LDs are transported along microtubules in a dynein-dependent manner and form tight associations with other cell organelles like the ER and mitochondria [268, 269]. This seems to be regulated by specific, LD-resident proteins. Perilipin-5 for example facilitates the interaction of LDs with mitochondria. This interaction between LDs and mitochondria appears to be crucial for stress-induced β-oxidation of FAs [270]. However, it is not clear what the exact functions of LDs and LD-associated proteins are. LDs might be used to simply deliver proteins, hold them for degradation, keep them on hold in an inactive state for later use, or they might be used as a recovery place of incorrectly or unfolded proteins [271].

LDs also play roles in host-pathogen interactions where they often serve as replication or assembly platforms, for example in HCV, dengue, rotavirus or Chlamydia infection [272-275]. Abnormalities in terms of size or numbers have also been associated with various pathologies, such as atherosclerosis, diabetes, inflammation, and cancer [276]. Accumulation of LDs has been found in response to apoptosis, and cell-cycle arrest. In the absence of extracellular lipids, LDs are formed independent of *de novo* fatty acid synthesis but regulated by phospholipase A_2 [270, 277, 278].

2.4 Host lipid metabolism dependence of the HCV lifecycle

The HCV lifecycle is strongly interlaced with host lipid and cholesterol metabolism. The viral particle, replication, and assembly rely on a distinct lipid environment [279]. Virus isolated from patient sera and separated on a density gradient shows distinct, separate populations. The gradient can be separated into a low-density fraction (<1.06 g/ml), which describes the density range of VLDL and LDL, and a population at higher density (>1.06 g/ml), which comprises HDL. HCV RNA, derived from plasma, can be detected across a range of 1.03 g/ml to 1.2 g/ml on a sucrose gradient. This effect can be attributed to the association of viral particles with host lipoproteins and immune complexes [280, 281]. High-density fractions are less infectious compared to low-density fractions [210]. This may be due to the association of virus with antibodies [282]. Low-density viral particles (also termed lipo-viral particles (LVP)) consist of a minimum of HCV RNA and core protein, and are associated with apolipoproteins ApoB, ApoE, ApoCI, CII, and CIII [283]. In this low-density fraction also present are sub-viral particles. They do not carry a nucleocapsid or RNA, but consist only of envelope proteins associated with ApoB [284]. Non-infectious particles make up a large proportion of the viral particles released from infected cells. Out of 10^{12} viral particles released per day, 1:100 to 1:1.000 are infectious versus non-infectious viral particles *in vivo* [284].

2.4.1 The HCV viral particle

In 1994 Kaito *et al.* purified for the first time HCV particles from patient sera and analysed them by electron microscopy. The particles appeared very heterogeneous in size and density [285]. The RNA containing nucleocapsid is believed to be icosahedral in accordance with other members of the family. It is surrounded by an ER-derived lipid bilayer containing heterodimers of the viral envelope proteins E1 and E2. Recent cryo-electron microscopy studies highlight the strong association of the viral particle with host lipoproteins. They confirm the variation in particle size, ranging between 40-100 nm in diameter. Catanese *et al.* describe the majority of particles to be asymmetrical, and unevenly covered with proteins. Those observations are in agreement with the LVP model (Figure 16). HCV appears to be heavily decorated with ApoE, one copy of ApoB and some ApoA-1 molecules. The extent of antibody accessible ApoE exceeds that of E2 significantly [286]. Several immuno-precipitation experiments with antibodies directed against ApoB, ApoE, ApoA-1, and ApoC have resulted in the isolation of HCV particles [286-288].

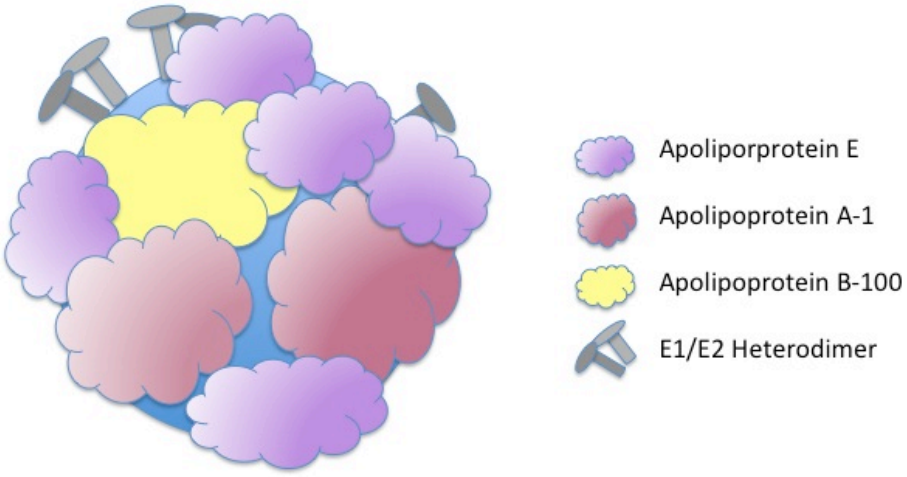

Figure 16: The HCV particle according to the LVP model. The viral particle is associated with lipids and several copies of ApoE, ApoA-1 and one copy of ApoB-100. The number of lipoproteins on the surface exceeds the number of accessible viral glycoproteins.

2.4.2 Viral entry

Viral entry is facilitated using, amongst others, cellular receptors involved in lipid metabolism: LDLR, SR-BI, and NPC1L1 receptor [126]. This is due to the tight association of the viral particle with lipoproteins as described above. Each of these receptors is involved in cellular lipid and cholesterol metabolism. LDLR imports cholesterol-rich LDL into hepatocytes, increasing intracellular cholesterol levels [289]. Soluble LDL directly competes with HCV for binding and uptake, shown in the HCVcc and primary human hepatocyces [118]. LDLR binds ApoE, which is highly prevalent on the viral surface, through electrostatic interactions, hence aiding viral attachment and entry [290]. The receptor further recognises ApoB100, which is presented on VLDL, LDL, and chylomicrons [291]. SR-B1 facilitates the uptake of cholesterol ester rich HDL from the hepatocellular environment through

binding to ApoA1 [292]. It aids attachment and entry but is also utilised post-binding. The latter is not fully understood, yet it is known to be dependent on the lipid transfer activity, but independent of the association of SR-B1 with HDL [293]. NPC1L1 functions as a cholesterol importer on the apical side of hepatocytes [294]. Therefore, it is believed that NPC1L1 does not directly interact with HCV during cell entry, which is thought to take place on the basolateral side. The role of NPC1L1 in HCV entry may lay in regulating cholesterol [126]. Cholesterol-rich micro-domains at the plasma membrane serve to concentrate and organise receptors, such as CD81 and SR-B1. Interaction of these is necessary to facilitate efficient viral entry [295].

2.4.3 Viral replication

Viral replication and assembly depend on the interaction of viral and host proteins with LDs. NS5A and core form a complex with DGAT-1 which facilitates the loading of core and NS5A onto LDs [296]. Rab18 provides access of the replication complex to LDs [297]. Studies with mutant NS4B have shown that the localisation of NS4B to LDs is necessary for infectivity [298]. The authors speculate that this is because NS4B is required for the formation of a micro-environment for replication in close proximity to the ER and LDs. The formation of the membranous web also requires the host factors annexin-2 and phosphatidylinositol 4-kinase (PI4Kα) [89, 299]. The latter is especially important for the replication process where it interacts with NS5A and enriches the web with posphatidylinosityl 4-phosphate. Silencing of PI4Kα alters the web morphology and diminishes the expression of non-structural proteins [89]. The exact mechanism of formation however remains

unknown. It is possible that the membranous web is an extension of the ER and LDs. This would explain the tight association of LDs, ER and the membranous web. The membranous web is known to contain ER membranes and the LD marker TIP47 positively regulates HCV replication through the interaction with NS5A [144, 149].

Another example of the delicate interplay between HCV and cellular lipid homeostasis is the effect of varying expression levels of miR-27a. This micro RNA negatively regulates the expression of the apolipoproteins ApoB100, ApoE, and ApoA1, but also other cellular genes that regulate the lipid metabolism, like SREBP-1/2, peroxisome proliferator-activated receptors (PPARs) and ABCA-1. Overexpression of miR-27a decreases viral infectivity; repression in turn increases viral replication and infectivity. MiR-27a repression leads to an increase in cellular lipid contents; however, in infection miR-27a levels are elevated [300].

2.4.4 Viral assembly and release

Lipoproteins are crucial for viral assembly. HCV uses the VLDL secretion pathway for its own assembly and release [184, 301]. Inhibition of MTP, ApoB, and ApoE, proteins, which are needed for VLDL assembly, leads to a reduced production of infectious particles [184, 301, 302]. The viral envelope proteins E1 and E2 form particles associated and secreted with ApoB only if lipoprotein assembly is supported by the cell line *in vitro* [254].

2.5 HCV pathology

Chronic HCV infection causes a deregulation of host lipid homeostasis. HCV positive patients often present with metabolic diseases like steatosis, diabetes, hypocholesterolemia or hypobetalipoproteinemia [303-307]. One of the defining characteristics of infected hepatocytes is the accumulation of neutral lipids in the form of lipid droplets. This was identified as a distinct pathological feature for non-A, non-B hepatitis in 1982 [308]. Animal studies in chimpanzees and mice, as well as tissue culture experiments have shown the induction of key regulators of regulatory genes within the lipid metabolism by HCV [309-311]. Hepatic steatosis can occur in insulin resistant HCV patients, but also in HCV patients who do not present any other metabolic disorders. Viral steatosis develops due to the interference of HCV with the cellular lipid metabolism (reviewed in [312]). The core protein plays a crucial role by decreasing the LD turnover and leading to an accumulation of LDs in hepatocytes [313]. However, steatosis predominantly develops in genotype 3 infections. There is a direct correlation between the viral load and the advance of hepatic steatosis [303]. Viral clearance can reverse steatosis in genotype 3 infections, in contrast to genotype 1 infections [314].

During infection, cellular glucose levels decrease in response to down-regulated glucose uptake. The expression levels of glucose importers GLUT1, 2, 3, and GLUT4 are significantly lowered *in vitro* [315-317]. *In vivo*, chronic HCV infection has been associated with type 2 diabetes mellitus and insulin resistance. Up to 30% of HCV positive patients are also diabetic [307, 318]. The development of insulin resistance in HCV infected patients is independent from visceral adipose tissue, which implicates that it is virus

induced and different from the classical metabolic syndrome [319, 320]. HCV induced insulin resistance is likely to be caused by a core mediated increased phosphorylation of insulin receptor substrate-1 (IRS-1) [321]. This leads to inhibition of the Akt-signalling pathway causing up-regulation of the down-stream signaling events. This ultimately leads to down-regulation of IRS-1 cell surface expression and thereby increased susceptibility to insulin resistance with GLUT-4 suppression and phosphoenolpyruvate carboxykinase 2 (PCK2) up-regulation [322].

2.6 Liposomes

Liposomes are colloidal particles of a lipid bilayer, surrounding an aqueous core, formed through the self-arrangement of phospholipids in an aqueous solution. Liposomes can be uni-lamellar, consisting of one lipid bilayer, oligo-lamellar or multi-lamellar. The size ranges between 50 to 250 nm in diameter for uni-lamellar liposomes and 1-5 μm in the case of multi-lamellar liposomes. The variation in size is dependent on the method of preparation.

Liposomes were first developed in the 1970s as a drug delivery system and further improved and developed since then. They allow specific targeting of tissue, cell types or subcellular organelles. This is achieved through the incorporation of tissue specific receptors, mode of administration or modulation of the lipid composition of the liposomes. Delivering a drug in liposomes thereby minimises the drug concentration necessary to reach specific concentration at the target site. It also provides a delivery tool for hydrophobic compounds. The composition of the lipid bilayer determines the physical properties of the liposome and consequently its physical and

biological stability in the bloodstream. Liposomes administered intravenously will be quickly targeted by opsonins such as antibodies or complement components and thereby marked for uptake by macrophages, neutrophils, or monocytes [323]. Lipoproteins and liposomes may interact and exchange lipids, which could result in disintegration of the liposomes and premature leakage of the drug into the bloodstream. These obstacles can be overcome by manipulating the lipid composition and the addition of protective groups, e.g. the polymer polyethylene glycol (PEG), which increases the circulation time presumably by inhibiting opsonisation and aggregation [324].

Liposomes have been developed for cancer treatment, chronic infections, and auto-immune diseases, delivering nucleic acids, drugs or peptides (reviewed in [325]). Furthermore, liposomes are used and developed as vaccines, e.g. Epaxal® (Hepatitis A) and Inflexal® (Influenza) are viral vaccines on liposome basis already available. In these cases, viral proteins are displayed and antigens delivered in a safe way, with liposomes mimicking viral particles (reviewed in [326]). Empty liposomes can elicit immune modulatory effects and are therefore also considered for cancer treatment or investigated as treatment for infectious diseases [327, 328], ClinicalTrials.gov identifier: NCT01083979.

Our laboratory has developed ER-targeting polyunsaturated liposomes (PERLs), originally designed as a drug delivery system for antiviral drugs against HCV [229]. The endocytotic uptake of PERLs involves the receptors SR-B1 and LDLR. This has been shown by competition assays and in the case of SR-B1 by knock-out experiments. Following uptake, PERLs follow

retrograde transport through the Golgi and PERL lipids have been shown to fuse with the ER membrane [229]. The lipid formulation of PERLs roughly resembles the lipid composition of the ER, the site of replication of HCV. Early characterisation experiments have shown that PERLs elicit antiviral activity against HCV, HIV, and Hepatitis B Virus. This can partly be explained by their cholesterol-lowering effect, determined by cholesterol measurements of spent cell culture media and intracellular cholesterol levels [230]. However, since statins, cholesterol-lowering drugs, do not exert an antiviral effect to the same extent it is unlikely that this exhausts the mechanism of action of PERLs. With regards to drug development, this work investigates the antiviral effect of fully synthetically optimised (SO)-PERLs in the context of hepatocellular lipid metabolism. Naturally derived lipids used in the original PERL composition were replaced with identical, synthetic counterparts, ensuring reproducibility.

2.7 Materials and methods

2.7.1 Lipids

Lipids were obtained from Avanti® Polar Lipids, Inc., including 1,2-dioleoyl-*sn*-glycero-3-phosphoethanolamine (22:6 PE), 1,2-didocosahexaenoyl-*sn*-glycero-3-phosphocholine (22:6 PC), 1,2-dioleoyl-*sn*-glycero-3-phospho-L-serine (18:1 PS), 1,2-dioleoyl-sn-glycero-3-phospho-(1'-myo-inositol) (18:1 PI) (gift from United Therapeutics Corporation).

2.7.2 Liposome preparation

Liposomes were prepared from lipids in chloroform solution in a 1.5 : 1.5 : 1 :1 molar ratio PE (22:6) : PC (22:6) : PI (18:1) : PS (18:1) (Avanti Polar Lipids). Lipids were transferred into glass vials and chloroform evaporated under nitrogen gas. The resulting lipid film was resuspended in PBS to a final concentration of 5 mM by rigorous shaking for at least 4 h at room temperature. The emulsion was passed 11 times through a mini extruder (Avanti Polar Lipids) with 100 nm pore diameter to create uniform unilamellar liposomes. Liposomes were stored at 4 °C for 24 h and subsequently analysed with dynamic light scattering for size and uniformity before they were used in experiments. The size of SO-PERLs used in the experiments described was determined to range between 62 nm and 64 nm (dynamic light scattering data is shown in supplement, section iii).

2.7.3 Cell culture

Huh7.5 cells were maintained in high glucose Dulbecco's Modified Eagle Media (PAA) supplemented with 10% (v/v) fetal bovine serum, 1% (v/v) penicillin streptomycin (Gibco®), and 1% (v/v) MEM non-essential amino acids (Gibco®) at 37 °C and 5% CO_2 (cells obtained from C.Rice, Rockefeller University, New York). They were passaged about every 3 days: Spent media was removed, cells were washed once with phosphate buffered saline (PBS) (Sigma) and 0.1% trypsin was added to cover all cells and incubated for 3 min at 37 °C. Lifted cells were taken up in twice the amount of media as trypsin used and split 1:4 in fresh media. Mycoplasma tests performed on a regular basis by PCR confirmed that all cells cultured and used for experiments were mycoplasma free.

2.7.4 HCV Jc1 infection

Cells were seeded 24 h before infection to 50-60% confluence at the time of infection as determined by eye using a light microscope. Jc1 virus stock, kept at -80°C, was thawed and added at multiplicity of infection (moi) 0.1 to the culture media. Cells were passaged and infection levels monitored by anti-core immunofluorescence (see 2.6.5) starting 4 days post infection until an infection level of 70% was reached as determined by eye. All experiments involving Jc1 infected cells were carried out at 70 % infection rate.

Jc1 virus stock was originally generated from the pFL-J6/JFH1 plasmid (provided by R. Bartenschlager, Universitäts Klinikum Heidelberg) [209]. In brief, the DNA plasmid was linearised, phenol-chloroform extracted, and transcribed into RNA. RNA was phenol-chloroform extracted under acidic

conditions and electroporated into Huh7.5. Infectious culture media was collected, concentrated with 50 ml 100 kDa filter columns (Ambion) and stored at -80 °C until required.

2.7.5 Anti-core immunofluorescence

Cells to be stained were seeded 16 h before in a 48-well plate. Cells were washed with PBS (Sigma) once and treated with methanol-acetone (1:1) to fix and permeabilise the cells. After 20 min incubation at room temperature (RT) cells were washed 3 times with PBS-Tween® (0.01% (v/v)) and the primary monoclonal anti-core antibody (Pierce, 1 mg/ml) was added 1:300 for 1 h incubation at RT. The primary antibody was washed off with PBS-Tween® and the secondary, AlexaFluor®488 (Invitrogen, 2 mg/ml) was added 1:1 000 for 1 h at 4 °C. The secondary antibody was washed off with PBS-Tween®, the last 2 washes were performed with MilliQ water. Cells were mounted and DAPI stained with VECTASHIELD® containing 4', 6-diamidino-2-phenylindole (DAPI) (Vector Laboratories). The stained and mounted cells were analysed for core signals representing the infection level with a fluorescence microscope (Nicon Eclipse TE2000-V). The infection level was judged by eye, based on the DAPI and anti-core stain ratio.

2.8 Results

2.8.1 Microarray sample preparation

Huh7.5 cells were infected with concentrated Jc1 stock at moi 0.1, incubated and monitored for infection level as determined by anti-core immunofluorescence (see methods section 2.6.5). Cells were seeded to a density of $2x10^6$ cells per T25 flask, and cultured in supplemented DMEM. The next day, at 70% infection level, SO-PERLs were added to a final concentration of 50 μM and incubated for 6 h or 24 h. 50 μM is the concentration that elicits the highest antiviral effect (viral infectivity <10%) with minimal cytotoxic effect (< 5%) [229]. Mock treated controls were cultured in parallel and harvested together with the 6 h and 24 h treated samples. RNA was extracted using the QIAGEN Viral RNA extraction kit, following the manufacturer's protocol for mammalian cells. The efficiency and quality of the RNA extraction were evaluated using the RT^2 RNA QC PCR Array from QIAGEN. cDNA was prepared using the QIAGEN RT^2 First Strand kit and further used as a template in the Qiagen RT^2 Profiler™ PCR Array for lipoprotein signalling and cholesterol metabolism. 1 μg of this cDNA together with the RT^2 qPCR Master Mix were used according to manufacturer's instructions.

Four different conditions were analysed, each in triplicates (see matrix in Table 2).

Naïve, untreated	Naïve, SO-PERL treated
HCV infected, untreated	HCV infected, SO-PERL treated

Table 2: Sample organistation in a matrix of four different conditions. Technical triplicates were included for each condition.

The microarray contained the following genes (the full list containing Unigene, GeneBank, gene names and non-abbreviated protein descriptions as provided by the supplier, is attached in the supplementary section):

LDL receptors and associated proteins

LDL receptors: CXCL16, LDLR, LRP10, LRP12, LRP1B, LRP6, OLR1, STAB1, STAB2, VLDLR, ZMYND15

LDL receptor associated proteins: LRPAP1, PCSK9, SNX17

LDL associated proteins

ANKRA2, APOA4, CDH13, COLEC12, SCARF1, SORL1

HDL associated proteins

APOA1, APOD, APOF, APOL2, APOL5

Cholesterol transport

- Cholesterol transporters: ABCA1, ABCG1, APOA1, APOE, CETP, STARD3
- Cholesterol efflux: ABCA1, ABCG1, APOA1, APOA4, APOE

- Reverse cholesterol transport: ABCA1, APOA1, APOA2, APOA4, APOE, CETP, LCAT
- Other genes involved in cholesterol transport: APOB, LDLR, NPC1L1, OSBPL5

Cholesterol metabolism:

- Cholesterol absorption: CEL, LDLR, NPC1L1
- Cholesterol catabolism: AKR1D1, APOE, CEL, CYP39A1, CYP46A1, CYP7A1, SCARF1, SNX17, TRERF1
- Cholesterol homeostasis: ABCA1, ABCG1, ANGPTL3, APOA1, APOA2, APOA4, APOE, CETP, LCAT, LDLR, LDLRAP1, PCSK9
- Cholesterol biosynthesis: ACAA2, CNBP, CYB5R3, CYP51A1, DHCR24, DHCR7, FDFT1, FDPS, HMGCR, HMGCS1, HMGCS2, IDI1, IDI2, MVD, MVK, NPC1L1, NSDHL, PMVK, PRKAA1, PRKAA2, PRKAG2, TM7SF2
- Other genes involved in cholesterol metabolism: APOB, APOF, APOL1, APOL2, CYP11A1, CYP7B1, CELA3A, CELA3B, HDLBP, IL4, INSIG1, INSIG2, LEP, LIPE, MBTPS1, NR0B2, NR1H4, OSBPL1A, OSBPL5, PPARD, SCAP, SOAT1, SORL1, SREBF1, SREBF2, STARD3, VLDLR

2.8.2 Microarray data analysis

Microarray data analysis was performed following the QIAGEN data analysis instructions. The RNA quality control plate confirmed that there were no impurities affecting the reverse transcription or qPCR, nor was the PCR

system contaminated with exogenous nucleic acids. Small amounts of genomic DNA were detected in 3 out of 12 samples. Those amounts were too small to impede the qPCR reaction as levels were below a threshold set by the manufacturer (Table 3). Therefore, all samples prepared were used in the microarray experiment on an MJ research Opticon2 instrument according to the manufacturer's guidelines.

Reverse Trascription Control (RTC): Are RNA sample impurities affecting reverse transcription?													
$C_t^C - C_t^G$		3.89	3.95	3.99	3.97	3.94	3.36	3.28	4.91	3.30	3.93	2.95	3.78
Cut-off	**5**	NO	NO	NO	NO	NO	NO	NO	NO	NO	NO	NO	NO
Positive PCR Control (PPC): Are RNA sample impurities affecting PCR?													
$C_t^D - C_t^G$		-0.79	-0.50	-0.01	0.10	-0.29	0.09	-0.22	0.43	-0.08	0.04	-0.45	-0.69
Cut-off	**3**	NO	NO	NO	NO	NO	NO	NO	NO	NO	NO	NO	NO
No Reverse Transcription (NRT) control: Is genomic DNA contamination detectable?													
C_t^F		32.28	32.82	35.00	35.00	34.77	35.00	35.00	35.00	35.00	35.00	35.00	35.00
Cut-off	**35**	YES	YES	NO	NO	YES	NO	NO	NO	NO	NO	NO	NO
Genomic DNA Contamination (GDC) control: Will it affect the results?													
C_t^E		35.0	35.0	35.0	35.0	35.0	35.0	35.0	35.0	35.0	35.0	35.0	35.0
Cut-off	**35**	NO	NO	NO	NO	NO	NO	NO	NO	NO	NO	NO	NO
No Template Control (NTC): Is the PCR system clean?													
C_t^H		35	35	35	35	35	35	35	35	35	35	35	35
Cut-off	**34**	YES	YES	YES	YES	YES	YES	YES	YES	YES	YES	YES	YES

Table 3: Quality control test results. Summary of the results of the quality control plate to evaluate the extracted sample RNA. Samples were analysed for RNA impurities, genomic DNA contamination, and endogenous DNA contamination. All RNA samples extracted and purified from cell culture were found suitable for the microarray experiment.

The raw microarray data were copied into the Excel spreadsheet template provided by QIAGEN. Data points were normalised using the levels of 3 housekeeping genes on the array rather than all 5 as preselected: The genes

for actin-β, and GAPDH were differentially regulated in infected compared to non-infected samples and were therefore excluded from the analysis. Expression values of technical replicates were averaged and normalised, and then used for fold-change and Student's t-test calculations. P-values below 0.05 were considered significant.

Expression data were compared and analysed for the following combinations:

A) Naïve versus Jc1 infected, untreated (Figure 17)
B) Jc1 infected, untreated versus Jc1 infected, SO-PERL treated (6 and 24 h time points) (Figures 20, 22)
C) Naïve versus uninfected, SO-PERL treated (6 and 24 h time points) (Figures 25, 26)

For graphical representation, the standard deviation for the difference between two datasets was calculated by the propagation of the error, using the standard deviations of test and control dataset as variables. Control and test datasets, each containing 3 repeats, have been converted into variances (S^2_x), combined and plotted as combined standard deviations.

$$Sx_1\,x_2 = \sqrt{\frac{1}{2}(S^2x_1 + S^2x_2)}$$

Equation 1: S_{x1x2} is the pooled standard deviation from both datasets. S^2_x describes the variance of one dataset.

These data were further analysed with Ingenuity Pathway Analysis® to identify upstream regulators.

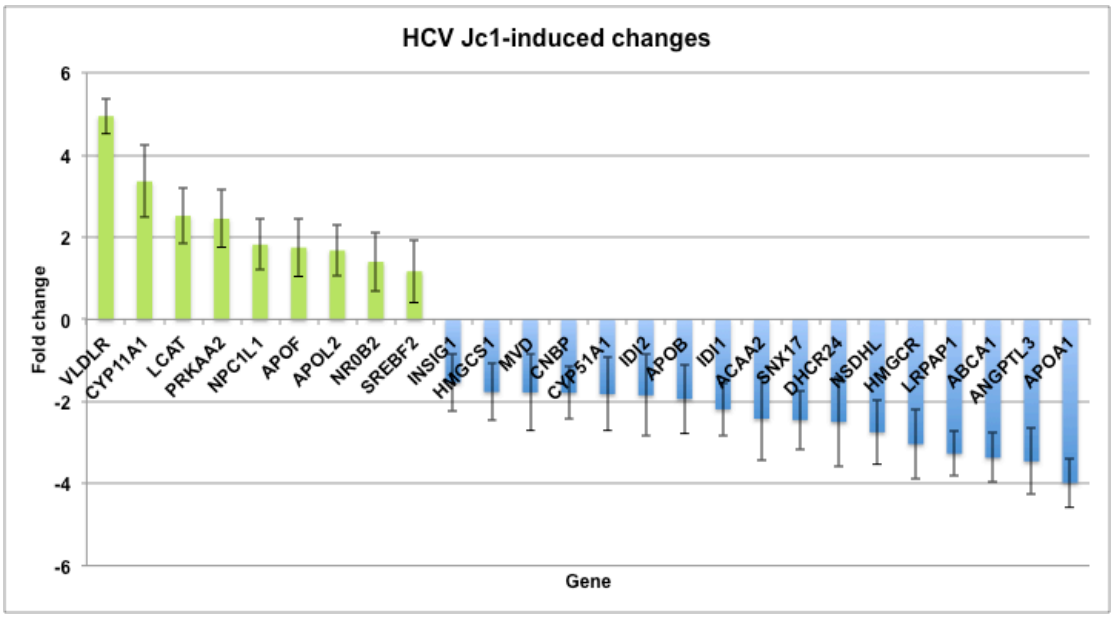

Figure 17: Naïve versus Jc1 infected gene expression data. Genes shown here are differentially regulated in Jc1 infected cells compared to naïve cells. Out of 83 genes analysed, 9 are significantly up-regulated and 17 are significantly down-regulated. Represented are fold changes with p-values <0.05. Error bars are based on standard deviations of both datasets according to equation 1. Exact values are listed below in Table 4.

Gene	Fold change	p-value	Description
VLDLR	4.95	0.0457	Lipoprotein receptor
CYP11A1	3.36	0.0384	Catalyses the conversion of cholesterol to pregnenolone, the first and rate-limiting step in the synthesis of steroid hormones
LCAT	2.52	0.0004	Esterification of cholesterol for cholesterol transport
PRKAA2	2.45	0.0002	Catalytic subunit of the AMP-activated

			protein kinase, which upregulates *de novo* biosynthesis of FA and cholesterol when cellular energy levels are low
NPC1L1	1.82	0.0351	Membrane protein for cholesterol uptake
APOF	1.75	0.0354	Minor apolipoprotein; may be involved in transport and/or esterification of cholesterol
APOL2	1.68	0.0178	May be involved in the cytoplasmic movement of lipids or binding of lipids to organelles
NR0B2	1.40	0.0201	Nuclear receptor for transcription modulation
SREBF2	1.17	0.0368	Controls cholesterol homeostasis by stimulating transcription of sterol-regulated genes
INSIG1	-1.54	0.0270	Insulin induced; regulates cholesterol homeostasis through the liver X receptor (LXR)-, and SREBP-mediated signalling pathways
HMGCS1	-1.77	0.0129	Condenses acetyl-CoA with acetoacetyl-CoA resulting in HMG-CoA; cholesterol biosynthesis
MVD	-1.78	0.0255	Converts mevalonate pyrophosphate into isopentenyl pyrophosphate;

			cholesterol biosynthesis
CNBP	-1.79	0.0202	ssDNA/RNA-binding protein, specifically to the sterol regulatory element leading to sterol-mediated repression
CYP51A1	-1.82	0.0109	Catalyses the de-methylation of lanosterol reaction in cholesterol biosynthesis
IDI2	-1.85	0.0440	Catalyses the conversion of isopentenyl (IPP) to dimethylallyl diphosphate (DMAPP)
APOB	-1.94	0.0030	Main apolipoprotein of chylomicrons and low density lipoproteins
IDI1	-2.19	0.0022	Catalyses the conversion of isopentenyl (IPP) to dimethylallyl diphosphate (DMAPP)
ACAA2	-2.42	0.0171	Catalyses the last step of the mitochondrial fatty acid beta-oxidation
SNX17	-2.45	0.0007	Intracellular sorting protein with phosphoinositide binding domain
DHCR24	-2.50	0.0046	ER-resident reductase in the cholesterol biosynthesis pathway
NSDHL	-2.75	0.0001	ER-localised dehydrogenase involved in cholesterol biosynthesis
HMGCR	-3.04	0.0041	Rate limiting enzyme for cholesterol

			biosynthesis, suppressed by cholesterol
LRPAP1	-3.27	0.0206	Adapter protein for efficient LDL uptake
ABCA1	-3.37	0.0076	Cholesterol exporter
ANGPTL3	-3.46	0.0007	Regulates and inactivates lipoprotein lipase which clears triacylglycerols from the plasma
APOA1	-3.98	0.0184	Cholesterol efflux through: a) acting as LCAT co-factor b) reverse transport of cholesterol from tissue to liver

Table 4: Gene expression data for virus-induced changes. Genes shown here are differentially regulated in Jc1 infected cells compared to naïve cells. These data correspond to the regulation chart in Figure 17.

The main upstream regulators for those genes are cholesterol and its metabolite 25-hydroxycholesterol.

25-hydroxycholesterol elicits a suppressive effect on the expression of cholesterol and FA biosynthesis genes to maintain cholesterol homeostasis. It is also elevated in serum upon TLR-ligand binding and interferon response (reviewed in [329]). The enzyme cholesterol-25-hydroxylase, which converts cholesterol into 25-hydroxycholesterol, has been shown to be broadly antiviral, inhibiting replication and entry processes of various enveloped viruses [330]. It has also been reported to be elevated in liver biopsy samples of HCV positive patient [331].

The microarray data in Table 4 indicate that HCV infection affects a number of steps in the cholesterol biosynthesis pathway, mainly by down-regulation of genes involved.

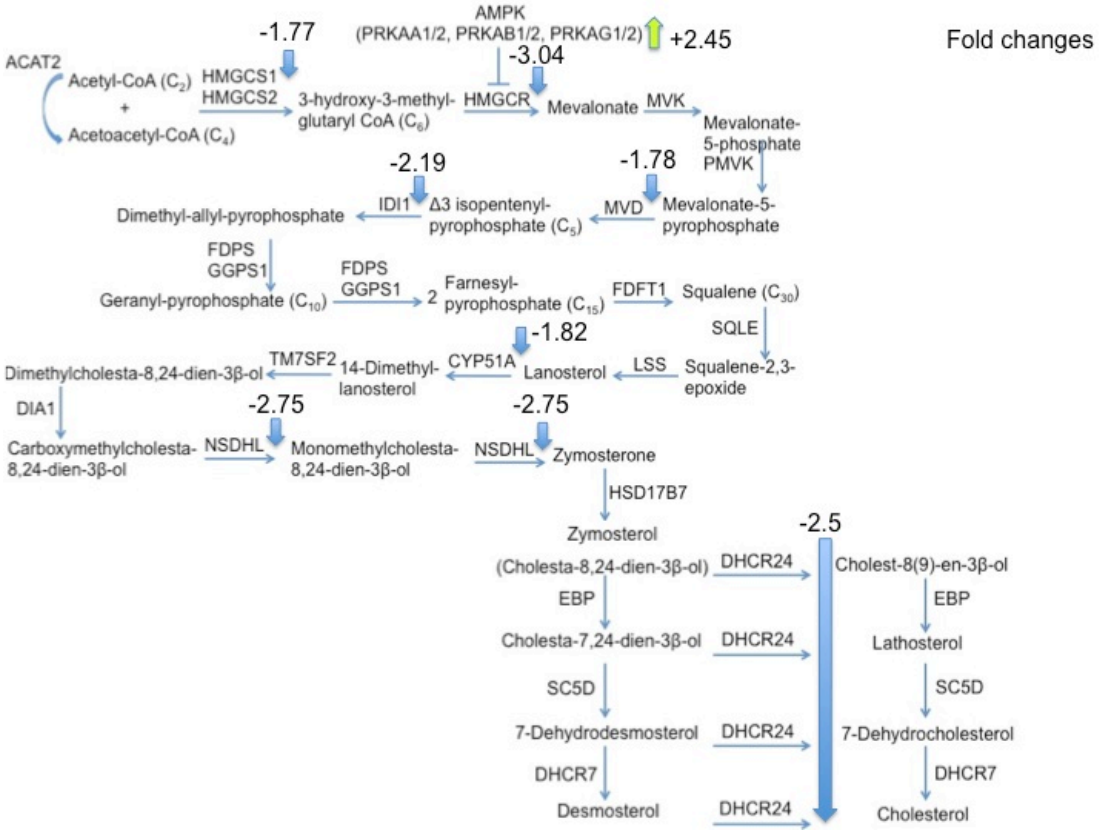

Figure 18: HCV Jc1 induced changes within the cholesterol biosynthesis pathway. HCV down-regulates the biosynthesis pathway of cholesterol at various steps. Numbers indicate fold changes of gene expression levels.

The rate-limiting enzyme HMGCR is 3-fold down-regulated whereas its inhibitor, PRKAA2, is 2.45-fold up-regulated (Figure 18). HMGCS1, MVD, IDI1, NSDHL, and DHCR24 are further down-regulated within this pathway. This is also reflected by the negative regulation of the cholesterol exporter ABCA1, which is over 3-fold down-regulated.

Summarising the changes observed in infected cells, genes involved in intracellular cholesterol biosynthesis are down-regulated, and genes involved in lipoprotein uptake are up-regulated.

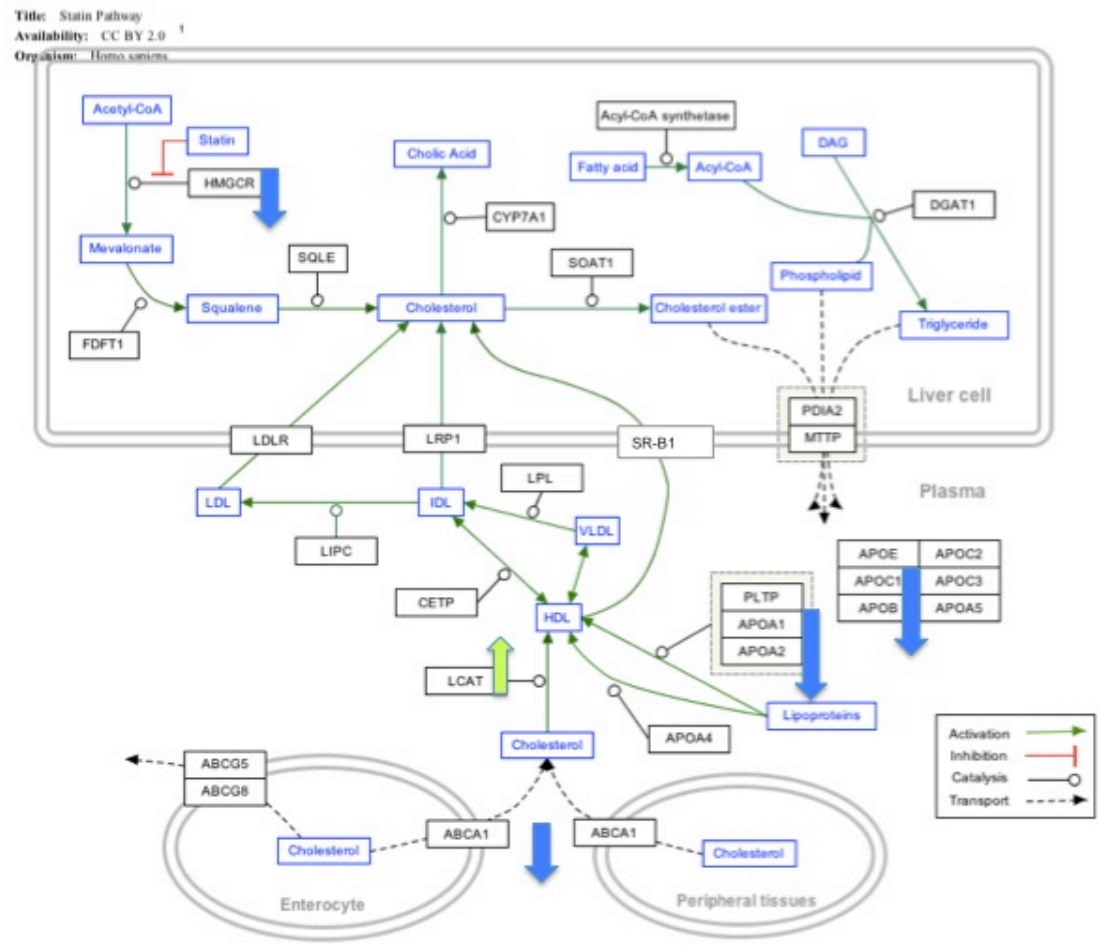

Figure 19: The effect of HCV infection on the statin pathway. This figure illustrates that infection does not only affect cholesterol biosynthesis but extends beyond and also involves apoliproteins and lipid transport (adapted from PharmGKB).

To compare the effect of SO-PERL treatment on HCV Jc1 infected cells, the same analysis was carried out. This represents the deviation of gene expression from the infected state upon SO-PERL treatment. Shown here are the effects of SO-PERLs on lipoprotein signalling and cholesterol metabolism genes after 6 h (Figure 20 and 21, Table 5) and 24 h (Figure 22, Table 6) of treatment.

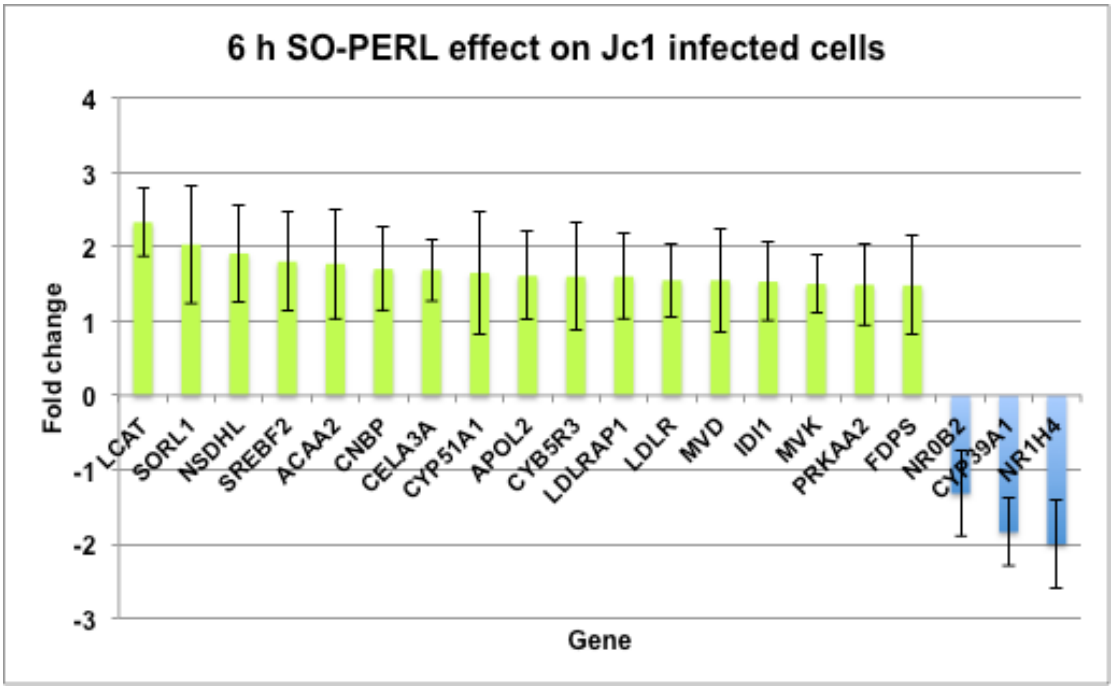

Figure 20: Gene expression data for 6 h SO-PERL treatment versus non-treated, Jc1 infected cells. Genes shown here are differentially regulated in Jc1 infected, and 6 h SO-PERL treated cells compared to Jc1 infected, untreated cells. Out of 83 genes analysed, 17 are significantly up-regulated and 3 are significantly down-regulated. Represented are fold changes with p-values <0.05. Error bars are based on standard deviations of both datasets according to equation 1. Exact values are listed below in Table 5.

Gene	p-value	Fold change	Description
LCAT	0.0029	2.33	Esterification of cholesterol for cholesterol transport
SORL1	0.0069	2.03	Endocytic receptor for LDL, potentially for lipoprotein and protease (β-secretase) uptake
NSDHL	0.0027	1.91	ER-localised dehydrogenase involved in cholesterol biosynthesis
SREBF2	0.00009	1.80	Controls cholesterol homeostasis by stimulating transcription of sterol-regulated genes
ACAA2	0.0108	1.77	Catalyses the last step of the mitochondrial fatty acid beta-oxidation
CNBP	0.0212	1.70	ssDNA/RNA-binding protein, specifically to the sterol regulatory element leading to sterol-mediated repression
CELA3A	0.032	1.69	Serine protease; may be involved in cholesterol transport and metabolism
CYP51A1	0.0123	1.65	Catalyses the de-methylation of lanosterol reaction in cholesterol biosynthesis
APOL2	0.0037	1.61	May be involved in the cytoplasmic

			movement of lipids or binding of lipids to organelles
CYB5R3	0.0395	1.60	Desaturation and elongation of fatty acids
LDLRAP1	0.0281	1.60	Adapter protein for efficient LDL uptake
LDLR	0.0317	1.55	Binds and endocytoses LDL
MVD	0.0107	1.55	Converts mevalonate pyrophosphate into isopentenyl pyrophosphate; cholesterol biosynthesis
IDI1	0.0162	1.53	Cholesterol biosynthesis
MVK	0.0196	1.50	Mevalonate kinase; regulatory site in cholesterol biosynthetic pathway
PRKAA2	0.0223	1.49	Catalytic subunit of the AMP-activated protein kinase, which up-regulates *de novo* biosynthesis of FA and cholesterol when cellular energy levels are low
FDPS	0.0215	1.48	Catalyses the production of geranyl pyrophosphate and farnesyl pyrophosphate, the latter being a key intermediate in cholesterol and sterol biosynthesis
NR0B2	0.0138	-1.32	Nuclear receptor for transcription modulation
CYP39A1	0.0099	-1.84	ER-resident monooxygenase; involved

			in cholesterol to bile acid conversion
NR1H4	0.0022	-2.00	Ligand-activated transcription factor; represses bile acid synthesis and transport through NR0B2 induction

Table 5: Gene expression data for the 6 h timepoint after SO-PERL treatment in HCV infected cells. Genes shown here are differentially regulated in Jc1 infected, 6 h SO-PERL treated cells compared to Jc1 infected, untreated cells. These data correspond to the regulation chart in Figure 20.

The majority of differentially regulated genes in 6 h SO-PERL treated, HCV infected cells are up-regulated. This is in contrast to virus-induced changes in naïve cells. Focusing on the cholesterol biosynthesis pathway, the 6 h SO-PERL treatment appears to up-regulate genes involved in relation to the infected state.

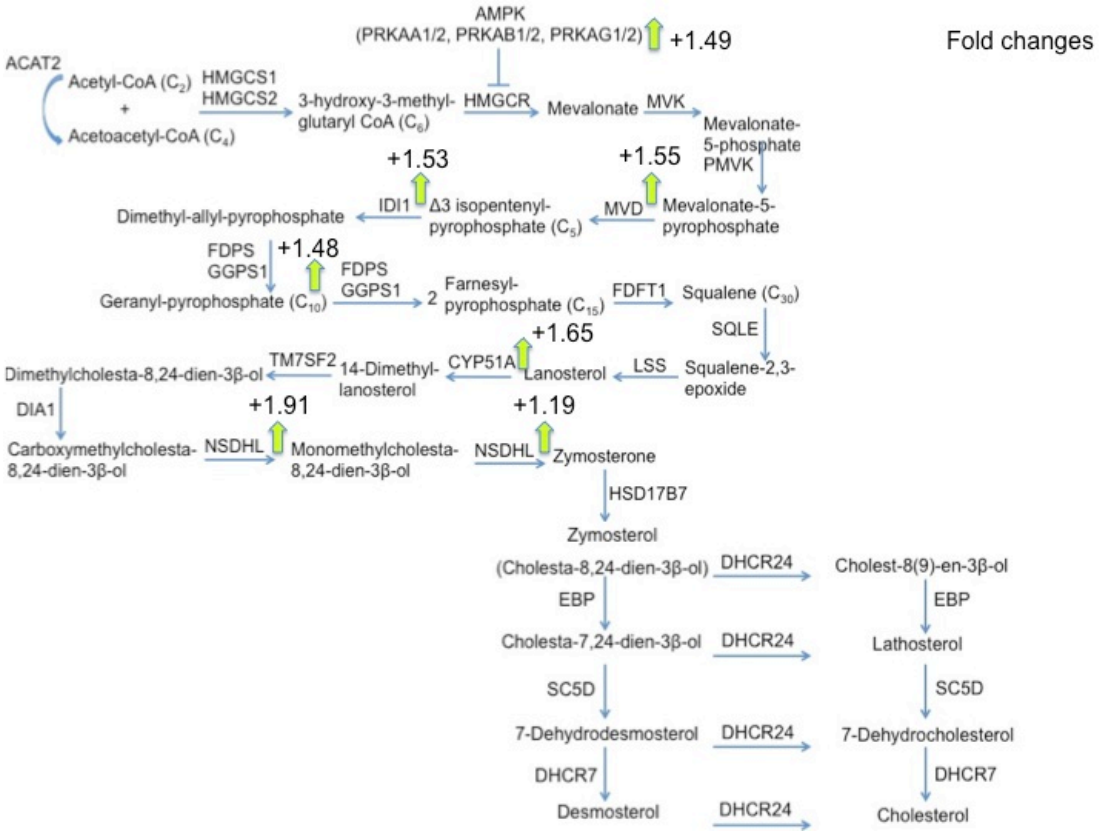

Figure 21: Changes within the cholesterol biosynthesis pathway after 6 h SO-PERL treatment of HCV infected cells, normalised to the infected state. Numbers indicate fold changes in gene expression of the respective enzyme. Arrows indicate whether the regulation is positive or negative.

Genes within the cholesterol biosynthesis pathway that are up-regulated, when normalised to infection, include MVD, IDI1, FDPS, CYP51A, and NSDHL.

After 24 h of SO-PERL treatment, the gene expression pattern is different from the 6 h treatment pattern. The effect after 24 h of SO-PERL treatment on infected cells is shown in Figure 22 and Table 6 below.

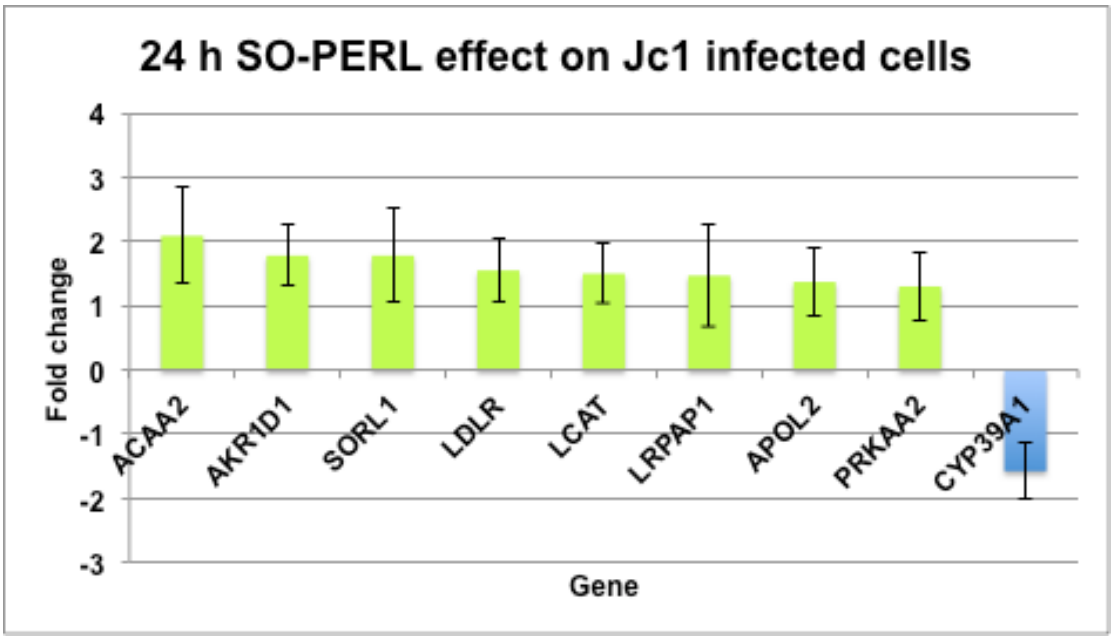

Figure 22: Gene expression data for 24 h SO-PERL treatment versus non-treated, Jc1 infected cells. Genes shown here are differentially regulated in Jc1 infected, and 24 h SO-PERL treated cells compared to Jc1 infected, untreated cells. Out of 83 genes analysed, 8 are significantly up-regulated and 1 is significantly down-regulated, when normalised to infection. Represented are fold changes with p-values <0.05. Error bars are based on standard deviations of both datasets according to equation 1. Exact values are listed below in Table 6.

Gene	p-value	Fold change	Description
ACAA2	0.0099	2.09	Catalyses the last step of the mitochondrial fatty acid beta-oxidation
AKR1D1	0.0037	1.78	Catalyses bile acid intermediates and steroid hormones with a delta(4)-3-one structure
SORL1	0.0037	1.78	Endocytic receptor for LDL, potentially

			for lipoprotein and protease (β-secretase) uptake
LDLR	0.02	1.55	Binds and endocytoses LDL
LCAT	0.0381	1.50	Esterification of cholesterol for cholesterol transport
LRPAP1	0.0499	1.47	Adapter protein for efficient LDL uptake
APOL2	0.0409	1.37	May be involved in the cytoplasmic movement of lipids or binding of lipids to organelles
PRKAA2	0.0138	1.30	Catalytic subunit of the AMP-activated protein kinase, which up-regulates *de novo* biosynthesis of FA and cholesterol when cellular energy levels are low
CYP39A1	0.0313	-1.58	ER-resident monooxygenase; involved in cholesterol to bile acid conversion

Table 6: Gene expression data for the 24 h timepoint after SO-PERL treatment. Genes shown here are differentially regulated in Jc1 infected, 24 h SO-PERL treated cells compared to Jc1 infected, untreated cells. These data correspond to the regulation chart in Figure 22.

There are fewer genes differently expressed after 24 h of treatment compared to 6 h treatment; that is 9 genes after 24 h SO-PERL treatment compared to 20 genes after 6 h of SO-PERL treatment; all normalised to infection. This is highlighted in the comparison below (Table 7).

Gene	Untreated, Infected cells	6 h SO-PERLs on infected cells	24 h SO-PERLs on infected cells
VLDLR	4.95		
CYP11A1	3.36		
LCAT	2.52	2.33	1.50
PRKAA2	2.45	1.49	1.30
NPC1L1	1.82		
APOF	1.75		
APOL2	1.68	1.61	1.37
NR0B2	1.40	-1.32	
SREBF2	1.17	1.80	
INSIG1	-1.54		
HMGCS1	-1.77	1.53	
MVD	-1.78	1.55	
CNBP	-1.79	1.70	
CYP51A1	-1.82	1.65	
IDI2	-1.85		
APOB	-1.94		
IDI1	-2.19		
ACAA2	-2.42	1.77	2.09
SNX17	-2.45		
DHCR24	-2.5		
NSDHL	-2.75	1.91	
HMGCR	-3.04		

LRPAP1	-3.27	1.60	1.47
ABCA1	-3.37		
ANGPTL3	-3.46		
APOA1	-3.98		
CELA3A		1.69	
CYB5R3		1.60	
FDPS		1.48	
LDLR		1.55	1.55
MVK		1.50	
NR1H4		-2.00	
SORL1		2.03	1.78
AKR1D1			1.78
CYP39A1		-1.84	-1.58

Table 7: Gene expression data represented as fold-change for infected, untreated, 6 h SO-PERL treated and 24 h SO-PERL treated Huh 7.5 cells. The table lists and compares significant changes in gene expression as analysed between infected, untreated cells and 6 h and 24 h SO-PERL treated cells. Blanks indicate that there is no significant change in mRNA expression levels detected, normalised to the infected state.

In an attempt to dissect the influence of SO-PERLs on hepatocellular lipid and cholesterol metabolism, naïve cells were treated and analysed.

The results are listed below in Figure 23 and Table 8.

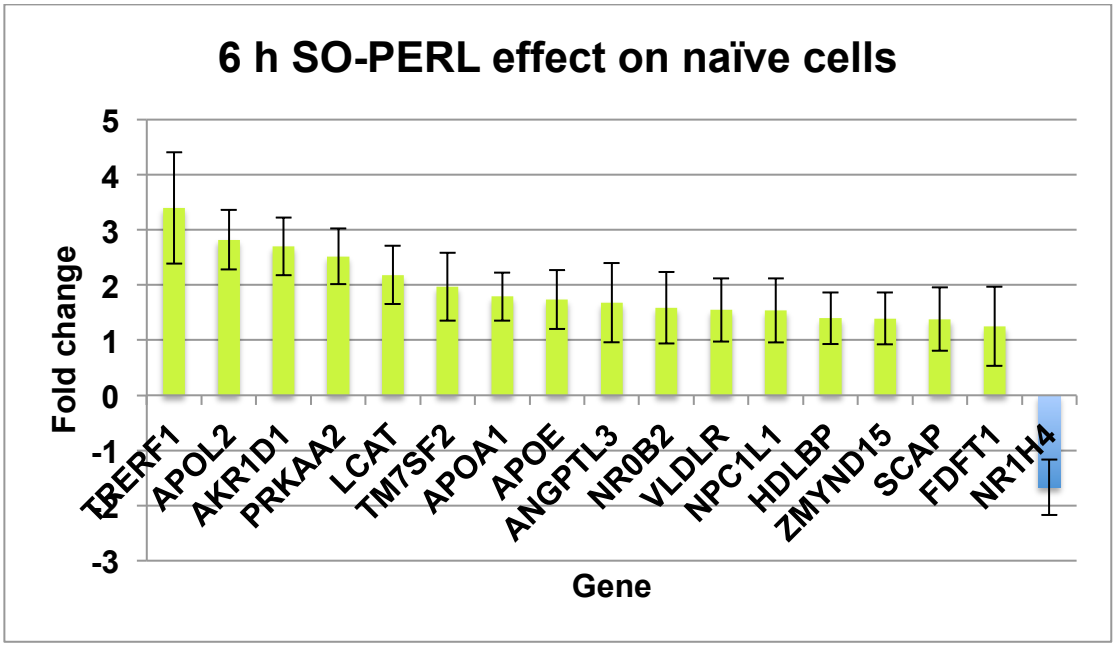

Figure 23: Gene expression data for 6 h SO-PERL treatment versus naïve cells. Genes shown here are differentially regulated in naïve cells compared to naïve, 6 h SO-PERL treated cells. Out of 83 genes analysed, 16 are significantly up-regulated and 1 is significantly down-regulated. Represented are fold changes with p-values <0.05. Error bars are based on standard deviations of both datasets according to equation 1. Exact values are listed below in table 8.

Gene	p-value	Fold change	Description
TRERF1	0.0237	3.40	Activates transcription of CYP11A1 for steroid biosynthesis
APOL2	0.0063	2.82	May be involved in the cytoplasmic movement of lipids or binding of lipids to organelles
AKR1D1	0.0001	2.70	Catalyses bile acid intermediates and steroid hormones with a delta(4)-3-

			one structure
PRKAA2	0.0005	2.52	Catalytic subunit of the AMP-activated protein kinase, which up-regulates *de novo* biosynthesis of FA and cholesterol when cellular energy levels are low
LCAT	0.000004	2.18	Esterification of cholesterol for cholesterol transport
TM7SF2	0.0381	1.97	SREBP-2 regulated, ER-resident sterol reductase
APOA1	0.0227	1.79	Cholesterol efflux through: a) acting as LCAT co-factor b) reverse transport of cholesterol from tissue to liver
APOE	0.0395	1.74	Major VLDL component
ANGPTL3	0.0405	1.68	Regulates and inactivates lipoprotein lipase which clears triacylglycerols from the plasma
NR0B2	0.0225	1.59	Nuclear receptor for transcription modulation
VLDLR	0.0437	1.55	Lipoprotein receptor
NPC1L1	0.0009	1.54	Membrane protein for cholesterol uptake
HDLBP	0.0044	1.4	HDL binding protein
ZMYND15	0.0181	1.39	Transcriptional repressor through interaction with histone deacetylases

SCAP	0.0189	1.38	Sterol-sensing protein; binds SREBP upon low cholesterol
FDFT1	0.041	1.25	Catalyses squalen formation in the mevalonate pathway; first enzyme in cholesterol biosynthesis
NR1H4	0.0249	-1.67	Ligand-activated transcription factor; represses bile acid synthesis and transport through NR0B2 induction

Table 8: Gene expression data for the 6 h timepoint after SO-PERL treatment on naïve cells. Genes shown here are differentially regulated in naïve, 6 h SO-PERL treated cells compared to naïve, untreated cells. These data correspond to the regulation chart in Figure 26.

After 6 h of SO-PERL treatment we observe 16 out of 17 differently regulated genes involved in lipoprotein and cholesterol metabolism up-regulated, as opposed to untreated, infected cells. Cholesterol trafficking and metabolism appear to be influenced to a great extent. Cholesterol biosynthesis however is not directly affected apart from PRKAA, the HMGCR inhibitor, which is 2.5-fold up-regulated.

For comparison, naïve cells were also analysed after 24 h of SO-PERL treatment. The results are shown in Figure 24 and Table 9 below.

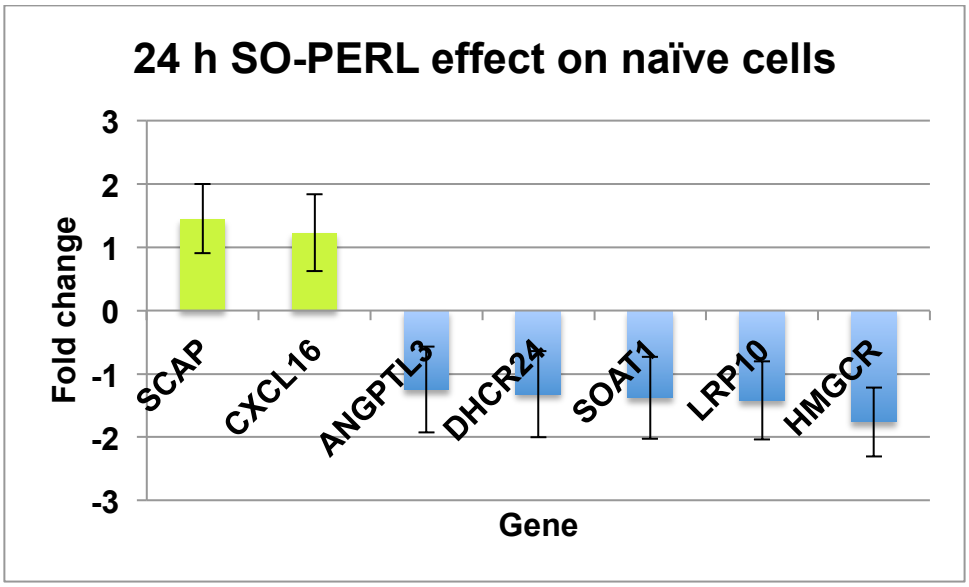

Figure 24: Gene expression data for 24 h SO-PERL treatment versus naïve cells. Genes shown here are differentially regulated in naïve cells compared to naïve, 24 h SO-PERL treated cells. Out of 83 genes analysed, 2 are significantly up-regulated and 5 are significantly down-regulated. Represented are fold changes with p-values <0.05. Error bars are based on standard deviations of both datasets according to equation 1. Exact values are listed below in Table 9.

Gene	p-value	Fold change	Description
SCAP	0.0082	1.45	Sterol-sensing protein; binds SREBP upon low cholesterol levels
CXCL16	0.025	1.23	Scavenger receptor; binds phosphatidyl serine and oxidised LDL
ANGPTL3	0.0404	-1.25	Regulates and inactivates lipoprotein lipase which clears triacylglycerols from the plasma
DHCR24	0.0256	-1.32	Cholesterol biosynthesis

SOAT1	0.0384	-1.38	Or ACAT1; forms cholesterol esters from cholesterol in the ER
LRP10	0.029	-1.42	Involved in uptake of lipophilic proteins, possibly ApoE
HMGCR	0.0158	-1.76	Rate limiting enzyme for cholesterol biosynthesis, suppressed by cholesterol

Table 9: Gene expression data for 24 h treatment of naïve cells with SO-PERLs. Genes shown here are differentially regulated in naïve, 24 h SO-PERL treated cells compared to naïve, untreated cells. These data correspond to the regulation chart in Figure 26.

The main upstream regulators for these genes are the ribosomal protein S6 kinase (RPS6KB1), 25-hydroxycholesterol, miR-4540, and miR-4433.
The 70 kDa kinase RPS6KB1 (S6K1) is regulated by mTOR, which is involved in cell proliferation, cell growth, and protein synthesis. S6K1 drives glycolysis and if suppressed, activates FA oxidation to compensate and provide energy from an alternative source [332]. There is no functional information available for the two miRNAs.

In naïve cell, in comparison to the previous analyses in HCV-infected cells, 24 h SO-PERL treatment seems to affect only a small number of genes. Out of those seven genes, two are up-regulated. If reflected in protein expression, both would lead to an increase in intracellular cholesterol and may be stimulated by low cholesterol levels. At the same time, two cholesterol biosynthesis genes, HMGCR and DHCR24, are down-regulated. ACAT1, which converts cholesterol into its storage form, is also down-regulated.

In order to evaluate the mechanism of the antiviral effect, gene expression profiles in infected cells after 6 h and 24 h SO-PERL treatment compared to infected cells, all normalised to naïve cells, were analysed (Table 7). This comparison highlights the effect of SO-PERL treatment on analysed gene expression and reveals the deviation of the infected, treated status from the naïve state. 7 genes that were differently regulated when comparing non-infected cells with HCV infected cells were changed in their mRNA expression levels after 6 h treatment but returned to their non-treated levels after 24 h. These gene include: VLDLR, CYP11A1, APOF, INSIG-1, INSIG-2, HMGCS-1, and APOB.

Gene	Infected	6 h SO-PERLs on infected cells	24 h SO-PERLs on infected cells
VLDLR	4.95		5.94
CYP11A1	3.36		3.68
LCAT	2.52	3.41	4.30
PRKAA2	2.45	3.31	3.61
NPC1L1	1.82	2.47	2.03
APOF	1.75	2.36	1.71
APOL2	1.68	2.27	2.62
NR0B2	1.40	1.89	2.24
SREBF2	1.17	1.58	
INSIG1	-1.54		-1.73
HMGCS1	-1.77		-1.74
MVD	-1.78	-1.32	-1.38

CNBP	-1.79		
CYP51A1	-1.82		-1.82
IDI2	-1.85		
APOB	-1.94	-1.44	-1.71
ACAA2	-2.09	-1.79	-1.02
IDI1	-2.19	-1.62	-1.80
SNX17	-2.45	-1.81	-1.48
DHCR24	-2.50	-1.85	-1.89
NSDHL	-2.75	-2.03	-1.99
HMGCR	-3.04	-2.25	-2.31
LRPAP1	-3.27		
ABCA1	-3.37	-2.49	-3.09
ANGPTL3	-3.46	-2.56	-3.05
APOA1	-3.98	-2.94	-2.73
ABCG1			1.96
AKR1D1			1.62
APOA4			1.97
CEL			-1.53
CELA3A			1.54
CETP			3.22
COLEC12			3.26
CYP39A1			-1.64
FDFT1			-1.23
HMGCS2			-2.08

INSIG2		2.25	2.01
LDLR		1.62	2.11
LDLRAP1			-1.27
SCAP			1.83
SCARF1			5.57
SOAT1			-1.61

Table 7: Changes of gene expression in infected cells with SO-PERL treatment compared to naïve cells. The table summarises significant changes ($p<0.05$) represented as fold-changes in mRNA expression levels, comparing uninfected cells with infected untreated (column 2), infected 6 h (column 3) and infected 24 h (column 4) SO-PERL cells. This involves 38 genes out of 86 genes analysed.

Changes within the cholesterol biosynthesis pathway, cause by infection, seem dampened after 24 h SO-PERL treatment.

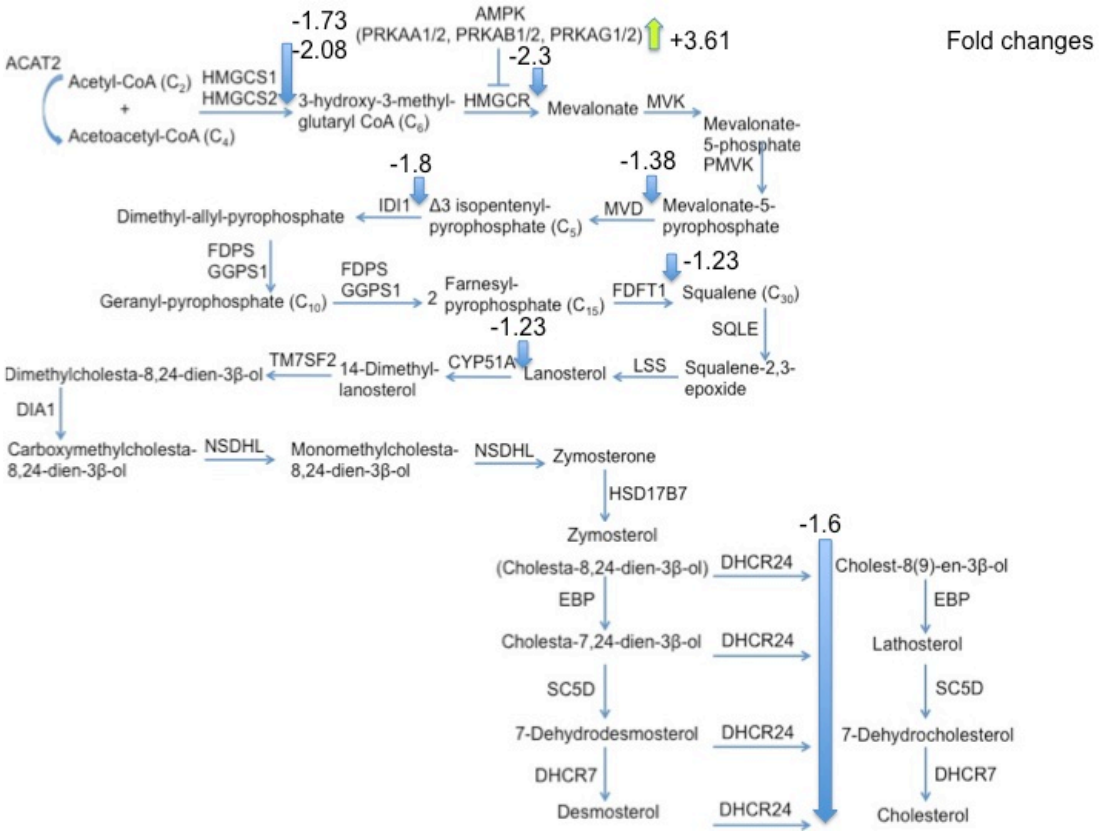

Figure 23: Gene regulation within the cholesterol synthesis pathway comparing naïve cells with 24 h SO-PERL treated infected cells. Numbers indicate fold changes in gene expression of the respective enzyme. Arrows indicate whether the regulation is positive or negative.

From Figure 23 it is evident that the gene expression profile of enzymes, involved in cholesterol biosynthesis, is not normalised after 24 h SO-PERL treatment. The effect of infection however is dampened, although HMGCS2 and CYP51A are only negatively regulated compared to naïve cells after 24 h SO-PERL treatment.

To summarise the gene expression data, Table 12 compares the effect of SO-PERL treatment in naïve and infected cells to infection.

Gene	6 h SO-PERLs on naiive cells	24 h SO-PERLs on naiive cells	6 h SO-PERLs on infected cells	24 h SO-PERLs on infected cells	Influence of infection
VLDLR	1.55			5.94	4.95
CYP11A1				3.68	3.36
LCAT	2.18		3.41	4.30	2.52
PRKAA2	2.52		3.31	3.61	2.45
INSIG2				2.01	2.25
NPC1L1	1.54		2.47	2.03	1.82
APOF			2.36	1.71	1.75
APOL2	2.82		2.27	2.62	1.68
NR0B2	1.59		1.89	2.24	1.40
SREBF2			1.58		1.17
INSIG1				-1.73	-1.54
HMGCS1			-1.31	-1.74	-1.77
MVD			-1.32	-1.38	-1.78
IDI2					-1.85
APOB			-1.44	-1.71	-1.94
IDI1			-1.62	-1.80	-2.19
SNX17			-1.81	-1.48	-2.45
DHCR24		-1.32	-1.85	-1.89	-2.50

NSDHL					-2.75
HMGCR		-1.76	-2.25	-2.31	-3.04
LDLRAP1					-3.27
ABCA1			-2.49	-3.09	-3.37
ANGPTL3	1.68	-1.25	-2.56	-3.05	-3.46
ACAA2			-1.79	-2.09	-2.42
APOA1	1.79		-2.94	-2.73	-3.98
TRERF1	3.4				
AKR1D1	2.7			1.62	
TM7SF2	1.97				
APOE	1.74				
HDLBP	1.4				
ZMYND15	1.39			2.04	
SCAP	1.38	1.45		1.83	
FDFT1	1.25			-1.23	
NR1H4	-1.67				
SORL1			1.90	2.83	
SOAT1		-1.38		-1.61	
SCARF1				5.57	
LRP10		-1.42			
LDLR			1.62	2.11	
HMGCS2				-2.08	
CYP51A1				-1.82	
CYP39A1				-1.64	

CXCL16		1.23			
CETP				3.22	
CELA3A				1.54	
CEL				-1.53	
APOA4				1.97	
ABCG1				1.96	

Table 8: Effect of SO-PERL treatment in infected and naïve cell compared to the effect of infection on gene expression. In this table, gene expression data for treated or untreated cells, as indicated, were compared to naïve cells.

From this table (Table 8), those genes can be identified, whose expression is changed by infection, and that are also influence by SO-PERL treatment (last three columns). From the same table the following genes can be identified as normalised in their mRNA expression levels after a 24 h treatment period.

Gene	Regulation
SREBF2	1.17 → 0
IDI2	-1.85 → 0
NSDHL	-2.75 → 0
LDLRAP1	-3.25 → 0

Table 9: Normalised gene expression after 24 h SO-PERL treatment. SREBF2, transcription regulator for cholesterol biosynthesis, IDI2, transcription regulator with a preference for sterol response elements, and NSDHL, cholesterol biosynthesis enzyme and catabolizing enzyme for long chain FAs, are 3 genes directly involved in cholesterol regulation. LDLRAP1 is involved in efficient LDL uptake and transport across the plasma

membrane. The mRNA levels of all 4 genes are not differently regulated compared to naïve cells after a 24 h treatment period with SO-PERLs.

To illustrate the different effect of SO-PERLs depending on the gene expression in the infection state of the cell, Table 8 is represented in Figure 25.

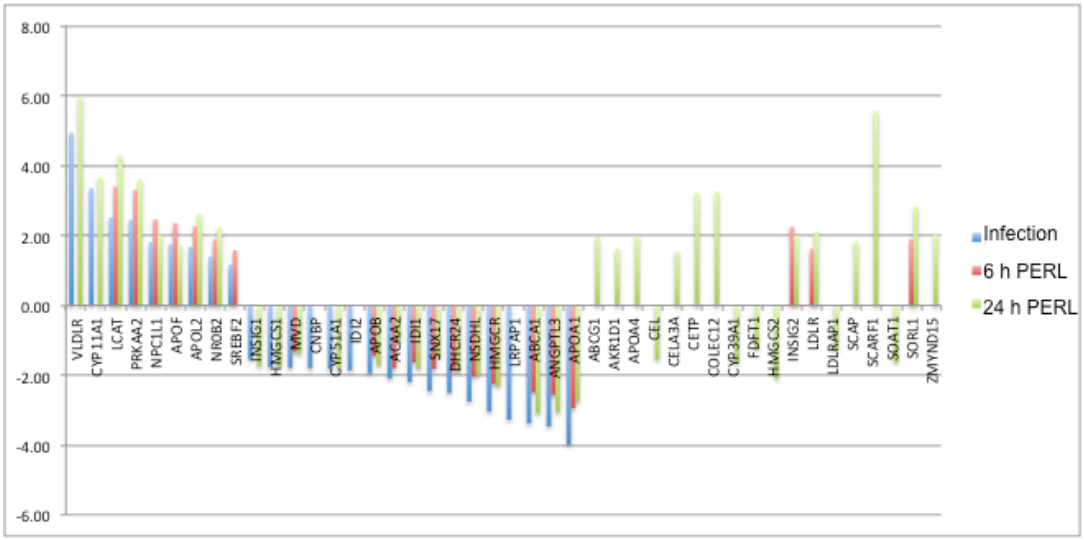

Figure 25: Diagram of the effect of SO-PERL treatment in infected cells compared to the effect of infection on gene expression. This diagram is a graphical representation of table 12. All values are normalised to the naïve state.

Summarising these data, HCV Jc1 down-regulates genes involved in cholesterol biosynthesis. SO-PERL treatment interferes by dampening this down-regulation of genes involved in cholesterol biosynthesis. Treatment normalises NSDHL, SREBF2, LDLRAP1 and IDI2 mRNA levels over 24 h. VLDLR, CYP11A1, INSIG1, and INSIG2 mRNA levels appear normalised after 6 h of treatment but are reversed to infection levels after 24h of SO-

PERL treatment. SO-PERLs thereby interfere with aberrations in cholesterol sensing, trafficking, and synthesis caused by HCV Jc1 infection.

In uninfected cells, SO-PERL treatment triggers a genetic, homeostatic response towards increased uptake of lipids.

2.9 Discussion

To investigate the degree of host cell lipoprotein and cholesterol metabolism manipulation by HCV, microarray experiments were performed, focusing on lipoprotein signalling and cholesterol metabolism. Additionally, the effect of antiviral SO-PERL treatment in the context of those processes was analysed.

Analysis of the microarray results, comparing infected and non-infected cells, indicates that HCV interferes with the cholesterol biosynthesis pathway at numerous levels (Figure 18). It is known that HCV infection causes hypocholesterolemia and that the late cholesterol synthesis pathway is negatively affected as determined by the measurement of synthesis metabolites in patient sera [305, 333]. Furthermore, early microarray studies were done analysing the effect of HCV replicons, the polyprotein or just HCV core in cell culture in an attempt to understand the pathology of HCV infection [334-336]. More recently, Wu et *al.* analysed the expression of genes involved in lipid metabolism from liver tissue of HCV cirrhotic and HCV cirrhotic cancer patients [331]. There is only little overlap with the dataset presented here. However, expression levels or trends of VLDLR, ACAA2, and APOA1 are the same (Supplement iv). The discrepancy is likely to arise due major differences in the experimental design. The main points to consider are that Wu et *al.* are analysing liver tissue from biopsies and do not separate their samples into different HCV genotypes. However, Blackham et *al.* conducted a microarray study in Huh-7 cells infected with JFH-1 [331]. This study's results are more comparable to the microarray study described in this thesis and there is considerable overlap in expression values and trends

(Supplement iv). The here presented study presents a microarray study using the Jc-1 isolate in Huh-7.5 cells, the most common cell culture system for HCV studies besides JFH-1. This work thereby provides valuable information to the HCV community and highlights the importance of noting different sample conditions, which is reflected in the significant variability, and partly contradiction in study results.

The different studies cited above show, to various extents, a suppressed cholesterol biosynthesis in HCV infection. This may seem contradictory to established observations that viral infectivity is dependent on cholesterol and that cholesterol depletion of infected cells results in loss of viral infectivity, which can be reversed by cholesterol supplementation, making cholesterol an essential molecule for HCV [337]. The cholesterol dependency of HCV has lead to investigations into whether statins, cholesterol lowering drugs prescribed to patients with high serum LDL levels, and dietary restrictions may have a synergistic antiviral effect in addition to SOC [338]. Indeed, the administration of Fluvastatin in particular, together with SOC HCV treatment results in a 7.5 % increase in SVR compared to SOC only. At the same time, this statin treatment shows no effect on serum LDL levels [339]. Statins differ in their antiviral treatment effect and the mechanism is not clear [340]. Fluvastatin however, is one of the most potent statins with regards to HCV treatment. Compared to less potent statins it is metabolised by a different cytochrome P450 enzyme and is hydrophilic rather than lipophilic [341]. Nevertheless, all statins are HMGCR inhibitors. In my experiments, HMGCR is 3-fold down-regulated in HCV infected cells. These data also show that expression of the HMGCR negative regulator PRKAA2 is increased by 2.45-

fold, resulting in HMGCR phosphorylation and therefore inhibition (Figure 18). To summarise briefly: HCV down-regulates the biosynthesis of essential cholesterol at 8 out of 21 points within this pathway, including a regulatory enzyme, HMGCR. The regulator of this enzyme, PRKAA2, is up-regulated thereby having an inhibitory effect on HMGCR. Statins, HMGCR antagonists, show antiviral potential in HCV positive patients. This suggests that the direct down-regulation of the cholesterol biosynthesis by HCV may be part of a more extensive manipulation of the host cell metabolism. The Ingenuity® analysis revealed 25-hydroxycholesterol is a main upstream regulator, which has an inhibitory effect on cholesterol biosynthesis. This supports the notion that cholesterol biosynthesis is also actively inhibited from outside the pathway. Indeed, Wu et *al.* found 25-hydroxycholesterol up-regulated in their dataset and concluded that 25-hydroxycholesterol is the regulator behind the down-regulation of the cholesterol synthesis pathway. However, even though this may appear reassuring, it has also to be considered cautiously due to the differences in study design as discussed above.

I have identified and quantified 8 out of 21 steps in the cholesterol synthesis pathway that are inhibited by HCV. However, data presented here show that cholesterol transport is also highly affected by infection. The cholesterol importer and viral entry receptor NPC1L1 is up-regulated, other genes for proteins involved in cholesterol trafficking are also up-regulated, e.g. VLDLR, LCAT, and APOF. I further found that the regulatory genes CYP11A1, NR0B2, and SREBF2, involved in steroid hormone regulation, are up-regulated. This may be a compensatory effect due to the cholesterol

synthesis shutdown by HCV or may be due to increased levels of cholesterol from up-regulated cholesterol import. Though not only is cholesterol itself crucial for viral infectivity but also the down-stream product bile acid is a positive regulator of viral replication [342]. With regards to steroid hormones, Murakami *et al.* demonstrate how different selective estrogen receptor modulators negatively affect different steps in the viral life cycle. The estrogen receptor antagonist Tamoxifen, for example, reduces intracellular levels of viral RNA and to a greater extent extracellular levels of RNA in a dose-dependent manner [343]. This suggests that steroid hormones play a regulatory role in replication and post-replication steps of the viral lifecyle.

In HCV positive patients testosterone levels are lower compared to control subjects [344]. This observation ties in with insulin resistance observed in HCV positive patients. Low testosterone levels are connected to insulin sensitivity, which is linked to a more severe disease progression [345]. On the other hand, female sex hormones, estrogen and progesterone, illicit a suppressive effect on interferon response, making females better responders to interferon therapy. But the fact that viral loads are decreased in pregnant women with elevated progesterone and estradiol levels indicates that the relationship between sex hormones and HCV is more complex (reviewed in [346]). A noteworthy change of 1.4-fold elevated gene expression of NR0B2 was observed in this dataset. This gene is implicated in suppression of estrogen receptor function and bile acid production [347].

The data presented here further show that genes involved in insulin regulation are also affected by infection. ABCA-1, essential for insulin secretion, is 3.37-fold down-regulated [348]. ABCA-1 is regulated by miR-33a, which is coupled to miR-122 and SREBF-2 expression as described in the introductory section [349]. SREBF-2 is up-regulated in our dataset. Because of the co-transcription of SREBF-2 and miR-33a/b, miR-33a/b is expected to be up-regulated causing ABCA-1 down-regulation [350]. This results in suppressed insulin secretion and cholesterol efflux through ApoA1 [351]. My data show a down-regulation of ApoA1 and a decreased expression of ABCA-1 on mRNA level in infection, potentially contributing to decreased insulin secretion.
Furthermore, although SREBF-2 is up-regulated, and binds a target region in the HMGCS1 and LDLR region to facilitate cholesterol biosynthesis, LDLR expression does not seem to be affected and HMGCS1 gene expression is even decreased. HMGCR is significantly down-regulated, suggesting that cholesterol biosynthesis initiation by SREBF-2 is inhibited otherwise, potentially through 25-hydroxycholesterol.

The key regulatory enzyme HMGCR has been reported down-regulated across different studies [331, 352]. As discussed above, HMGCR antagonists are under investigation in terms of anti-HCV treatment, which with respect to this finding seems contradictory. However, it is another indication that the change in cholesterol regulation by HCV is strongly connected to another pathway.

To analyse the effect of SO-PERL treatment on lipoprotein signalling and cholesterol metabolism in infected cells, two time points were chosen: 6 h post-treatment, in order to detect early regulation of transcription, and 24 h post-treatment to detect later or long-lasting changes in gene expression. The latter also covers a full round of viral replication and compares to previously published data on polyunsaturated liposome treatment from our laboratory [230].

As shown in Table 5, comparing gene expression patterns of 6 and 24 h for the infected and non-infected state, they are very different between each other and compared to untreated cells.

6 h post-treatment gene expression levels of cholesterol biosynthesis enzymes are restored or partially up-regulated, and lipoprotein trafficking is up-regulated. This suggests that polyunsaturated liposome treatment specifically interferes with virus-induced changes within the cholesterol synthesis pathway. The interference of SO-PERL treatment with virus-induced aberrations is illustrated in Figure 25.

The effect of SO-PERL treatment on infection can be assessed with the help of Table 7. The expression levels of VLDLR, CYP11A1, INSIG2, and INSIG1 are strongly changed in response to 6 h SO-PERL treatment. The mRNA levels are normalised after this time but bounce back to infected state levels after 24 h. Both proteins, INSIG1 and INSIG2, are mediators of cholesterol biosynthesis regulation by blocking the transport of SREBP to the nucleus hence preventing transcriptional activation of cholesterol biosynthesis genes. CYP11A1 is involved in the conversion of cholesterol to prednisolone, which

is the preceding step of steroid hormone synthesis. VLDLR is the receptor for uptake of VLDL. Together with Figure 21, which illustrates the effect of 6 h SO-PERL treatment specifically on the cholesterol biosynthesis pathway, it can be concluded that the liposome treatment strongly interferes with the cholesterol regulation and synthesis. This is also apparent when looking at gene regulation after 24 h treatment. There, SREBF2, a major transcriptional regulator for cholesterol biosynthesis, is normalised in gene expression to naïve state levels. Further, IDI2 and NSDHL, both involved in cholesterol biosynthesis, are also normalised. These observations reflect early, published observations of negative changes in released cholesterol upon PERL treatment [230].

Furthermore, the gene ANGPTL3 is 3.46-fold down-regulated in infected cells, however, mRNA levels increase 1-fold after 6 h SO-PERL treatment before going to 3.05-fold down-regulation again (compared to naïve cells). Since suppression of ANGPTL3 expression has been shown to be critical for HCV infectivity, it would be interesting to investigate how the expression levels progress over a longer treatment period. ANGPTL3 hydrolyses LVP lipids and thereby destabilises the viral particle and renders it less infectious. In the same publication, Foak et *al.* report ANGPTL3 3-fold down-regulated in HCVcc, which provides a validation for the work presented here [353].

In line with the observed trend of ANGPTL3 expression, numerous genes appear changed in regulation after 6 h treatment but trending towards untreated, infected levels again after 24 h. It is possible that after 24 h the effective, antiviral concentration of SO-PERLs is no longer ensured and the previously determined half-life of PERLs of 27 h is slightly less [354]. This

can be assessed by reapplication of liposomes. However, it may also be possible that the 4 genes that were found normalised are the key players, which are targeted by SO-PERL treatment. Possibly, these regulations cannot be bypassed or compensated for as opposed to others, contributing to the antiviral effect of these liposomes.

The host-pathogen interaction on the level of metabolic pathways appears very finely tuned. Host survival is crucial for the replication and proliferation of viruses or other intracellular pathogens. There is a fine balance to be struck between hijacking host pathways for pathogen advantage and survival of the host. Therefore, it may not be necessary to induce a very strong deregulation in gene or protein expression in order to interfere with pathogen induced aberrations. To achieve a meaningful therapeutic effect, several small interferences may be just as effective, if not even better than one or a few very strong inhibitions.

Comparing the expression profile of infected, SO-PERL treated cells after 6 h treatment period with 24 h treatment period, there is a considerable overlap possibly due to the fact that there are 18 more genes induced after 24 h treatment compared to 6 h treatment. Noteworthy, however, SREBF2 is the only gene whose mRNA level is elevated in infection and after 6 h treatment but are normalised after 24 h treatment. The other 3 genes, whose gene expression levels are normalised after 24 h treatment, are already normalised at the 6 h time point. Numerous genes are induced after 24 h SO-PERL treatment but are not differentially regulated after 6 h or in infected, untreated control cells.

In order to investigate the effect of SO-PERLs on the cellular lipoprotein and cholesterol metabolism further, the same experiment was conducted with naïve cells as opposed to Jc1 HCV infected cells.

6 h SO-PERL incubation in uninfected cells does not result in significant cholesterol biosynthesis pathway alterations. Considering the results in infected cells, this implies that there are three possible SO-PERL treatment effects: i) it affects the regulation of the synthesis pathway rather than the pathway itself, thereby interfering with virus-induced changes and resulting in pathway normalisation, ii) SO-PERLs target the cholesterol synthesis pathway due to its virus-induced de-regulation or iii) the mechanism of action is fundamentally different between naïve and infected cells.

After the 24 h treatment period in naïve cells, genes for cholesterol and lipoprotein mobilisation are positively regulated. This regulation increases cellular cholesterol levels, and conversion into bile acid and steroid hormones. These genes comprise APOL2, LCAT, APOA1, APOE, ANGPTL3, VLDLR, NPC1L, and HDLBP.

APOL2 is up-regulated in both, naïve and infected SO-PERL treated cells. It is thought to be involved in cellular lipid transport possibly induced by lipids from SO-PERLs, which are freed after uptake. ApoL2 may be involved in cellular distribution of such explaining its up-regulation after 24 h, independent of the infection state. At the same time, sterol sensing SCAP and PRKAA2 are increased in their expression.

Comparing the effect of treatment in uninfected cells with infected cells further, it is to note that after 6 h the following genes are differently regulated in uninfected, treated but not infected, treated cells: TRERF1, AKR1D1,

TM7SF2, APOE, HDLBP, ZMYND15, FDFT1, and NR1H4. After 24 h, the same comparison reveals LRP10 and CXCL16 as changed on mRNA level in uninfected, but not infected samples. These differences imply that there is a shift towards bile acid and steroid hormone synthesis upon SO-PERL treatment in uninfected cells, which is not apparent in infected cells, as mentioned above. Also, APOE itself and ApoE uptake are down-regulated only in uninfected cells but not in infected cells when analysing the 6 h treatment time point. The first effect may be explained by the fact that cholesterol is an important molecule in the HCV lifecycle. Because the biosynthesis is down-regulated, bile acid and steroid hormone biosynthesis, which are based on cholesterol, are suppressed to make cholesterol available for other purposes. The second effect, the lack APOE and ApoE uptake suppression, as indicated by LRP10 down-regulation only in uninfected cells, can most likely be contributed to the important role of ApoE as a component of the LVP. These two examples, of differences in the effect of SO-PERLs on gene expression between infected and uninfected samples, could be an example for treatment-induced effects that can be bypassed by the virus as opposed to others. However, SO-PERL treatment does affect cholesterol biosynthesis in uninfected, as well as infected samples.

Concluding this analysis, HCV suppresses the expression of key regulators throughout the cholesterol biosynthesis pathway. This effect was identified and quantified in Huh7.5 cells using microarray analysis. SO-PERL treatment abrogates virus-induced changes possibly through driving the expression of bile acid and steroid hormone production, down-stream of cholesterol

biosynthesis thereby potentially driving cholesterol biosynthesis in infected cells. This is supported by the lack or minimal differential expression of cholesterol synthesis pathway genes in uninfected cells and an increase in bile acid and steroid hormone metabolism genes. From these data it can be hypothesised that the positive regulatory shift in expression profiles towards cholesterol- and down-stream metabolism is part of the antiviral effect of SO-PERLs in human hepatocytes in the context of Jc1 HCV infection. To further support this hypothesis silencing RNA (siRNA) experiments of key proteins could be performed. However, this would provide a novel and interesting treatment approach. The liposome formulation tested does not specifically target a single factor like most antiviral drugs, e.g. small-molecules. In contrast, SO-PERLs influence the expression of numerous factors.

A comparison of 0 h time point with uninfected, untreated 6 and 24 h later would indicate if changes occur “naturally” over time, meaning 6 and 24 h, in culture that are currently hidden by the identified changes. It would allow a subtraction of background expression. Other data obtained in our laboratory suggests that there may only be a minimal change in expression levels within 24 h of genes that were analysed on the microarray. Furthermore, it was ensured that cells used in this study were not over-confluent and had not entered a stationary phase, which is indicated by active lipogenesis.

In addition to these conclusions, it should be noted that the experiments were performed once in technical triplicates. Ideally, the experiments need to be repeated to increase confidence and minimise errors. This was not possible due to time constraints. Key regulators could be followed up by Western blot analysis to see if mRNA levels correspond to protein levels. Knock-out

experiments with siRNA would provide further insights into the relevance of the target protein.

3. Analysis of lipid droplets

3.1 Objective

To analyse the antiviral effect of SO-PERL treatment and complement the microarray data, lipid droplets were analysed using confocal microscopy, Western blot and mass spectrometry.

Lipid droplets were isolated and subjected to mass spectrometric analysis. The analysis comprises phospholipids, sphingolipids, and cholesterol esters and identifies different lipid species based on saturation levels and carbon chain length. In addition, confocal microscopy focusing on the association of HCV core and NS5A was carried out. These results were further assessed by Western blot. All analyses were done using the same sample matrix as introduced for the microarray analysis (Chapter 2) and samples for mass spectrometry were prepared in parallel to microarray samples to make results comparable.

3.2 Materials and methods

3.2.1 HCV JFH-1 electroporation

Infection of Huh 7.5 cells with the JFH-1 isolate was performed according to Kato et *al.* Nature Protocols [355].

3.2.2 Lipid droplet isolation

Huh7.5 cells were grown to 90% confluence in 4 x 225 cm^2 flasks (Greiner) per sample preparation. For harvest, cells were washed with PBS, lifted with trypsin and pelleted for 5 min at 1,200 rpm. Cell pellets were washed twice with ice-cold PBS and resuspended to make up a 20% cell solution in hypotonic HLM buffer (20 mM Tris-Cl, 1mM EDTA, 1 x protease inhibitor cocktail (Roche) at pH 7.4). Cell membranes were disrupted with 30 strokes in a tightly fitted hand-held glass homogeniser on ice. The homogenate was centrifuged for 10 min at 10,000 rpm in order to remove cell debris. The supernatant was collected and adjusted to 20% (w/w) sucrose in HLM by adding ⅓ volume of 60% (w/w) sucrose in HLM. The solution was transferred into 8 ml ultracentrifuge tubes (Beckmann) and topped with 2.5 ml 5% (w/w) sucrose in HLM and 2 to 3 ml HLM to fill up the tubes. Samples were centrifuged at 30,000 rpm for 45 min at 4 °C in a Beckmann ultracentrifuge using a SW Ti 41 rotor. The floating white lipid layer was taken off with 200 µl gel loading tips and the gradient centrifugation was repeated.

3.2.3 Confocal microscopy

Cells were seeded in Lab-Trek®-II chamber slides (Nunc) 16 h before sample preparation. In case of SO-PERL treatment, cells were treated for 24 h before they were washed with PBS and fixed with 4 % paraformaldehyde for 20 min at RT. Cells were washed with PBS and permeabilised with 0.1% Triton-X/PBS or 0.1% digitonin/PBS in case of LipidTOX™ staining. Primary antibodies were incubated for 90 min at 4 °C and washed off with PBS-Tween®. Secondary AlexaFluor® (Invitrogen) antibodies were incubated for 1 h at 4 °C and washed off with PBS-Tween® and rinsed twice with PBS. LipidTOX™ was added 1:750 in PBS for 30 min at RT. The LipidTOX™ solution was aspirated and cells were mounted with VECTASHIELD®DAPI or ProLong® Gold antifade without DAPI (Invitrogen).

Samples were imaged on Olympus FV1000 laser scanning microscope with Becker and Hickel FLIM system, using a 100x/1.40 Oil UPlanSApo objective and recorded as Z-stacks of approximately 20 slices of ~0.3 µm thickness.

Image processing was done in Fiji using the Coloc2 plugin for colocalisation analysis.

3.2.4 Western blot

Samples were prepared for SDS-PAGE with 10-20 µl sample, NuPAGE® sample buffer (Invitrogen), NuPAGE® reducing agent (Invitrogen), and 1.2% (v/v) sodium dodecyl sulfate (SDS). Equal protein loading was ensured by protein quantification using a NanoDrop 1000 and subsequent protein adjustment of all samples. They were incubated for 5 min at 70 °C and immediately transferred to 4 °C. Chilled samples were loaded on 4-12%

NuPAGE® Novex® Bis-Tris gels (Invitrogen) and run in NuPAGE® MES SDS running buffer at 200 V for 35 min. Gels were rinsed with MilliQ water and transferred on to a with methanol pre-soaked Amersham Hybond-P PVDF membrane (GE Healthcare Life Sciences), run on a wet blotting system XCell II™ (Invitrogen) using NuPAGE® transfer buffer with 20% methanol at 25 V for 2:20 h.

After the transfer, membranes were transferred into I-Block™ blotting buffer (Invitrogen) for 1 h at 4 °C. Primary antibodies were incubated for 1.5 h at 4 °C, followed by 3 x 10 min washes with PBS-Tween®. Horseradish peroxidase-conjugated secondary antibodies were incubated for 1 h at 4 °C, followed by 3 x 20 min washes with PBS-Tween® and rinsed with PBS. The ECL Prime western blotting detection reagent (GE Healtcare Life Sciences) was used on a Fuji LAS 1000 imaging machine.

3.2.5 Lipid droplet analysis

Isolated lipid droplets were sent to APlipid (Paris, France) for mass spectrometric analysis. APlipid analysed the lipid droplet preparations by extracting the lipids according to a modified method based on Bligh and Dyer [356]. Of the resulting chloroform extract, ¼ was used for gas chromatography mass spectrometry (GCMS) and ¾ for high-performance liquid chromatography-MS/MS (HPLC-MS2). Total fatty acid composition was obtained by chemical conversion of lipids into methyl esters and analysis by GCMS. Triacylglycerol species, phospholipids, ceramides, and cholesterol esters were determined by tandem-MS and quantified based on synthetic internal standards.

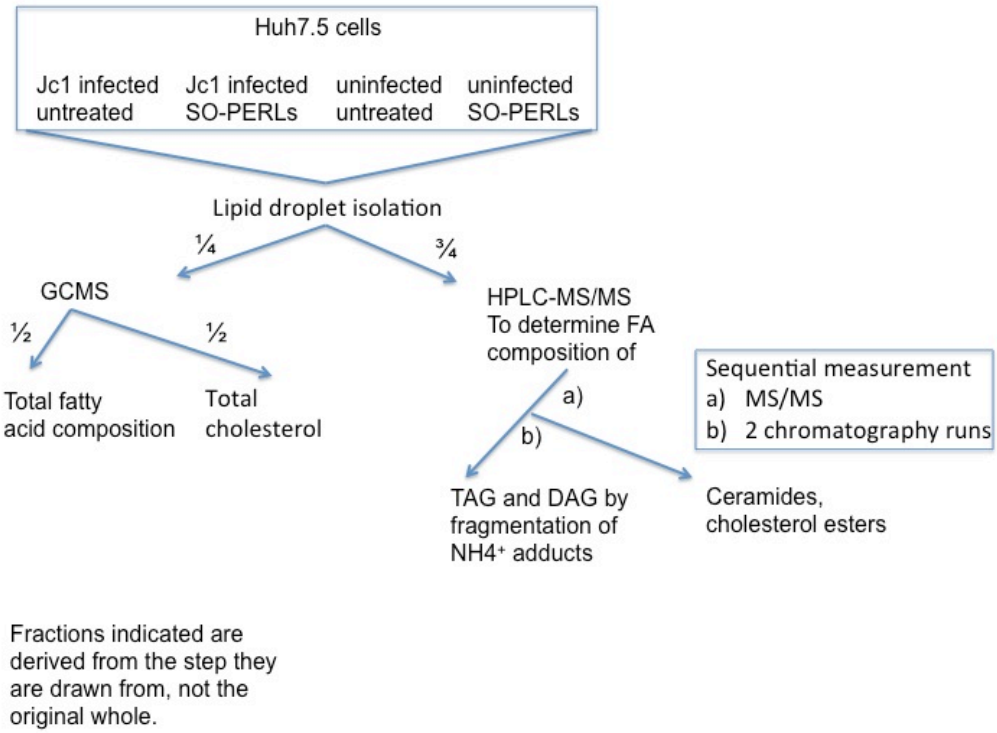

Figure 26: Lipidomics workflow. The flowchart above describes the workflow for the analysis of LD preparations by mass spectrometry. The initial LD preparation is divided into a fraction for total FA determination, including TAG and DAG, and total cholesterol. For detailed FA composition analysis, the remaining sample fraction is treated with ammonium to results in ammonium adducts, TAG-$NH4^+$, DAG-$NH4^+$, and MAG-$NH4^+$, which are fragmented in the collision chamber. Various ceramide species and cholesterol esters are measured independent from TAG and DAG by re-injecting a fraction of the sample.

3.3 Results

HCV Jc1 infected Huh7.5 cells, SO-PERL treated and untreated, were stained for lipid droplets, and the HCV proteins core and NS5A. Confocal microscopy analysis revealed colocalisation of both viral proteins with lipid droplets in infected, untreated cells (Figure 27). Upon 24 h SO-PERL treatment core association with lipid droplet was less defined and the core staining seemed more disperse compared to infected, untreated controls. NS5A localisation did not change with treatment and was therefore not followed up.

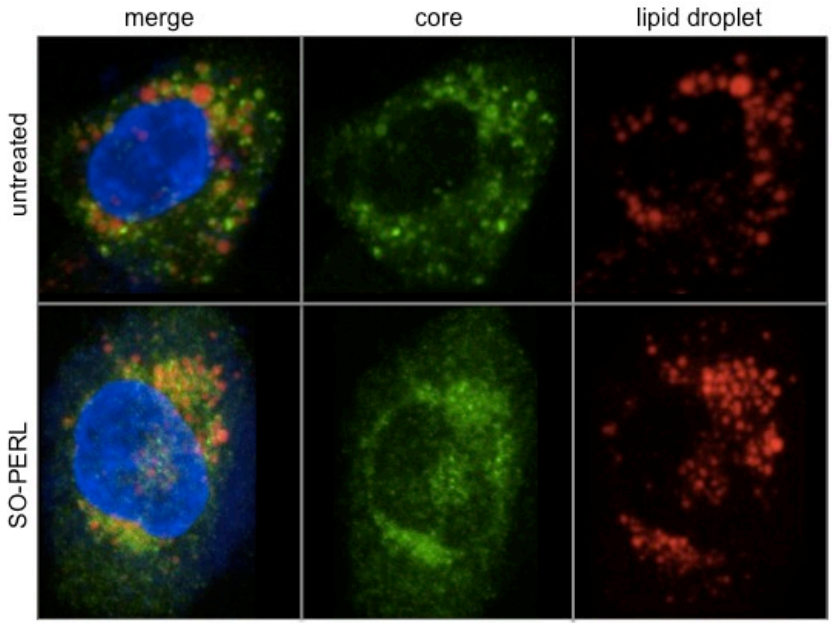

Figure 27: HCV Jc1 core association with lipid droplets. Cells were fixed with PFA, permeabilised with digitonin, and stained for HCV core with monoclonal anti-core antibody (Pierce) and Alexa®Fluor488 secondary antibody. Lipid droplets were visualised using the neutral lipid stain LipidTOX™. Cells were mounted and nuclei stained with VECTASHIELD®DAPI. Images were taken with an Olympus FV1000 laser scanning confocal microscope with a 100x oil lens, and processed using Fiji software.

The same experiment was conducted using the JFH-1 strain, with a similar result (Figure 28).

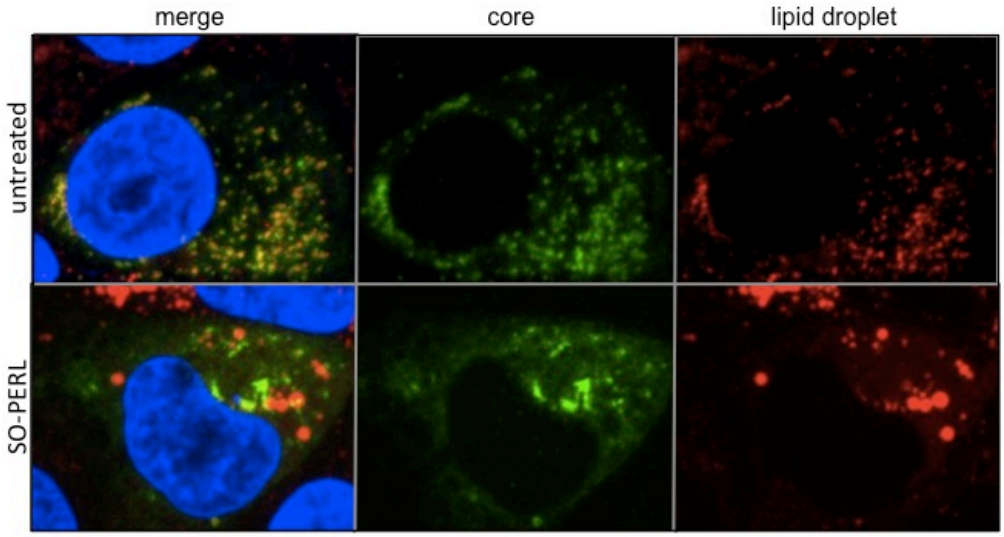

Figure 28: HCV JFH-1 core association with lipid droplets. Cells were fixed with PFA, permeabilised with digitonin and stained for HCV core with monoclonal anti-core antibody (Pierce) and Alexa®Fluor488 secondary antibody. Lipid droplets were visualised using the neutral lipid stain LipidTOX™. Cells were mounted and nuclei stained with VECTASHIELD®DAPI. Images were taken with an Olympus FV1000 laser scanning confocal microscope with a 100x oil lens, and processed using Fiji software.

Colocalisation of core protein and lipid droplets in infected cells with both HCV strains was quantified and determined using the Pearson's coefficient, measuring covariability of 2 signals. The background levels were minimal, as measured with Fiji, and regions of interest were selected. Core proteins localised to 46% and 65% of LDs in untreated Jc1 (n=9) and JFH-1 (n=6) samples, respectively, compared to 25% and 41% in SO-PERL treated Jc1

(n=9) and JFH-1 (n=8) samples, respectively. This translates into a decrease of core associated with LDs after 24 h SO-PERL treatment of 2-fold in Jc1 infected cells and ⅓ decrease in JFH-1 infected cells (Figure 29).

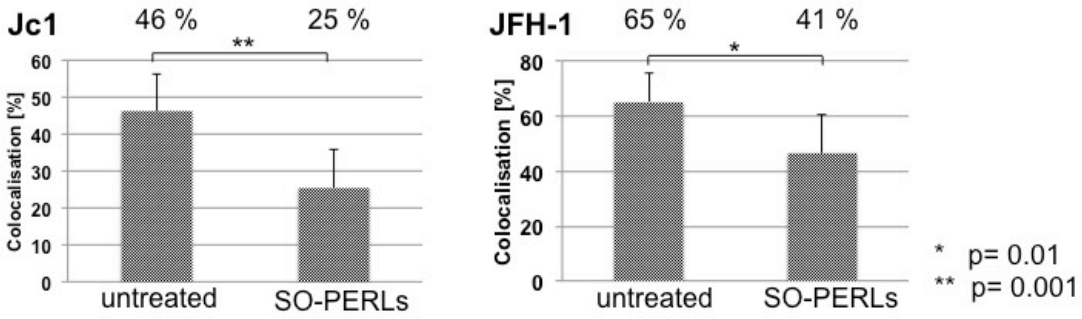

Figure 29: Quantification of HCV core and lipid droplet colocalisation. Microscopy images were analysed in Fiji and the resulting Pearson's coefficients converted into percentage colocalisation. A two-tailed, unpaired t-test was performed, showing changes in colocalisation of core and LDs were significant with p=0.001 (Jc1) and p=0.01 (JFH-1).

To further assess the observed association of core protein with lipid droplets and the effect of SO-PERLs, purified lipid droplets were analysed for core protein using Western blot and band intensities were quantified using Fiji imaging software (Figure 30). The 2D-densitometry determined a 26% difference in core levels between untreated and SO-PERL treated LD preparations for Jc1 (n=4), and 17% for JFH-1 infected cells (n=2).

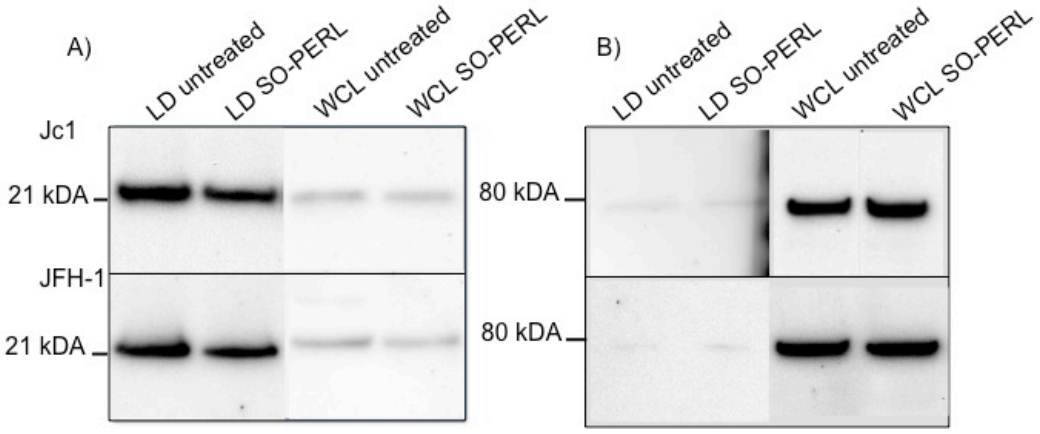

Figure 30: Western blot analysis of HCV core dissociation from LDs. All samples were protein adjusted according to total protein concentration of individual samples using a NanoDrop 1000. LD preparations and whole cell lysates (WCL) from cells infected with either of both strains, Jc1 or JFH-1, were analysed by Western blot for HCV core (A). Quantification was performed using Fiji imaging software. Only protein bands that did not contain saturated pixels were used. Pixel intensities were measured and plotted. The area under the curve was calculated and compared between samples. The same samples were also analysed for calnexin (B) as a measure of purity of the LD preparation, and for comparison in WCL.

In order to investigate possible changes in the lipid composition of lipid droplets, samples were analysed with mass spectrometry. The sample preparations did not contain other cellular membranes, as concluded from the absence of glycolipids. Results of sample duplicates are graphically represented in scatter plots. Each data point is depicted as a black cross and the sample mean as a red minus.

Triacylglycerol content of each sample group is represented in Figure 31.

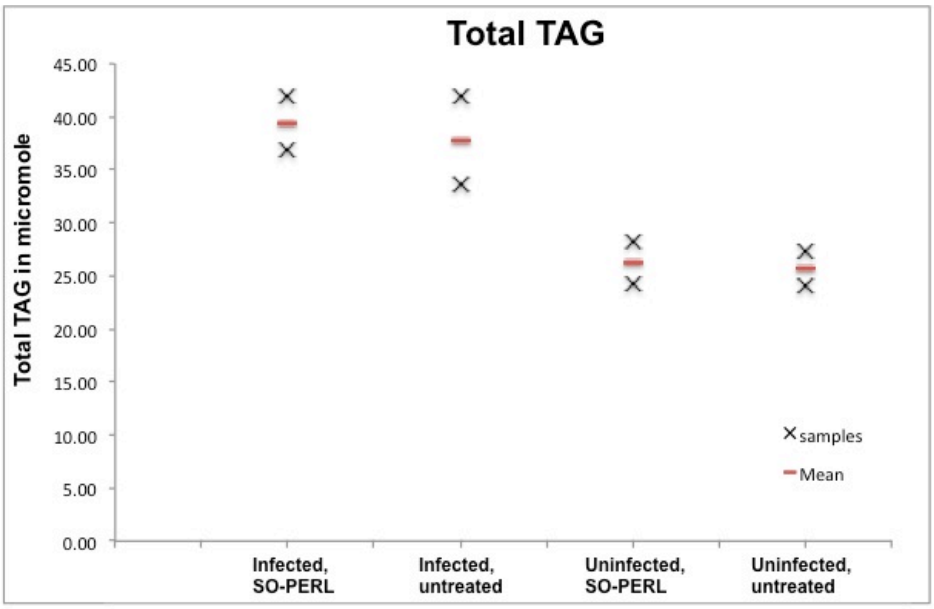

Figure 31: Total TAG of each sample group from duplicates. The TAG content in infected samples is about ⅓ higher than in uninfected samples. This difference is significant with p=0.0034 after conducting a two-tailed Student's t-test. This is irrespective of treatment. If treatment is taken into account, differences between infected, untreated versus uninfected, untreated are not significant with p=0.059 and comparing infected, treated versus infected, untreated p=0.171. However, the sample size of 2 for the latter two comparisons is very low which should be considered when drawing any conclusions. Samples were originally normalised to cell number. However, since this is a subcellular preparation there is no internal standard for sample normalisation.

Lipid droplet extractions were further analysed by mass spectrometry to determine their fatty acid composition in Figure 32.

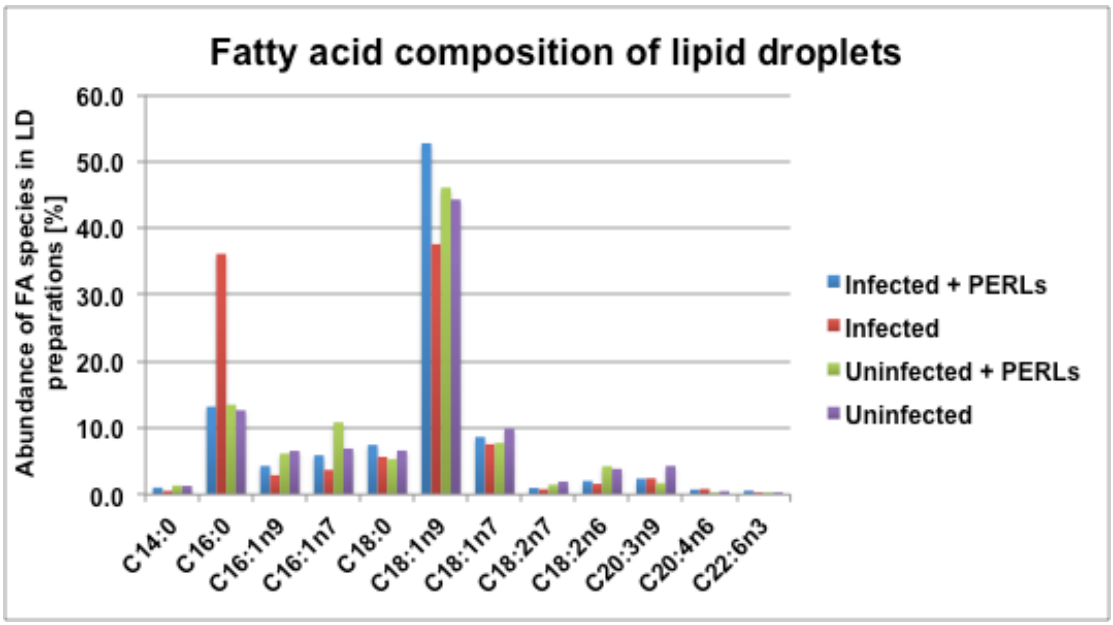

Figure 32: Fatty acid composition of lipid droplets from Huh7.5 cells and the influence of SO-PERL treatment. Fatty acids were measured as methyl esters using GCMS. Mean fatty acid abundances from total fatty acid contents of duplicate samples are plotted as percentages.

Analysis indicates that there are no changes in 22:6 PUFA (docosahexaenoic acid, DHA) between SO-PERL treated samples compared to non-treated samples (Figure 32). 22:6 fatty acids are components of SO-PERLs and an increase in 22:6 lipids is therefore expected if SO-PERL lipids were to be readily incorporated into LDs. Furthermore, the 16:0 fatty acids in infected, non-treated cells are more than 20% elevated compared to any other group. All LD preparations are low in PUFAs and high in monounsaturated species, and 20:3 mead fatty acid, which are markers for active *de novo* lipogenesis [357].

Since SO-PERL lipids do not seem to be readily incorporated into LDs, the effect of HCV infection on the triacylglycerol composition of LDs was analysed (Figure 33). This was done to investigate the detailed TAG composition

behind the change in total TAG between infected and uninfected samples as seen in Figure 33.

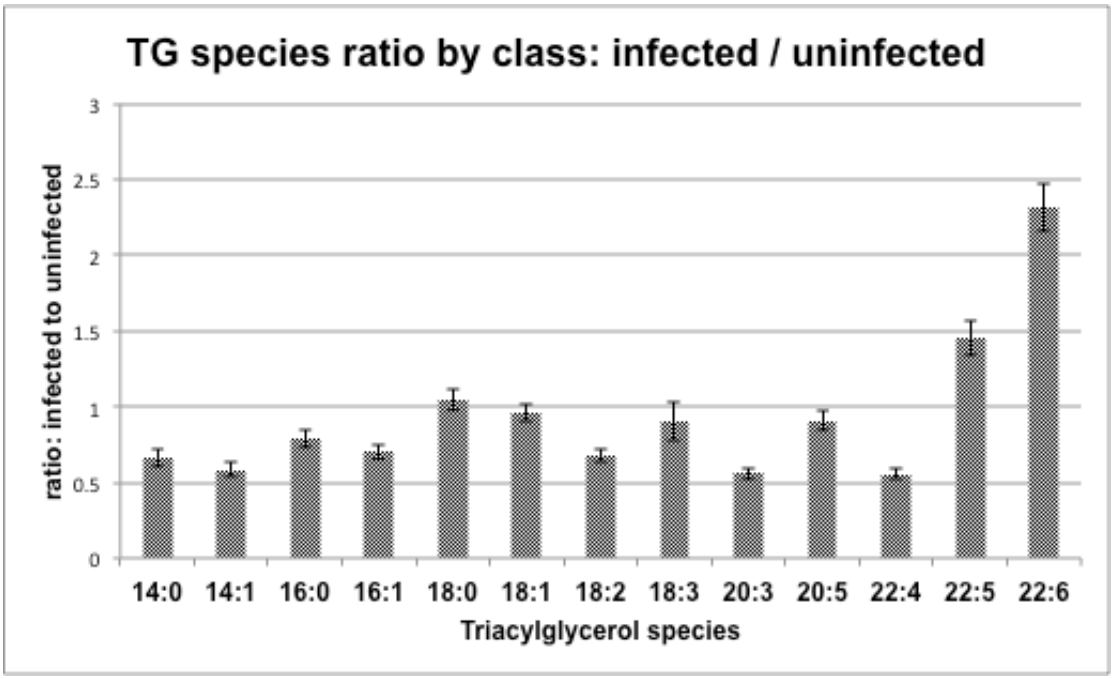

Figure 33: The effect of HCV infection on the TAG composition of LDs. Presented here is the ratio of analysed TAG species for infected to uninfected samples. X-axis represents the neutral loss element of the different TAG species; error bars represent the standard error of the mean taking duplicates for each sample set into account.

The in depth analysis of TAG composition of infected and uninfected cells shows an increase in polyunsaturated species, 22:6 and 22:5 in particular, in infected compared to uninfected samples irrespective of SO-PERL treatment [1]. Furthermore, 20:3 mead acid seems to be reduced 1.9-fold in infection.

[1] Since no influence of SO-PERL treatment was detected, treated and untreated samples were analysed combined, forming untreated and treated sample groups with 4 individual measurements each.

Both observations indicate that either *de novo* lipid biosynthesis or β-oxidation are inhibited.

Analysis of total DAG reflects the majority of the changes observed analysing TAG species (Figure 37). Infected samples seem to contain more DAG compared to uninfected samples.

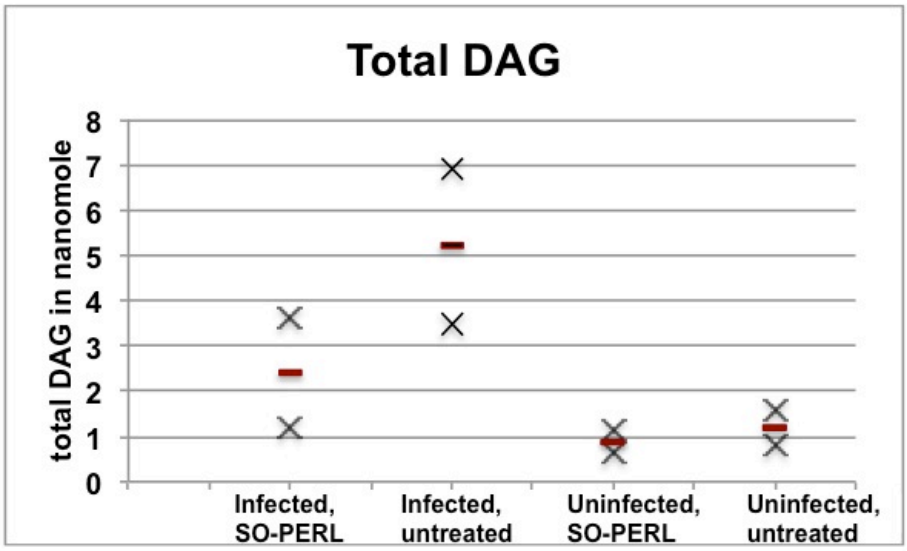

Figure 34: Total amounts of DAG in LD preparations. All samples were analysed for DAG. A Student's t-test was performed comparing infected samples with uninfected samples, irrespective of treatment. There is no significant difference with p=0.294 between infected and uninfected samples. There is also no significant difference with treatment taken into account with p=0.419 and p=0.244 for treated and untreated samples, respectively. However, samples were only measured in duplicates and there seem to be differences between infected and uninfected sample groups by looking at the plotted distribution above. The t-test, expressed as the p-value, accounts for the likelihood that the observation described occurs by chance. An increased number of repeats thereby increases certainty and would be advised.

Looking at the FA profile of DAG, monounsaturated and saturated FAs are abundant (Figure 35).

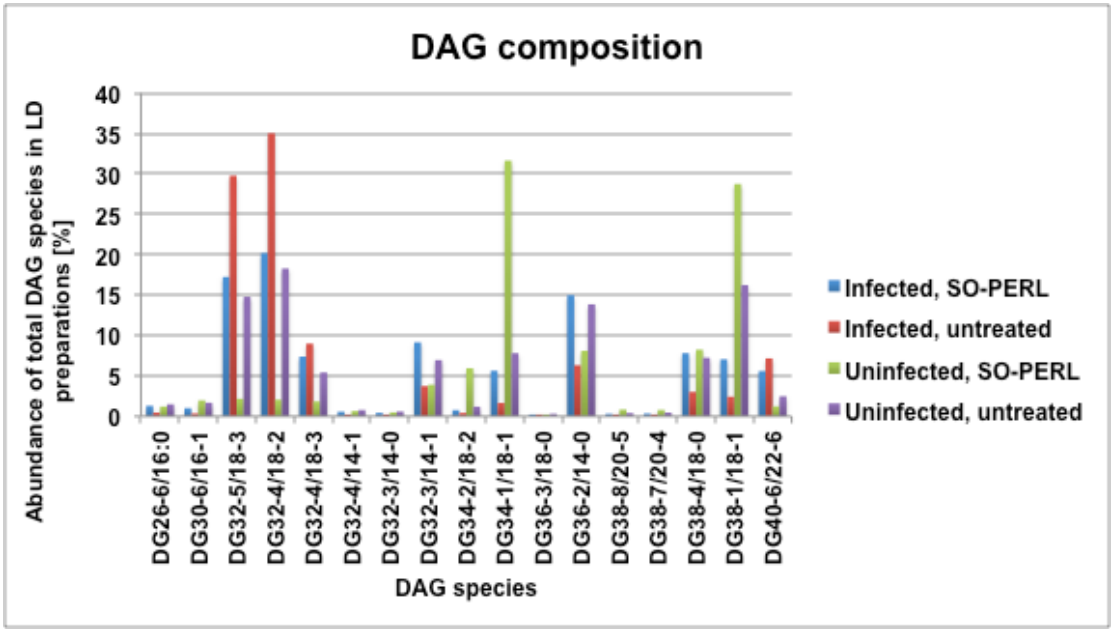

Figure 35: DAG species in LD preparations. In depth analysis of the DAG composition reveals a prominent abundance of saturated and monounsaturated FAs. PUFAs, FAs with 4 or more double bonds, are less abundant.

LD preparations were further analysed for phospholipid composition by LCMS/MS. Total PC remains unchanged across all sample groups (Figure 36).

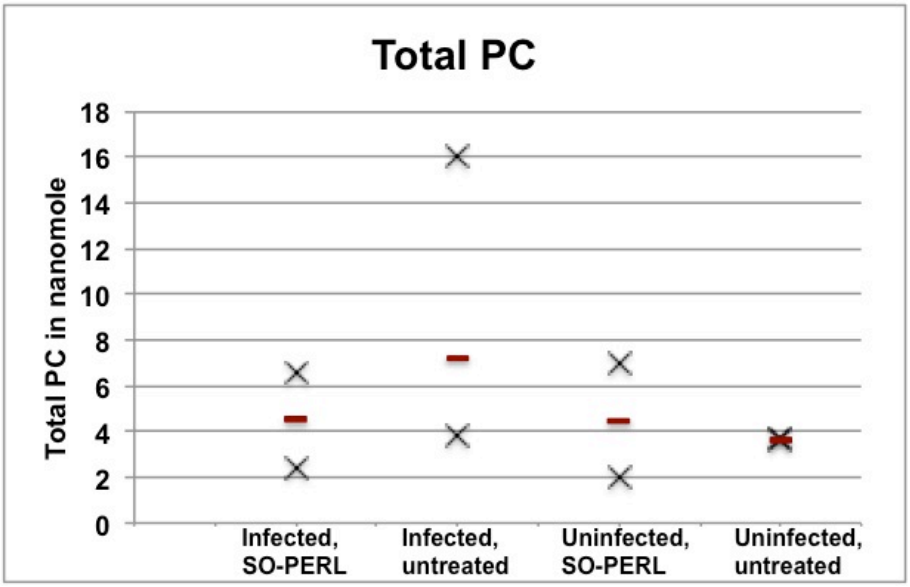

Figure 36: Total amounts of PC in LD preparations. Total PC was determined by summing up all molecular species measured and detected. Quantification was performed according to an internal standard. There is no difference in abundance of PC between sample groups.

Principal component analysis (PCA) of FA composition of PC revealed systematic differences between the 4 sample groups (Figure 37). A comparison of these groups showed that infection caused a decrease in principle component F1, which, in this dataset, corresponds to a reduction in the number of double bonds. Principal component F2 was reduced and resulted in a separation that was caused by SO-PERL treatment.

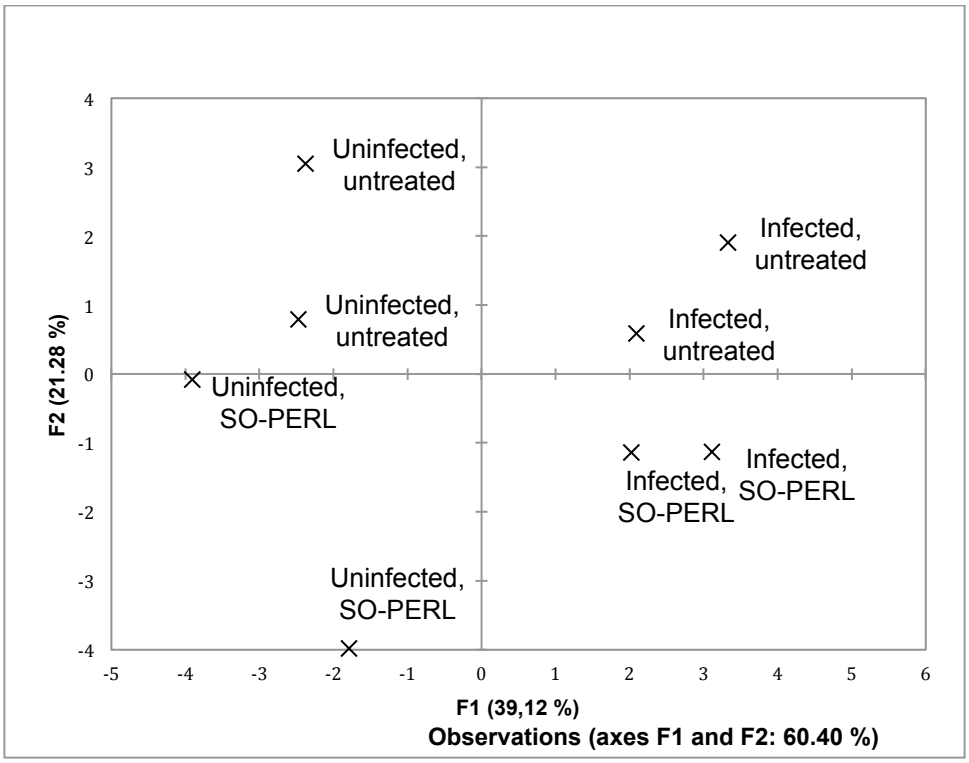

Figure 37: Principle component analysis for PC.

PCA of the FA composition of PC was performed by Claude Wolf (APlipid). Infected and uninfected sample groups cluster clearly into separate quadrants based on the length of the FA carbon chain and the number of double bonds. The dominant contributor to this separation is principal component F1, resulting in a separation of samples corresponding to the infected state. Principal component F2 had a minor contribution and was influenced by SO-PERL treatment,

	F1	F2	nC	nDB
PC38-5	0.954	0.131	28	5
PC36-4	0.822	0.444	36	4
PC36-1	0.716	-0.0073	36	1
PC38-4	0.704	0.622	38	4
PC38-2	0.424	0.220	38	2
PC34-1	0.420	-0.738	34	1
PC32-0	0.233	0150	32	0
PC36-2	0.156	0.114	36	2

Table 14: Correlations between variables and factor. F1 reflects the influence of infection as the major variable accounting for 39% of variance within the sample set performing PCA. F2 is the variable representing SO-PERL treatment and accounts for 21% of variance observed within the sample set analysing for PC using PCA (Figure 37). nC is the number of carbon atoms in the two FA carbon chains of one PC molecule, nDB the number of double bonds.

From these calculations, FAs constituting PC, with shorter carbon chain length and less unsaturation correspond to species dominant in uninfected samples (Table 14). This indicates higher *de novo* lipogenesis in uninfected samples compared to infected samples. Very active *de novo* lipogenesis in uninfected samples is represented by species with a high number of double bonds. This reflects a constitutive state of essential FA deficiency in the cultured Huh7.5 hepatoma cells.

To indirectly probe for lipase activity, which is important in membrane fusion events, lysoPC levels were measured (Figure 38).

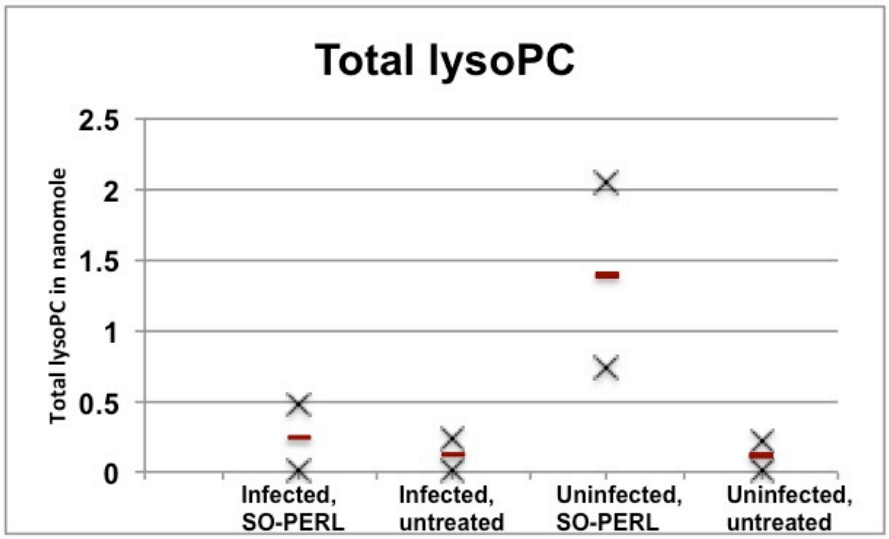

Figure 38: Total amounts of lysoPC in LD preparations. Scatter plot representing the total amounts of lysoPC in LD preparations. An individual data point is shown as a cross, the mean is indicated as a minus.

The levels of lysoPC in the LD preparation were low and inconsistent within sample sets and were therefore not interpreted further.
Sphingomyelin composition was unchanged throughout all samples.

Analysis for the second major phospholipid, PE, indicates that total amounts and composition do not change significantly (Figure 39 and 40).

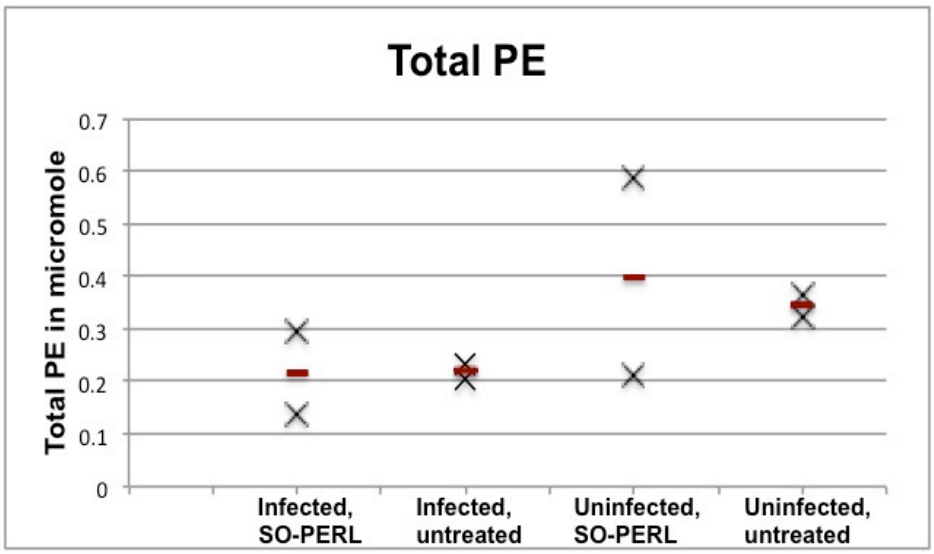

Figure 39: Total amounts of PE in LD preparations. All samples were analysed for PE. A Student's t-test was performed comparing infected samples with uninfected samples, irrespective of treatment. There is no significant difference with p=0.109.

Uninfected, SO-PERL treated samples appear less concisely clustered compared to other data points within sample groups (Figure 39). Additional analyses would increase certainty about the true distribution. Looking at the scatter plot there may be a true clustering of data points into infected and uninfected sample groups. To investigate this further, the analysis would have to be repeated.

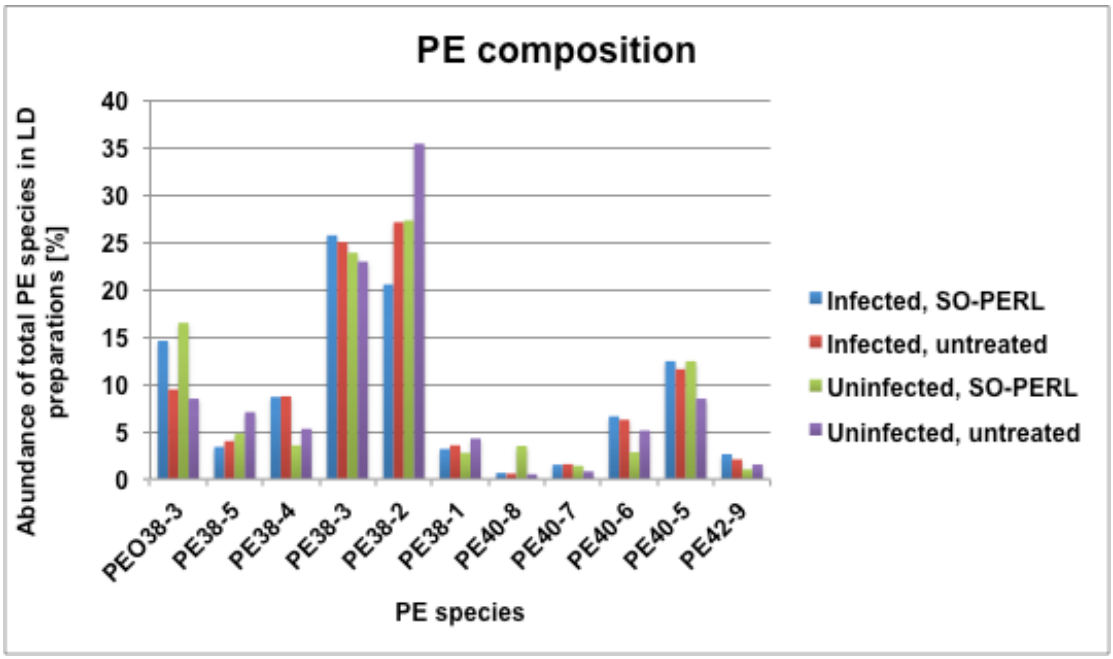

Figure 40: PE composition in LD preparations. The FA composition of PE is constant across all samples.

LD preparations were also analysed for ceramides and glycosphingolipids (Figure 41). Although ceramides were detected, their levels were below the limit of quantification of the instrument and should therefore be interpreted cautiously. However, no significant amounts of hexosyl-ceramide could be detected, which reflects a clean LD preparation and no cross-contamination with cellular membranes that would contain glycolipids.

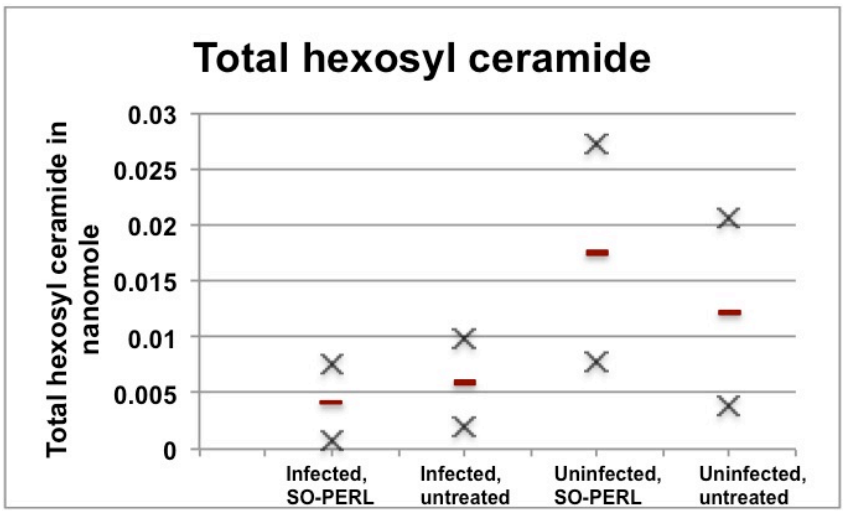

Figure 41: Total hexosyl ceramide in LD preparations. Hexosyl ceramide levels in LD preparations were measured with < 0.03 nanomole, which is below the limit of quantification of the instrument.

Hexosyl ceramide is a measure of purity of the sample preparation and levels indicate that there was no cross-contamination with cellular membranes.

The cholesterol ester amounts in LD preparations were less than 110 nanomol for all samples and the composition did not change in different sample groups (Figure 42).

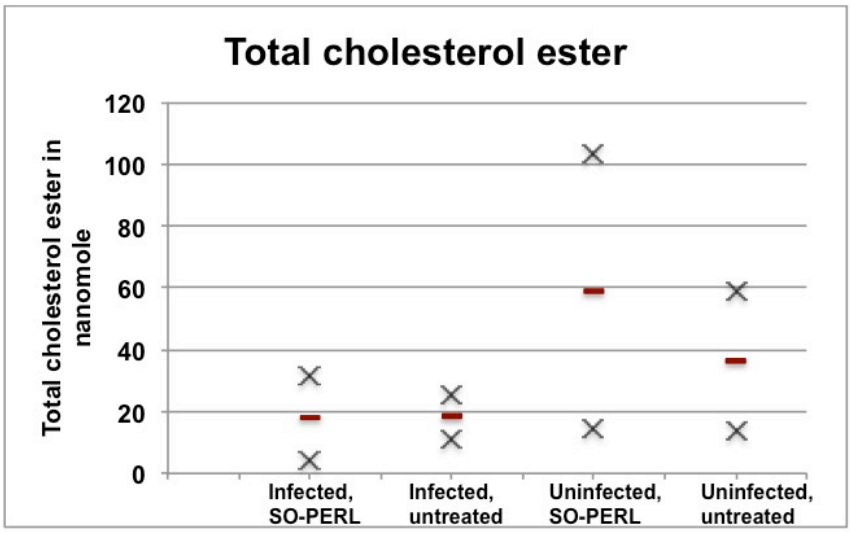

Figure 42: Total cholesterol ester in LD preparations. The data points and means representing cholesterol ester abundance for each sample are

represented in the scatter plot. This indicates that the total amounts of cholesterol ester are unchanged across the sample groups.

In depth analysis of cholesterol ester composition is shown below in Figure 43. The most abundant cholesterol ester species was 18:1 oleic acid but compared to human liver *in vivo*, the levels of 18:2 linoleic acid and 20:4 arachidonic acid species are very low in LD preparations [358].

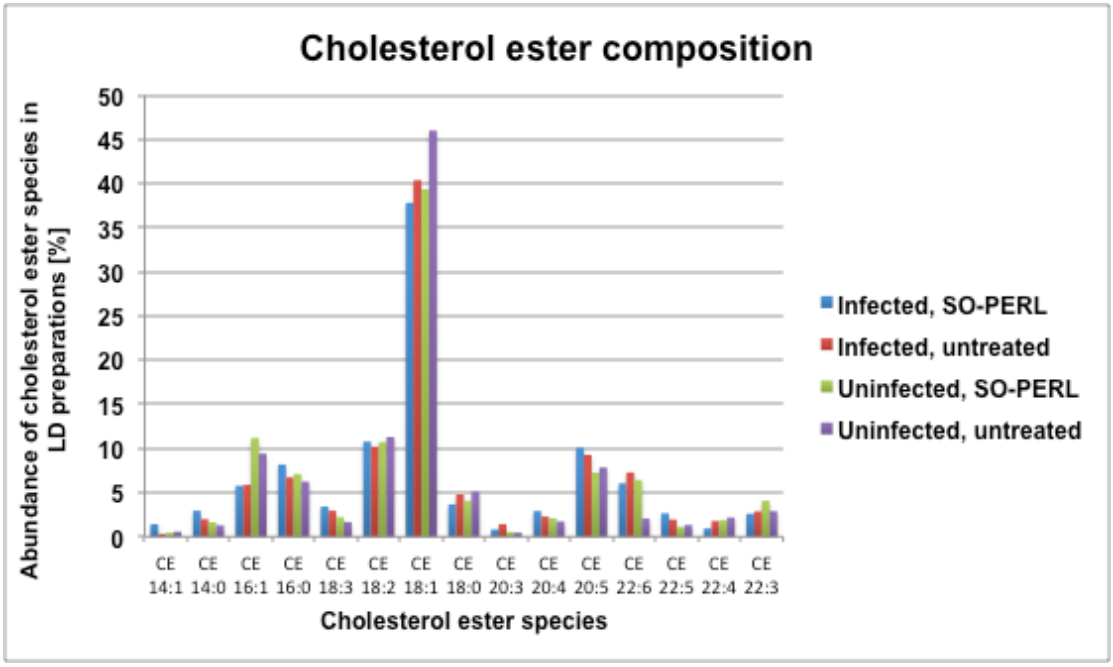

Figure 43: Cholesterol ester composition of LD preparations. The abundance of separate cholesterol ester species was unchanged across the sample groups analysed. The most abundant species was 18:1 oleic acid comprising 30-40% of all species measured. This is expected and in agreement with *in vivo* observations.

3.4 Discussion

The data presented here suggest that SO-PERL treatment does not grossly affect the lipid composition of LDs to the extent that their physical properties would be altered. SO-PERL lipids are not readily incorporated into LDs which is concluded from a lack of liposome constituting PUFAs in LD preparations of SO-PERL treated cells (Figure 32). This suggests that PERL lipids are degraded into FAs and used by the cell as fuel or are oxidised. Previous studies on the total FA composition of Huh7.5 cells have demonstrated that they seem to be deprived of lipids (Stephanie Pollock, unpublished data). Indeed, cells grown in cell culture are starved of lipids compared to *in vivo* tissue as reported by Lamaziere et *al.* [359]. This would explain and favour a rapid conversion of PERL lipids into FAs. Nevertheless, there was a statistically significant 30% elevation in content of total TAGs in infected compared to uninfected samples, irrespective of treatment. This may at first seem contradictory because cells are in a state of infection, within a lipid-deprived environment. FA synthesis is energetically expensive and under those circumstances TAG synthesis from liposome-supplied PUFAs may become critical for cell survival. This increase in total TAG content appears virus-induced and is favourable for viral infectivity and replication as described previously. The total lipid content of a cell is a net function of *de novo* synthesis, import and export. As described in the previous chapter, infection also impacts lipoprotein transport, and up-regulates VLDLR 5-fold on the mRNA level. However, elevated TAG levels have been observed *in vivo* as well. There, TAG levels in the form of VLDL increase early in infection and decrease later in infection [360]. Our HCVcc *in vitro* data therefore compare

to early infection events for total TAG levels. Furthermore, ER-linked FA synthesis is part of the cell's stress response. HCV is known to induce ER stress and cell cycle arrest [361-363]. The lipid-deprived culture environment poses an additional source of cellular stress, which may also be reflected in PRKAA2 up-regulation that was described previously (chapter 2). Cell survival under these circumstances becomes dependent on FA catabolism, which itself is dependent on mitochondrial β-oxidation. Stress response, cell-cycle arrest, and other virus-induced alterations of the host lipid metabolism are therefore likely to account for the elevated total TAG content in infected cells.

Detailed FA analysis reveals an about 20% increase of 16:0 palmitic acid in infected samples. Palmitic acid is an early marker for *de novo* lipogenesis, which has previously been reported to be elevated with infection [310, 338, 364]. Elevated 16:0 palmitic acid has been shown to impair insulin signalling through down-regulation of the insulin receptor signalling and may thereby also contribute to insulin resistance in HCV patients [365, 366]. This may have a synergistic effect to the core protein induced phosphorylation of IRS-1 and subsequent down-regulation of IRS-1 cell surface expression, leading to increased susceptibility to insulin resistance.

Together with 18:1 oleic acid, palmitic acid is the most abundant fatty acid in the liver [367]. S-palmitoylation is a lipid post-translational modification of proteins where palmitic acid is conjugated to a cysteine residue through a labile thioester bond in a reversible manner. Palmitic acid is the preferred FA

for this reaction; however, it can be substituted by 18:0 stearic acid, 18:1 oleic acid, or 20:4 arachidonic acid. The protein modification occurs at the cytosolic side of either ER- or Golgi membrane catalysed by palmitoyl-acyl transferases (PATs) (reviewed in [368]). Palmitoylation is involved in folding and targeting of membrane proteins, trafficking and protein-protein interactions. The latter includes clustering of proteins or accumulation of proteins and formation of a platform, as shown for $GABA_4$ receptor and tetraspanins, respectively (reviewed in [369]). Palmitoylation is a contributing factor, amongst others, to the association of membrane proteins with lipid-rich domains or membranes. This may be either by elongation of the hydrophic transmembrane domain or by alteration of the transmembrane domain orientation relative to the target membrane [369]. HCV core was found to be palmitoylated, primarily at cysteine^{172} (Cys), which is conserved amongst the genotypes but replaced by a phenylalanine in the JFH-1 isolate [370]. Phenylalanine has a hydrophobic side chain, which may partly compensate for the loss of Cys-palmitoylation at amino acid position 172, since JFH-1 core protein shows distinct localisation to LDs. Majeau et *al.* show that upon mutation of Cys^{172} core protein association with the ER is altered compared to wild-type (wt), resulting in a decreased association of mutated core with what the authors call “smooth ER associated with lipid droplets” [370]. However, the Cys^{172} mutant core protein was detected by Western blot in “dense (rough) ER” fractions that were taken from an iodixanol gradient after ultracentrifugation. Our in depth TAG analysis show that 16:0 palmitic acid is 3-fold increased in infected, untreated cells. However, levels in infected, treated samples resemble those of both uninfected sample groups. Based on

the report from Majeau et *al.*, together with the change in 16:0 palmitic acid levels measured by mass spectrometry in LD preparations under various conditions, and core dissociation from LDs upon SO-PERL treatment by immunofluorescence, let me hypothesise that SO-PERL treatment alters 16:0 palmitic acid abundance, thereby influencing S-palmitoylation of HCV core and its association with or trafficking between ER and LDs. S-palmitoylation may also be involved in core oligomerisation and capsid assembly on the surface of LDs. SO-PERLs may therefore interfere with capsid assembly directly, leading to particle defects, or indirectly through alterations of core trafficking between or association with ER and LDs. This could therefore be a major contributing antiviral mechanism of action of SO-PERLs in the context of HCV infection. To investigate the palmitoylation state of HCV core in SO-PERL treated cells, Western blot, 2D-gel or mass spectrometry can be applied in comparison to untreated cells, which would contribute to the evaluation of this hypothesis. Immunoprecipitation of HCV core protein will enrich the sample for palmitoylation analysis using hydroxylamine. Unmodified cysteine thiols are irreversibly blocked using N-ethylmaleimide. Subsequently, palmitoylated cysteine thiols are specifically cleaved and unmasked by hydroxylamine, and conjugated with a biotin label. A final immunoprecipitation using streptavidin will enrich formerly palmitoylated core protein. A potential inhibitory effect of SO-PERL treatment on the palmitoylation state of core can be compared to infected cells, which are treated with known palmitoylation inhibitors, such as 2-bromopalmitate, tunicamycin, or cerulenin.

The analyses of TAGs show further that LD preparations are high in monounsaturated FAs, and low in PUFAs across all sample groups, indicating active *de novo* lipogenesis, which in turn indicates that cells are not overgrown and are metabolically active. However, in relation to and comparing PUFAs of infected samples with uninfected, we observe a 2-fold increase in PUFA levels in HCV infected samples compared to non-infected samples as shown in Figure 33. This can be interpreted as an indication of inhibition of *de novo* lipogenesis or inhibition of β-oxidation. B-oxidation has been reported to be impaired *in vitro* and *in vivo* in HCV infection [371, 372]. Inhibited β-oxidation, possibly leading to a decrease in lipid turnover, in addition to a decrease in LD turnover induced by HCV core, may explain why LD composition does not change grossly in infection [313].

Analysis of DAG levels reveals an elevation of total DAG in infected compared to uninfected samples, irrespective of treatment. DAGs can either be precursors for TAGs or degradation products of the very same. Therefore, they can be regarded as either an indication for increased lipogenesis or lipodegradation.

Analyses of phospholipids reveal that the total abundance of PE and PC did not change across all sample groups. Together with the 30% increase in TAG levels in infected samples, this suggests that LD size increases in infection. HCV induced increase in LD size has been reported previously and is supported by these data [373]. My data show that in infected samples the fatty acids constituting PC is of shorter chain length and saturated to a higher

degree than shown in rats. This may be due to a shift in PC synthesis pathway utilisation. PC is predominantly synthesised by the CDP-choline pathway, generating mainly mono- and disaturated species. However, the alternative PEMT pathway generates polyunsaturated PC species.

The half-life of newly synthesised lipids is very diverse across various cell types. The time for incorporation of newly synthesised phospholipids in membranes varies between 10 min and >12 h, whereas newly synthesised cholesterol is distributed within the cell within minutes or up to 2 h. The movement of cholesterol from the plasma membrane to the intracellular space, however, can take up to 24 h [374]. In terms of intracellular lipid turnover, it is thought that about 50% of total lipids are turned over within one or two cell divisions. Huh7.5 cells in this study have been shown to be metabolically active and divide approximately every 18 h. At the same time, HCV infected cells are reported to be arrested in G_2/M phase [363]. Because of the extent of aberrations concerning the lipid metabolism in infection, it is not known how the lipid turnover is affected. Due to the finely tuned interaction between host and pathogen on this level, I would speculate that the lipid turnover is decreased once infection is established. With this assumption, a longer treatment period might result in more pronounced changes and might even result in changes that are not visible after this 24 h treatment period.

To summarise these data, 16:0 palmitic acid is important for S-palmitoylation of proteins, such as HCV core. This lipid species is elevated in HCV infection

but levels are negatively influenced by SO-PERL treatment and thereby possibly interfering with S-palmitoylation of HCV core. Reduced post-translational modification of core with palmitic acid provides an explanation for the dissociation of core with LDs upon SO-PERL treatment, as observed by microscopy. I therefore propose that the reduction in palmitic acid by SO-PERLs in infected cells constitutes a major contributory mechanism for the antiviral effects of SO-PERLs in the context of HCV infection. The microarray analysis indicates that in infection lipid trafficking is up-regulated on mRNA level. High levels of essential 22:6 DHA and 22:5 DPA may be a consequence of this up-regulation due to increased import from the extracellular environment. This in turn may not only reflect the increased demand for lipids by HCV for infectivity and replication.

With these conclusions it should be noted that each sample was only measured in duplicate even though samples were set up as triplicates but could not be analysed due to a technical problem. Ideally, the experiments described in this chapter should be repeated to create biological as well as technical replicates, decreasing any errors and increasing confidence in the results presented. However, conclusions drawn from the work in this chapter are supported by independent, similar experiments from our laboratory as indicated. With regards to LD isolation; it is a method involving numerous steps with each one introducing variability for each sample preparation. This cannot be avoided but emphasises the importance of experimental repeats, which could not be done, primarily due to time restraints.

4. Fluorescent labelling of HCV Jc1 RNA

4.1.1 RNA labelling

Labelled RNA provides a powerful tool for the study of RNA viruses like HCV. Especially for HCV, very little is known about the assembly, release and transmission mechanisms. Tagged, viral RNA would be a useful tool to investigate these processes.

There are many challenges involved in fluorescent RNA labelling. Due to a usually low abundance of a specific RNA the labelling has to be highly specific. However, viral RNA is expected to be present in high copy numbers at the site of replication but may remain at low abundance during trafficking events. Furthermore, delivery and toxicity of dyes have to be considered. The RNA label may compromise RNA folding, accessibility to interaction partners or targeting because of steric properties of the reporter or tag or overexpression [375, 376].

There are various techniques available e.g. fluorescent *in situ* hybridisation, fluorescently labelled nucleotides, molecular beacons, aptamers, or metabolic labelling of nascent RNA [377].

In this study, the aim was to label HCV RNA using the MS2 strategy, as well as Alexa®–labelled nucleotides. With regards to the latter, full-length HCV RNA is *in vitro* transcribed using Alexa®–labelled nucleotides. The resulting transcripts are transfected into naïve Huh7.5 cells and imaged. This labelling approach allows RNA tracking in live cells. Further to the Alexa®-labelling, the labelling approach using the MS2 coat protein has proven to be very

versatile and useful for endogenous RNA labelling in eukaryotic cells and additionally enables further characterisation of tagged RNA by co-immunoprecipitation experiments in contrast to the Alexa®-labelling approach [375, 378].

4.1.2 MS2 coat protein RNA labelling

The MS2 coat protein derived from the bacteriophage MS2 is a widely used tool for RNA trafficking studies. The MS2 protein binds with high specificity to a unique stem loop structure, not naturally present in eukaryotic cells. For RNA trafficking studies, the MS2 protein is fused to a sorting signal (SS), e.g. a nuclear localisation sequence (NLS) as well as a fluorescent reporter protein (FP), e.g. photoactivatable green fluorescent protein (paGFP). The unique stem loop RNA is introduced into the target RNA sequence. Stem-loops can be introduced as 6, 12 or 24 repeats with randomised spacers of 20 nucleotides between those repeats. Each repeat consists of 19 nucleotides.

The target cell line is stably transfected with MS2–SS–FP. Upon transfection of this cell line with the tagged target RNA, the MS2–reporter binds to the stem loop structure present in the target RNA (Figure 44).

In order to conduct single-molecule trafficking studies, the introduction of 24 stem-loop repeats into the target RNA sequence will be necessary. If the reporter construct is well expressed, the target RNA, tagged with 24 stem-loop repeats, will on averaged be occupied with 33 GFP proteins. In case of low expression levels only 11-15 GFP proteins will be bound [379, 380].

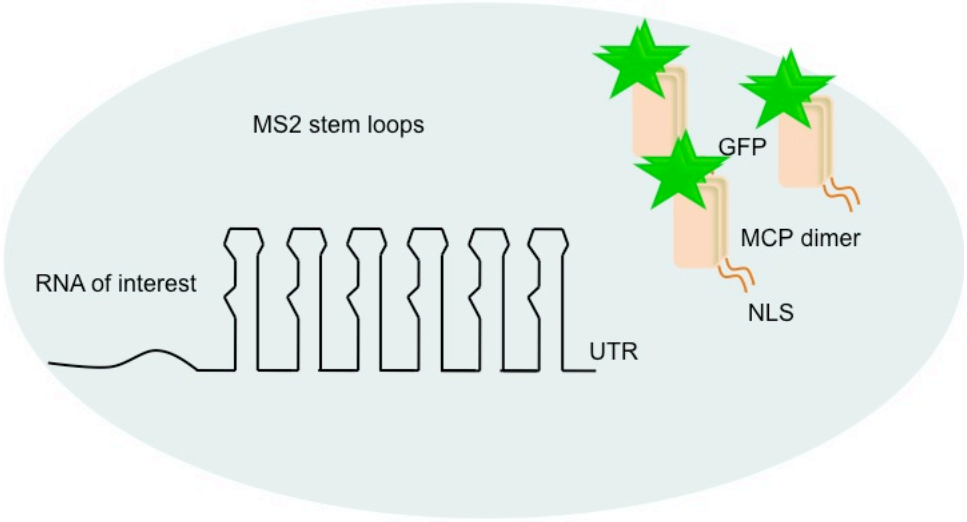

Figure 44: Principle of the MS coat protein labelling system. The RNA of interest is tagged with multiple copies of MS2 stem-loops in 6, 12, or 24 tandem repeats. The MCP-reporter construct binds to those stem-loops, resulting in fluorescently tagged RNA, which can subsequently be tracked in live cells.

Challenges of RNA labelling, like adjusting expression levels for reporter constructs, and background fluorescence, can be addressed in the following ways: Varying the inducible promoter, which drives the expression of the reporter construct, can optimise expression levels. Fluorescence of unbound reporter constructs will be restricted to one cellular compartment by the introduction of appropriate sorting signals. If the remaining fluorescence still significantly disturbs the signal of the labelled RNA, split fluorescent proteins would be an alternative. In case of split fluorescent proteins, one half of the fluorescent reporter protein is encoded and produced as a fusion at the target side, the complementing other half is delivered by the specific binding partner. Upon binding, the fluorescent reporter becomes complemented and emits

fluorescence. This system provides the advantage that there is no background fluorescence produced since the fluorescent reporter is only active after specific binding of the binding partners of choice.

This technique has been used successfully to study RNA movement in yeast cells, Drosophila cells and various mammalian cell lines [381-386]. In the context of human virus research, this method has been successfully used for studies of HIV, and Epstein-Barr Virus (EBV) [387, 388]. It was also used to prove the cell-to-cell transmission of the Turnip crinkle plant virus [389].

4.1.3 Alexa®-UTP RNA labelling

This labelling approach is based on the incorporation of fluorescently tagged uracil triphosphates (UTPs) during RNA *in vitro* transcription. Labelled nucleotides are randomly incorporated throughout the transcript. The fluorophore is attached at carbon 4 of the uracil nucleotide to not interfere with the Watson-Crick pairing.

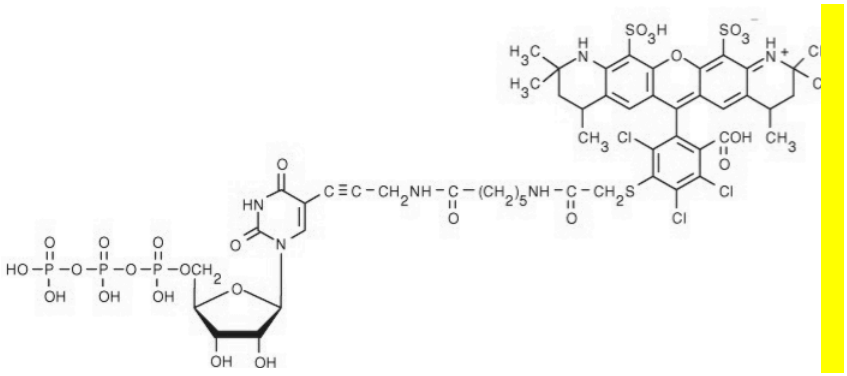

Figure 45: Alexa®-UTP structure

The advantage of this method is that the bright and stable label is directly and covalently attached to the target RNA. This labelling approach is suitable to investigate early RNA trafficking events, since it is not known if the label may interfere with the viral replication machinery and possibly accumulate. An

accumulation of transfected RNA at the site of viral replication may result in alterations of trafficking events. However, it is possible that transfected RNA gets incorporated into progeny viruses or is transmitted in a cell-dependent manner. Alexa®-nucleotide labelling of viral RNA had not been reported before.

4.2 Objective

The focus of this project was to develop a system for HCV trafficking using live cell imaging techniques. The aim was to develop labelling methods to track single viral RNAs *in vitro* in HCVcc, primarily to describe the extent to which cell−free transmission in HCV infection occurs. However, it was also designed to investigate interactions between host proteins and viral RNA, and possibly the HCV assembly process [208, 209, 211]. Because of its versatility the MS2 RNA tagging system was chosen as a primary approach [390]. This approach may not only be a tool for cell trafficking studies but also for immuno-precipitation experiments. In addition, viral RNA was labelled by incorporation of Alexa®–labelled nucleotides. This approach was aimed to investigate early RNA trafficking events and potential cell-to-cell transmission. Despite systematically altering various conditions and approaches, this project was not successful. None of the techniques and strategies resulted in tagged, infectious, full-length HCV RNA. Therefore, the project was discontinued after almost 2 years.

4.3 Materials and methods

4.3.1 Alexa®-UTP labeling

10 µg of HCV Jc1 plasmid were linearised with 20 units Mlu-I (New England Biolabs) for 1 h at 37 °C. Linearised DNA was purified with phenol:chloroform (Sigma) and resuspended in RNase free water. *In vitro* transcription was performed using 20 µl 5 x RLL buffer (400 mM Hepes pH 7.5, 60 mM $MgCl_2$, 10 mM spermidine, 200 mM DTT), 12.5 µl nucleotide triphosphate mix (equals 25 mM each nucleotide, Promega), 100 units RNasin (Promega), 5 – 7 µg DNA, 60 units T7-RNA polymerase (Promega), topped up with RNase-free water to 100 µl total reaction volume and left for 5 h at 37 °C. DNA was digested by 7.5 µl of RNase-free DNase-1 (Promega) for 45 min at 37 °C and precipitated with phenol:chloroform and isopropanol, and resuspended in RNase-free water.

RNA was transfected into Huh7.5 cells using Lipofectamine RNAiMax (Invitrogen) following the manufacturer's instructions.

4.3.2 RNA gel electrophoresis

Ethidium bromide gel electrophoresis was performed to analyse the *in vitro* transcribed RNA. As a marker for size B16 RNA was used showing bands at 5 kb, 2 kb, and 0.5 kb on a 1% agarose gel containing 2.2 M formaldehyde. The agarose was dissolved in deionised water and cooled down before running buffer and formaldehyde were added. Samples were prepared as described below (Table 10). The gel was run at 90 V.

RNA gel (100 ml)	1 g agarose	
	20 ml 5x running buffer	
	17.5 ml formaldehyde (2.2 M)	
	62.5 ml deionised water	
RNA sample preparation	5 µl RNA	10 min at 65 °C
	2 µl 5x running buffer	
	3.5 µl formamide	
	10 µl formaldehyde	
	4 µl loading buffer	
	1 µl ethidiumbromide (1 µg ml^{-1})	

Table 10: RNA gel electrophoresis. Running buffer (0.02 M MOPS, 8 mM sodium acetate, 1 mM EDTA, pH 7.0, in diethyl pyrocarbonate water), 10x loading buffer (50% glycerol (in DEPC-water v/v), 10 mM EDTA (pH 8.0), 0.25% (w/v) bromophenol blue, 0.25% (w/v) xylene cyanol FF).

4.3.3 Infectivity assay

50 ng of *in vitro* transcribed RNA were transfected into Huh7.5 cells using Lipofectamine RNAiMax (Invitrogen) following the manufacturer's instructions. Cells were cultured for 72 h and 6 days. Immunofluorescence analysis for core protein expression was performed as described previously (see 2.6.5).

4.3.4 Quantitative real-time PCR for HCV

Quantitative real-time PCR (qRT-PCR) was carried out using the SYBR®-Green RT-PCR kit (Roche) following the manufacturer's protocol. Both primers, RC21 and RC1 for positive strand and negative strand, respectively, are specific for the HCV UTR's and were used in 10 μM dilutions (Sigma according to [391]). The standard for quantification of transcripts was based on Jc1.

4.3.5 Jc1 MS2 mutagenesis

For the mutation of restriction sites within the Jc1 genome and subsequent introduction of MS2 coat protein stem loops into the Jc1 UTRs, QuikChange-II XL site-specific mutagenesis kit (Stratagene) was used according to the manufacturer's protocol. Primers were designed using the PrimerX software as recommended and synthesised by Sigma. The PCR was cleaned up using the PCR purification kit from Qiagen following the manufacturer's instructions.

4.4 Results

4.4.1 MS2-coat protein labelling

For the MS2-coat protein labelling, stem-loop repeats have to be inserted within the untranslated region. They cannot be inserted within the open reading frame since the repeats contain stop codons due to their original purpose in the MS2 bacteriophage. The HCV untranslated regions, are as described previously, highly structured and densely packed with regulatory regions. The 3'UTR insertion site is within the bulge of the stem loop preceding the poly(U/UC). Stem loops are very often regulatory regions and should therefore be avoided, however this is difficult in the case of HCV UTRs. Insertions within the poly(U/UC) repeats would likely have an effect on the replication efficiency, since it has been shown that the length of the poly(U/UC) influences the replication capability [155]. The MS2 repeats should ideally be placed as far towards the end of the transcript as possible to have a minimal effect on the target RNA. However, the HCV 3'UTR ends with 3 stem loops, the X region, instead of a poly(A) sequence. The X region is an important part of the replication process and should therefore not be disrupted. Inserting the MS2 repeats at the very end of this region, and thereby the end of the 3'UTR, could destabilise the RNA and significantly decrease its half-life since 3'UTRs are involved in the regulation of RNA stability. The 5'UTR insertion was planned to occur within the first stem loop in domain I. This is the only possible place preceding the miR-122 binding site (nt 23-29), which itself is followed by IRES-interacting sequences [392].

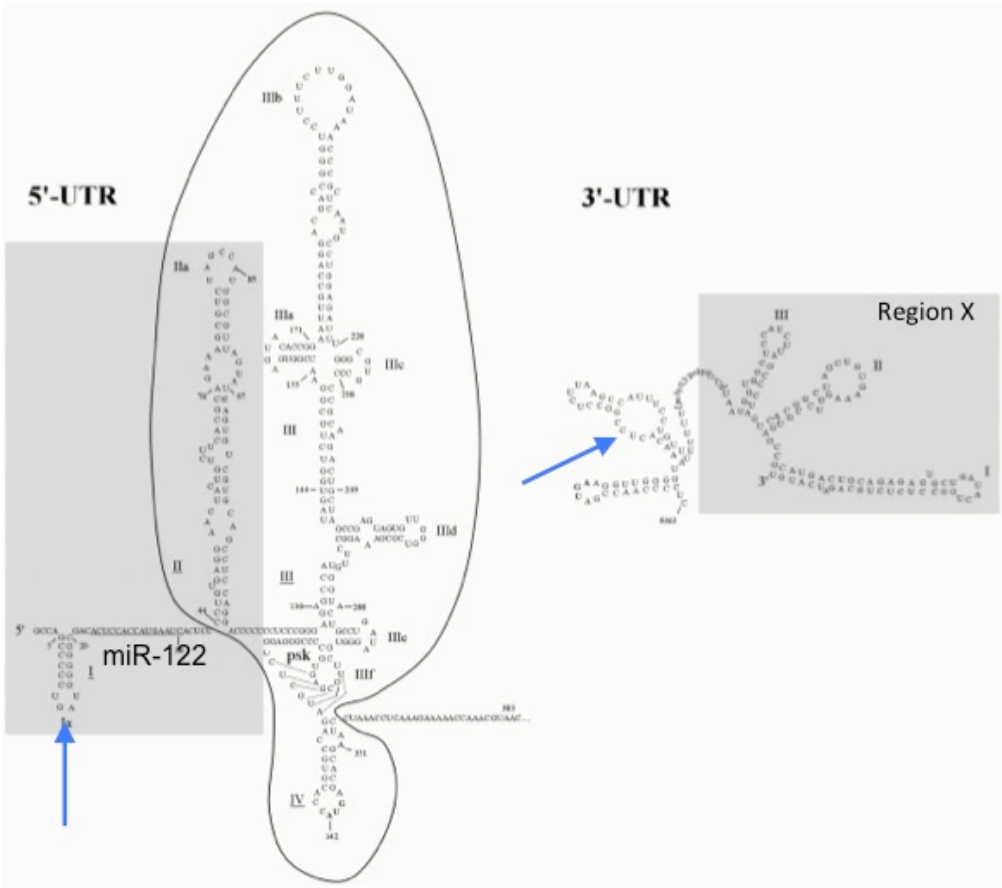

Figure 46: The arrows depict the insertion sites for the MS2 stem-loops for both, 3'UTR and 5'UTR. Grey shaded boxes contain RNA elements that are thought to be involved in replication. Outlined is the IRES. (Adapted from Hepatitis C Viruses: Genome and Molecular Biology)

MS2 stem loop constructs were obtained from RH Singer (Albert Einstein College of Medicine, New York) in a pSL1180 vector, flanked by Bgl-II and BamH-I restriction sites. The pFK-JFHI/J6/C-846 plasmid, encoding the Jc1 genome, was analysed for the presence of both restriction sites using ApE software. This search revealed 4 BamH-I recognition sequences at nucleotide positions 6003 (NS4B, aa 337-338), 6271 (NS5A, aa 1-3), 9763 (vector backbone), and 9895 (vector backbone). The NS5A BamH-I site lies outside domain I and is therefore unlikely to affect the zinc-binding or

membrane association properties of the protein [393]. The BamH-I site within the C-terminus of NS4B, however, might affect the membrane association of the protein [394].

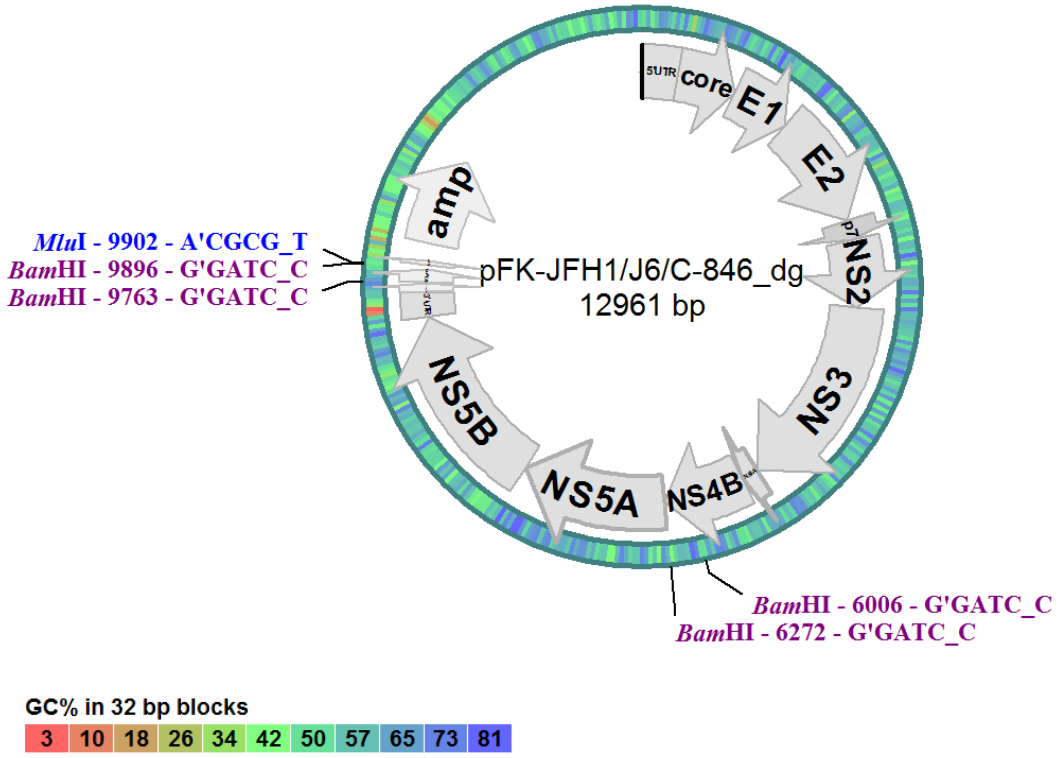

Figure 47: BamHI sites within the HCV genome. Vector map was produced based on the sequence of pFK-JFH1/J6/C-846_dg. Marked are the original BamHI sites, which were mutated as part of the described MS2 cloning strategy. 2 out of 4 identified BamHI sites are located within the genome. Also marked is the MluI site, which was used to linearise the vector for *in vitro* transcription (4.1.6). The outer ring illustrated the GC-content of the sequence.

In order to introduce the stem loops with both restriction sites, the 4 BamH-I sites present in pFK-JFHI/J6/C-846 needed to be mutated. Primers introducing point mutation were designed using PrimerX, designated Jc1_BamHImut6003_fwd/rv, Jc1_BamHImut6271_fwd/rv,

Jc1_BamHImut9763_fwd/rv, and Jc1_BamHImut9895_fwd/rv. The mutation PCR and transformation of XL10-Gold® ultracompetent bacteria was done using the QuikChange Mutagenesis II XL kit (Stratagene), following the manufacturer's protocols with the exception that all bacterial cultures were kept at 30 °C, instead of 37 °C to ensure correct amplification of the plasmid. Positive clones were confirmed by sequencing. The resulting mutated pFK-JFHI/J6/C-846 was renamed Jc1_4xmut and subjected to MS2 restriction site insertion PCR, using the QuikChange Lightning site-directed mutagenesis kit (Stratagene) following the manufacturer's instructions with a starting Jc1_4xmut DNA concentration of 50 ng and 18 PCR cycles. Two different sets of primers were used for both UTRs (Table 11). Set 1 primers included both restriction sites, BamH-I and Bgl-II, whereas set 2 was split into two primers, each containing one restriction site. This was done to minimise the length of the primers, and to reduce the possibility of secondary structure formation during PCR. PCR conditions were varied as listed in table 12.

Primer name	Sequence (5'→ 3')
5'UTR_fwd	acctgcccctaaGGATCCTCAAGATCTtaggggcgaca
5'UTR_split1_fwd	acctgcccctaaGGATCCtaggggcgaca
5'UTR_split2_fwd	acctgcccctaaTCAAGATCTtaggggcgaca
5'UTR_rv	tgtcgccccta AGATCTTGAGGGATCCttaggggcaggt
5'UTR_split1_rv	tgtcgccccta GGATCCttaggggcaggt
5'UTR_split2_rv	tgtcgccccta AGATCTTGATtaggggcaggt
3'UTR_fwd	ctcggtagagcgGGATCCCCAAGATCTgcacacactag
3'UTR_split1_fwd	ctcggtagagcgGGATCCgcacacactag
3'UTR_split2_fwd	ctcggtagagcgCCAAGATCTgcacacactag

3'UTR_rv	ctagtgtgtgcAGATCTTGGGGATCCcgctctaccgag
3'UTR_split1_rv	ctagtgtgtgcGGATCCcgctctaccgag
3'UTR_split2_rv	ctagtgtgtgcADATCTTGGcgctctaccgag

Table 11: MS2 restriction site insertion primers. Primers were designed with PrimerX, insertions are highlighted in blue.

Annealing temperature gradient	45 °C – 68 °C
DNA template concentration	2%, 5%, 7%, 10%
Glycerol/DTT/BSA	25 %/50 mM/5 mg ml^{-1}
$MgCl_2$ (25 mM, New England Biolabs)	1:20, 1:30, 1:40, 1:50
DMSO (Sigma)	2%, 5%, 7%, 10%
Glycerol (Sigma)	2%, 5%, 7%, 10%

Table 12: MS2 restriction site insertion PCR. Listed here are variations of PCR conditions. One variable was changes at a time.

PCR products were transformed into XL10-Gold® cells and cultured over night according to manufacturer's protocol. In the case of colonies resulting from this culture, the construct was further replicated in a second overnight culture, isolated and submitted for sequencing. No positive clones were identified for any of the conditions.

In a different approach the In-Fusion® kit (Clonetech) was used to insert the restriction sites Bgl-II, and BamH-I, and later the MS2 stem loops within the 3'UTR and 5'UTR of the Jc1 genome. This method was recommended by members of Ilan Davis' group (University of Oxford), who have used In-Fusion® successfully to insert MS2 stem loop repeats in the *Drosophila*

melanogaster genome. PCR, using the In-Fusion® kit, was carried out following manufacturer's protocols. This kit requires a linearised target vector for the insertion of the gene of interest with a 15 bp overhang on both sides. Primers were designed creating a 12 and 13 bp overhang on both UTRs, which overlaps with the insert sequence (Table 13). The overhang was slightly shorter to optimise primer characteristics.

Primer name	Sequence (5'→3')
Jc1_5NTR_ampInFusion_fwd	CTCACTATAACCTGCCCCTAA
Jc1_5NTR_ampInFusion_rv	TTAGGGGCAGGTTATAGTGAG
Jc1_3NTR_ampInFusion_fwd	CTCCCCGCTCGGTAGAGCGG
Jc1_3NTR_ampInFusion_rv	CCGCTCTACCGAGCGGGGAG

Table 13: Primer sequences for the amplification of both UTRs within the pFK-JFHI/J6/C-846 plasmid for further use with the In-Fusion® kit.

The linearisation PCR was performed using the OneTaq® polymerase (New England Biolabs) testing various conditions. Primer concentration was varied between 10 µM and 2.5 µM, DNA template concentration between 1 ng and 0.25 ng

Since this was not successful, the linearisation PCR was also performed using the QuikChange Lightning kit with DNA concentrations ranging from 20 ng to 100 ng, as well as two annealing temperatures of 56 °C and 70 °C for 5'UTR and 3'UTR amplification respectively. Reactions with ≥30 ng Jc1 DNA template resulted in very weak 3 kb and 9 kb product bands on a 2% agarose gel, stained with GelRed™ (Biotium), but not a full-length product.

Since none of the PCRs had been successful, the integrity of the template DNA was tested using a dilution series on a 2% agarose gel. No DNA degradation was visible indicating that the template DNA was intact.

The HCV UTRs provide great challenges in terms of molecular cloning due to their structural characteristics. Based on the existing NS5A-GFP construct designed by Moradpour *et al.*, another set of primers was designed, aiming to introduce the restriction sites within the NS5A sequence at nucleotide position 7222 in pFK-JFHI/J6/C-846, corresponding to domain III in NS5A [395]. Even though this would eventually lead to the insertion of MS2 stem loops within the open reading frame, early RNA trafficking events are not expected to be influenced by this as long as the transfected RNA does not accumulate.

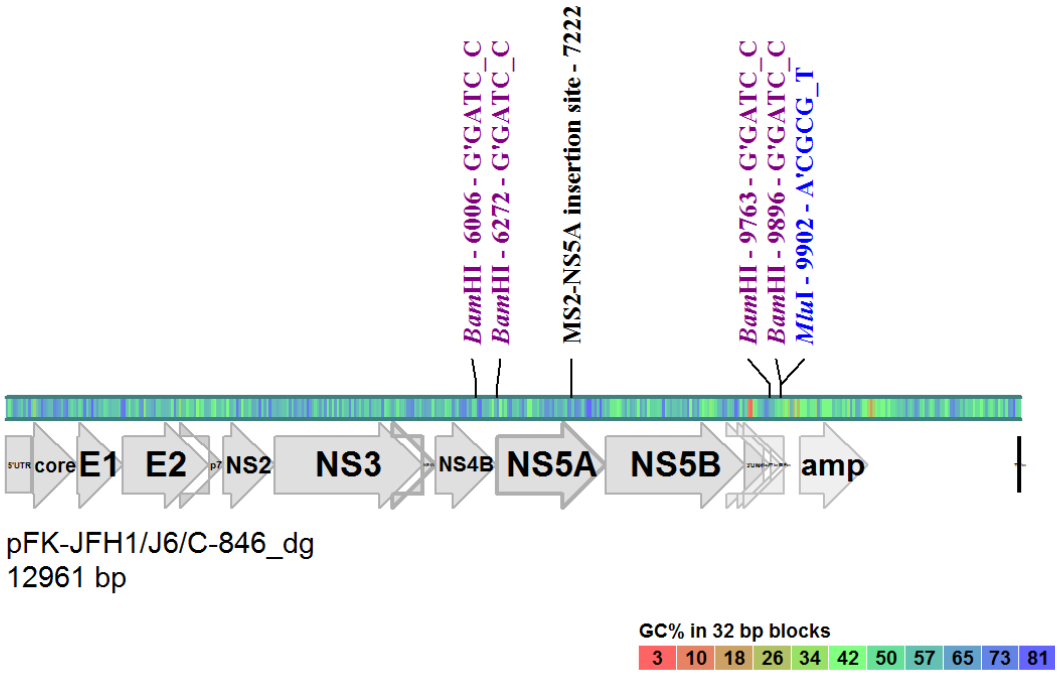

Figure 48: Insertion of MS2 stem loops within the ORF. The site of insertion lies within the intrinsically unstructured domain III of the NS5A protein.

Crimson Taq polymerase (New England Biolabs) was used as described below in a reaction with 0.5-30 ng DNA template (Table 14 and 15).

Step	Temperature	Time
1	94 °C	2 min
2	94 °C	30 s
3	60-80 °C temperature gradient	30 s
4	68 °C	14 min
5	68 °C	17 min

Table 14: PCR cycle parameters to introduce MS2 restriction sites within the NS5A sequence. Steps 2-4 were repeated 30 times, steps 1 and 5 were executed once.

Primer name	Sequence (5'→3')
Jc1_NS5A_MS2RS_fwd	ctgactacaaGGATCCTCAAGATCTcccgccgct
Jc1_NS5A_MS2RS_rv	agcggcgggAGATCTTGAGGATCCttgtagtcag

Table 15: MS2 restriction site insertion primers for NS5A region.

This PCR was not successful since it did not result in a full-length product but repeatedly in a 2.5 kb product. Analysis of the sequence using the ApE software did not reveal any obvious reasons within the sequence, like nucleotide repeats, why the reaction would stop at this point. Hence, both primers were also tested using the QuikChange Lightning site-directed mutagenesis kit using 100 ng DNA template, however, without resulting in any PCR product. In a final approach, the polymerase Herculase (Agilent Technologies) designed for challenging systems, optimised for high fidelity of

long amplifications was used according to the manufacturer's protocol, involving 50 ng Jc1 DNA template, DMSO titration ranging from 0 – 8% and 69 °C primer melting temperature. No PCR products were obtained.

At this point the project was discontinued.

4.4.2 Alexa®-UTP labelling

Uracil nucleotides, tagged with Alexa®Fluor546 were added in 3:7, 1:1, and 7:3 molar ratio to untagged uracil nucleotides. The presence and concentration of *in vitro* transcribed, fluorescently tagged RNA was determined on a NanoDrop 1000 spectrophotometer (Thermo Scientific). Transcription efficiency decreased with increased Alexa®-UTP concentration in a dose-dependent manner. Therefore, all subsequent experiments were carried out using the 7:3 (unlabeled to labelled UTPs) molar ratio.

Alexa®-labelled RNA was transfected into Huh7.5 cells and imaged on a widefield microscope (Applied Precision DeltaVision, 60x/1.35 Oil UPlanSApo objective). Images were deconvoluted with ImageJ software. Punctuate Alexa®546 signals were detected throughout the cytosol in cells fixed at various time points post transfection (Figure 49).

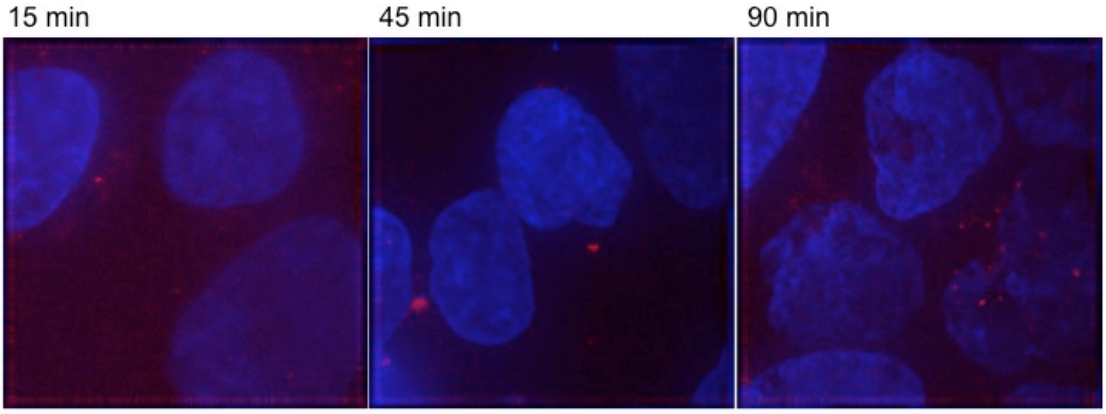

Figure 49: Time-course experiment with Alexa®-labelled HCV RNA. HCV Jc1 RNA was *in vitro* transcribed and transfected into naïve Huh7.5 cells as described. Cells were fixed with 4% PFA at time-points post-transfection as indicated. Samples were mounted with VECTASHIELD®DAPI and imaged on a DVCore widefield microscope using a 100x objective. Transfected RNA (Alexa®546) in red, nuclei in blue.

In order to investigate transmission of HCV RNA, naïve cells were labelled with CellTracker™Green CMFDA (5-chloromethylfluorescein diacetate; used according to the manufacturer's protocol) and subsequently co-cultured for 16 h with infected and Alexa®-RNA transfected cells (Figures 50 and 51).

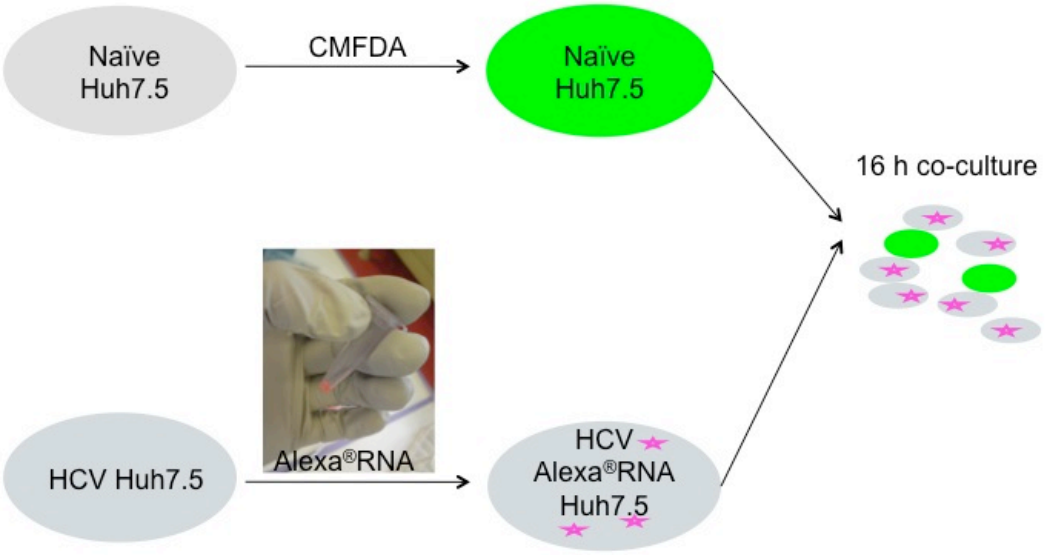

Figure 50: Experimental outline for HCV transmission analysis. This figure depicts the experimental design to investigate transmission of fluorescently labelled HCV RNA. CellTracker™Green was used to differentiate between donor and acceptor cells.

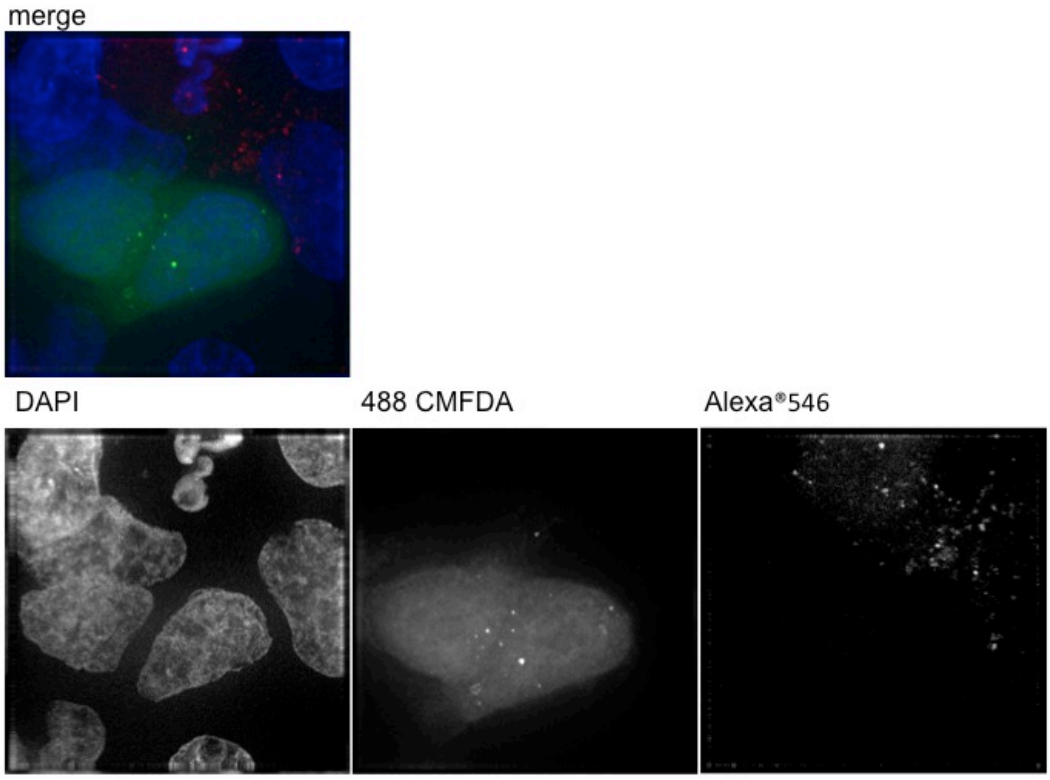

Figure 51: HCV transmission analysis. Alexa®-labelled HCV RNA (Alexa®546) was transfected into previously HCV Jc1 infected cells. Infected,

and transfected cells were co-cultured for 16 h with CellTracker™Green CMFDA (488 emitting) labelled naïve cells as outlined in Figure 49. Cells were fixed with 4% PFA, permeabilised with 0.1% TritonX/PBS, mounted with VECTASHIELD® DAPI, and imaged on a DVCore widefield microscope. Images recorded in a z-stack were projected and deconvoluted.

The co-culture experiment as described in Figure 50 did not reveal labelled and transfected viral RNA in CMFDA labelled naïve cells. The panel, depicting the image in separate channels shows a clear separation between the 488 CMFDA and Alexa®546 channels (Figure 51).

To investigate, whether Alexa®-labelled RNA is infectious, an infectivity assay was performed over 72 h and 6 days as described in the methods section. Very low-level infection was detected after transfection of unlabelled RNA. Since Alexa®-labelled RNA transfected into Huh7.5 cells did not result in an infection as determined by anti-core immunofluorescence, RNA was analysed by ethidiumbromide gel electrophoresis and by quantitative RNA PCR (qRT-PCR) to determine the transcript size. Both analyses revealed that no significant amounts of full-length RNA were obtained.

4.5 Discussion

4.5.1 MS2 coat protein labelling

The MS2 coat protein labelling approach was not successful. This may be due to the structural complexity of the HCV UTRs and the nature of restriction enzyme recognition sites, which make a manipulation using PCR difficult. Restriction enzyme recognition sites are palindromic sequences, which makes them prone to hairpin formation and dimerisation. This results in a reduced efficiency of the PCR. Restrictions in terms of placement of the insertions within the HCV genome very much limited optimisation of the primer design process leading to primers with high GC-contents. However, the latter has been taken into account by using reaction buffer optimised for high GC-content reactions and the addition of A/T nucleotides at the 5'-end of the primer where possible. Nonetheless, secondary structure formation could most likely not be prohibited at the point of primer design due to the palindromic nature of the insertion sequences. To address this problem, reaction conditions were modified using various additives. Small amounts of glycerol are used to increase the specificity and efficiency of PCR, whereas high concentrations inhibit polymerase activity. The beneficial effect of low concentrations of glycerol in the PCR may be due to lowering of the strand separation temperature, enhanced hydrophobic interactions between protein domains, and a raised thermal transition temperature of proteins. The addition of BSA and DTT to the reaction is thought to counteract the inhibitory effect of glycerol on the polymerase enzyme [396]. DMSO prevents secondary structure formation and increases PCR efficiency for high GC-

content sequences and was therefore tested as well. As another attempt to lower the potential for structural hindrances of the PCR due to primer dimerisation or hairpin formation, primers were split to only carry one restriction site rather than both. Temperature gradients were tested throughout since additives may interfere with melting temperatures of DNA. However, insertion of restriction sites within the HCV UTRs using PCR was not successful. This is also the case for the trialed introduction of stem loop repeats within the ORF. The fact that this experiment failed indicates that the reasons behind are, at least partly, fundamental since the site has been proven to tolerate smaller insertions, such as GFP sequences.

An alternative cloning strategy may be adopted for potential future experiments. To validate the MS2-labelling approach, the sub-genomic replicon system may be used, which is a much shorter construct and may therefore be easier to manipulated and amplified. Shorter amplifications will lower the risk of introducing replication errors into the sequence.

In order to simplify the amplification process when moving to the full-length genome, a shorter fragment of the genome may be isolated and used to insert the MS2 stem loop repeats before cloning it back into the full-length genome context. To evaluate the replication of MS2-tagged constructs, the luciferase-tagged HCV sub-genomic or full-length genomes could be used.

In terms of the insertion process of the stem loop repeats, the restriction sites chosen are likely to religate. Bgl-II would be sufficient for an introduction of repeats, which would make the mutation of BamH-I sites within the vector unnecessary, circumcising mutations that would potentially influence function,

localisation or interaction of proteins. In fact, the mutated NS4B BamH-I site might cause a disruption in the membrane association of NS4B, potentially having a negative effect on viral replication.

4.5.2 Alexa®-UTP labelling of HCV RNA

The Alexa®-UTP labelling approach did not result in infectious, fluorescently labelled, full-length RNA. That is due to the fact that the transcript was not of full length but only about 1.8 kb. This corresponds to the genome up to the E1 sequence; however, the sequence does not reveal any distinctive features, which would explain sequence-induced inhibition of the reaction. Furthermore, this seems unlikely since the Jc1 genome was successfully *in vitro* transcribed previously without the addition of Alexa®-tagged nucleotides. To slow down the reaction and possibly enhance polymerase efficiency, the reaction time was increased from 4 h to 16 h and the reaction temperature was decreased from 37 °C to RT. This increased reaction yield but had no effect on the length of the transcript. Titration of labelled nucleotides revealed that increased concentration of labelled UTPs decreases product yield. This hints towards an inhibition of the synthesis reaction by the Alexa®-label. Heinrich et *al.* reported an inhibition of the transcription reaction using Alexa®-labelled UTPs for the labelling of Vesicular Stomatitis Virus (VSV) RNA [397].

No Alexa®-labelled RNA was observed transmitted from infected to uninfected cell in the co-culture experiment (Figure 50-51). Since the process of cell-to-cell transmission is poorly understood, it is not possible to know whether this is because the RNA was not of full-length. It may also be that

the Alexa®-label sterically inhibits the encapsidation of Alexa®-labelled RNA. If there are indeed numerous encapsidation signals spread across the HCV genome, it may be that multiple interaction sites between core and the RNA are required for packaging and encapsidation [176]. This would ensure that only full-length RNA is packaged into progeny viruses and explain the lack of observed cell-to-cell transmission.

Although further trials could have possibly been conducted, such as mung bean digest to create blunt ends, or modifying the transcription protocol followed for JFH-1 in chapter 3, the Alexa®-labelling was discontinued as well due to time constraints.

Supplement

i) Abbreviations

Abbreviation	
aa	amino acid
ACC	acetyl-CoA carboxylase
ADRP	Adipocyte differentiation related protein
AGPAT	1-acylglycerol-3-phosphate-O-acyltransferase
Apo	apolipoprotein
CERT	ceramide transport-molecule
CLDN	claudin
CMV	cytomegalovirus
CPT	carnitine palmitoyltransferase
DAA	direct acting antiviral
DAG	diacylglycerol
DDX	DEAD (Asp-Glu-Ala-Asp) Box Polypeptide 3, X-Linked
DAPI	4',6-diamidino-2-phenylindole
DC-SIGN	dendritic cell-specific intracellular adhesion molecule-3-grabbing non-integrin
DHCR7	7-dehydrocholesterol reductase
DNA	deoxyribonucleic acid
DGAT	diacylglycerol acetyl transferase
EBP	emopamil binding protein
EGFR	epidermal growth factor receptor
eIF3	eukaryotic initiation factor-3

EphA2	ephrin receptor A2
ER	endoplasmic reticulum
FA	fatty acid
FP	fluorescent protein
GAG	glucosaminoglycan
GCMS	gas chromatography mass spectrometry
GPAT	glycerol-3-phosphate acyltransferase
HCC	hepatocellular carcinoma
HCV	hepatitis C virus
HCVpp	hepatitis C virus pseudoparticle
HFLC	human fetal liver cell
HIV	human immunodeficiency virus
Huh7/7.5	human hepatocyte cell line
hVAP-A	vesicle-associated membrane protein-associated protein A
HVR	hypervariable region
INSIG	insulin induced gene
iPSC	induced pluripotent stem cells
IRES	internal ribosome entry side
IRS	insulin
JFH-1	Japanese fulminant hepatitis
LCAT	lecithin-cholesterol acyltransferase
LD	lipid droplet
LDLR	low density lipid receptor
L-SIGN	liver/lymph node-specific intracellular adhesion molecule-3-grabbing non-integrin

LVP	lipoviral particle
MAPK	mitogen-activated protein kinase
MAVS	mitochondrial antiviral signaling protein
miR	micro RNA
moi	multiplicity of infection
MPCC	micropatterned co-culture
MTP	microsomal transfer protein
nC	number of carbon atoms
nDB	number of double bonds
NPC1L1	Niemann-Pick C1-like-1
NLS	nuclear localisation sequence
NS	non-structural
NTP	nucleotide triphosphate
OCLN	occludin
paGFP	photoactivatable green fluorescent protein
PAP	phosphatidic acid phosphohydrolase
PBS	phosphate buffered saline
PC	phosphatidylcholine
PCA	principal component analysis
PCK	phosphoenolpyruvate carboxykinase
PCR	polymerase chain reaction
PE	phosphatidylethanolamine
PEG	polyethyleneglycol
PEG-IFN	pegylated interferon
PEMT	phosphatidylethanolamine *N*-methyltransferase

PFA	paraformaldehyde
PI	phosphatidylinositol
PI4K	phosphatidylinositol-4-kinase
PKR	dsRNA-activated protein kinase
PPAR	peroxisome proliferator-activated receptor
PRK	protein kinase C-related kinase
PS	phosphatidylserine
PTB	polypyrimidine tract-binding protein
PUFA	polyunsaturated fatty acid
RdRp	RNA-dependent RNA polymerase
RIG-I	retinoic acid-inducible gene 1
RNA	ribonucleic acid
ROS	reactive oxygen species
SC5D	sterol-C5-desaturase
SCAP	SREBP cleavage-activating protein
SCID	severe combined immunodeficiency
S1/2P	site-1 and site-2 proteases
SNARE	soluble NSF attachment protein receptor
SO-PERL	synthetically optimised polyunsaturated ER targeting liposome
SOC	standard of care
SQLE	squalene epoxidase
SR-B1	scavenger receptor class B-1
SREBP	sterol regulatory element binding protein
ss/ds	single strand/double strand

SVR	sustained virological response
SYNCRIP	synaptotagmin binding cytoplasmic RNA interacting protein
TAG	triacyglycerol
TfR1	transferrin receptor 1
TLR	toll-like receptor
TIP47	tail-interacting protein of 47 kDa
USA	United States of America
UTR	untranslated region
wt	wild-type

ii) Microarray gene table

Unigene	GeneBank	Symbol	Description	Gene Name
Hs.429294	NM_005502	ABCA1	ATP-binding cassette, sub-family A (ABC1), member 1	ABC-1, ABC1, CERP, FLJ14958, HDLDT1, MGC164864, MGC165011, TGD
Hs.124649	NM_004915	ABCG1	ATP-binding cassette, sub-family G (WHITE), member 1	ABC8, MGC34313, WHITE1
Hs.200136	NM_006111	ACAA2	Acetyl-CoA acyltransferase 2	DSAEC, FLJ35992, FLJ95265
Hs.201667	NM_005989	AKR1D1	Aldo-keto reductase family 1, member D1 (delta 4-3-ketosteroid-5-beta-reductase)	3o5bred, CBAS2, SRD5B1
Hs.209153	NM_014495	ANGPTL3	Angiopoietin-like 3	ANGPT5, FHBL2

Hs.239154	NM_023039	ANKRA2	Ankyrin repeat, family A (RFXANK-like), 2	ANKRA
Hs.633003	NM_000039	APOA1	Apolipoprotein A-I	MGC117399
Hs.237658	NM_001643	APOA2	Apolipoprotein A-II	Apo-AII, ApoA-II, apoAII
Hs.591940	NM_000482	APOA4	Apolipoprotein A-IV	MGC142154, MGC142156
Hs.120759	NM_000384	APOB	Apolipoprotein B (including Ag(x) antigen)	FLDB, LDLCQ4
Hs.522555	NM_001647	APOD	Apolipoprotein D	-
Hs.654439	NM_000041	APOE	Apolipoprotein E	AD2, LDLCQ5, LPG, MGC1571
Hs.534302	NM_001638	APOF	Apolipoprotein F	Apo-F, DKFZp781G18150, LTIP, MGC22520
Hs.114309	NM_003661	APOL1	Apolipoprotein L, 1	APO-L, APOL, APOL-I, FSGS4
Hs.474740	NM_030882	APOL2	Apolipoprotein L, 2	APOL-II, APOL3
Hs.326561	NM_030642	APOL5	Apolipoprotein L, 5	APOL-V, APOLV
Hs.654386	NM_001257	CDH13	Cadherin 13, H-cadherin (heart)	CDHH, P105
Hs.533258	NM_001807	CEL	Carboxyl ester lipase (bile salt-stimulated lipase)	BAL, BSDL, BSSL, CELL, CEase, FAP, FAPP, LIPA, MODY8
Hs.89538	NM_000078	CETP	Cholesteryl ester transfer protein, plasma	HDLCQ10
Hs.518249	NM_003418	CNBP	CCHC-type zinc finger, nucleic acid binding protein	CNBP1, DM2, FLJ11631, PROMM, RNF163, ZCCHC22, ZNF9
Hs.464422	NM_130386	COLEC12	Collectin sub-family member 12	CLP1, NSR2, SCARA4, SRCL
Hs.708201	NM_022059	CXCL16	Chemokine (C-X-C motif) ligand 16	CXCLG16, SR-PSOX, SRPSOX
Hs.700572	NM_007326	CYB5R3	Cytochrome b5 reductase 3	B5R, DIA1

Hs.303980	NM_000781	CYP11A1	Cytochrome P450, family 11, subfamily A, polypeptide 1	CYP11A, P450SCC
Hs.387367	NM_016593	CYP39A1	Cytochrome P450, family 39, subfamily A, polypeptide 1	-
Hs.25121	NM_006668	CYP46A1	Cytochrome P450, family 46, subfamily A, polypeptide 1	CP46, CYP46
Hs.417077	NM_000786	CYP51A1	Cytochrome P450, family 51, subfamily A, polypeptide 1	CP51, CYP51, CYPL1, LDM, P450-14DM, P450L1
Hs.1644	NM_000780	CYP7A1	Cytochrome P450, family 7, subfamily A, polypeptide 1	CP7A, CYP7, CYPVII, MGC126826, MGC138389
Hs.667720	NM_004820	CYP7B1	Cytochrome P450, family 7, subfamily B, polypeptide 1	CBAS3, CP7B, SPG5A
Hs.498727	NM_014762	DHCR24	24-dehydrocholesterol reductase	DCE, KIAA0018, Nbla03646, SELADIN1, seladin-1
Hs.503134	NM_001360	DHCR7	7-dehydrocholesterol reductase	SLOS
Hs.654349	NM_005747	CELA3A	Chymotrypsin-like elastase family, member 3A	ELA3, ELA3A
Hs.728752	NM_007352	CELA3B	Chymotrypsin-like elastase family, member 3B	CBPP, E1, EL-1, ELA3B
Hs.593928	NM_004462	FDFT1	Farnesyl-diphosphate farnesyltransferase 1	DGPT, ERG9, SQS, SS
Hs.335918	NM_002004	FDPS	Farnesyl diphosphate	FPPS, FPS

			synthase	
Hs.471851	NM_005336	HDLBP	High density lipoprotein binding protein	FLJ16432, HBP, PRO2900, VGL
Hs.643495	NM_000859	HMGCR	3-hydroxy-3-methylglutaryl-CoA reductase	LDLCQ3
Hs.397729	NM_002130	HMGCS1	3-hydroxy-3-methylglutaryl-CoA synthase 1 (soluble)	HMGCS, MGC90332
Hs.59889	NM_005518	HMGCS2	3-hydroxy-3-methylglutaryl-CoA synthase 2 (mitochondrial)	-
Hs.283652	NM_004508	IDI1	Isopentenyl-diphosphate delta isomerase 1	IPP1, IPPI1
Hs.9270	NM_033261	IDI2	Isopentenyl-diphosphate delta isomerase 2	IPPI2
Hs.73917	NM_000589	IL4	Interleukin 4	BCGF-1, BCGF1, BSF-1, BSF1, IL-4, MGC79402
Hs.520819	NM_005542	INSIG1	Insulin induced gene 1	CL-6, CL6, MGC1405
Hs.7089	NM_016133	INSIG2	Insulin induced gene 2	MGC26273
Hs.387239	NM_000229	LCAT	Lecithin-cholesterol acyltransferase	-
Hs.213289	NM_000527	LDLR	Low density lipoprotein receptor	FH, FHC, LDLCQ2
Hs.590911	NM_015627	LDLRAP1	Low density lipoprotein receptor adaptor protein 1	ARH, ARH1, ARH2, DKFZp586D0624, FHCB1, FHCB2, MGC34705
Hs.194236	NM_000230	LEP	Leptin	FLJ94114, OB, OBS
Hs.656980	NM_005357	LIPE	Lipase, hormone-sensitive	HSL, LHS

Hs.525232	NM_014045	LRP10	Low density lipoprotein receptor-related protein 10	DKFZp564C1940, LRP9, MGC142274, MGC142276, MGC8675, MST087
Hs.600630	NM_013437	LRP12	Low density lipoprotein receptor-related protein 12	DKFZp781F1053, FLJ12929, ST7
Hs.656461	NM_018557	LRP1B	Low density lipoprotein receptor-related protein 1B	LRP-DIT, LRPDIT
Hs.584775	NM_002336	LRP6	Low density lipoprotein receptor-related protein 6	ADCAD2, FLJ90062, FLJ90421
Hs.533136	NM_002337	LRPAP1	Low density lipoprotein receptor-related protein associated protein 1	A2MRAP, A2RAP, HBP44, MGC138272, MRAP, RAP
Hs.75890	NM_003791	MBTPS1	Membrane-bound transcription factor peptidase, site 1	KIAA0091, MGC138711, MGC138712, PCSK8, S1P, SKI-1
Hs.252457	NM_002461	MVD	Mevalonate (diphospho) decarboxylase	FP17780, MPD
Hs.130607	NM_000431	MVK	Mevalonate kinase	FLJ96772, LRBP, MK, MVLK
Hs.567486	NM_013389	NPC1L1	NPC1 (Niemann-Pick disease, type C1, gene)-like 1	NPC11L1
Hs.427055	NM_021969	NR0B2	Nuclear receptor subfamily 0, group B, member 2	FLJ17090, SHP, SHP1
Hs.282735	NM_005123	NR1H4	Nuclear receptor subfamily 1, group H, member 4	BAR, FXR, HRR-1, HRR1, MGC163445, RIP14
Hs.57698	NM_015922	NSDHL	NAD(P) dependent steroid dehydrogenase-like	H105E3, SDR31E1, XAP104

Hs.412484	NM_002543	OLR1	Oxidized low density lipoprotein (lectin-like) receptor 1	CLEC8A, LOX1, LOXIN, SCARE1, SLOX1
Hs.370725	NM_018030	OSBPL1A	Oxysterol binding protein-like 1A	FLJ10217, ORP-1, ORP1, OSBPL1B
Hs.436166	NM_020896	OSBPL5	Oxysterol binding protein-like 5	FLJ42929, OBPH1, ORP5
Hs.18844	NM_174936	PCSK9	Proprotein convertase subtilisin/kexin type 9	FH3, HCHOLA3, LDLCQ1, NARC-1, NARC1, PC9
Hs.30954	NM_006556	PMVK	Phosphomevalonate kinase	HUMPMKI, PMK, PMKA, PMKASE
Hs.696032	NM_006238	PPARD	Peroxisome proliferator-activated receptor delta	FAAR, MGC3931, NR1C2, NUC1, NUCI, NUCII, PPARB
Hs.43322	NM_006251	PRKAA1	Protein kinase, AMP-activated, alpha 1 catalytic subunit	AMPK, AMPKa1, MGC33776, MGC57364
Hs.437039	NM_006252	PRKAA2	Protein kinase, AMP-activated, alpha 2 catalytic subunit	AMPK, AMPK2, PRKAA
Hs.647072	NM_016203	PRKAG2	Protein kinase, AMP-activated, gamma 2 non-catalytic subunit	AAKG, AAKG2, CMH6, H91620p, WPWS
Hs.531789	NM_012235	SCAP	SREBF chaperone	KIAA0199
Hs.647430	NM_003693	SCARF1	Scavenger receptor class F, member 1	KIAA0149, MGC47738, SREC, SREC-I, SREC1
Hs.278569	NM_014748	SNX17	Sorting nexin 17	KIAA0064
Hs.496383	NM_003101	SOAT1	Sterol O-acyltransferase 1	ACACT, ACAT, ACAT1, RP11-215I23.2, SOAT, STAT

Hs.368592	NM_003105	SORL1	Sortilin-related receptor, L(DLR class) A repeats containing	C11orf32, FLJ21930, FLJ39258, LR11, LRP9, SORLA, SorLA-1, gp250
Hs.592123	NM_004176	SREBF1	Sterol regulatory element binding transcription factor 1	SREBP-1c, SREBP1, bHLHd1
Hs.443258	NM_004599	SREBF2	Sterol regulatory element binding transcription factor 2	SREBP2, bHLHd2
Hs.301989	NM_015136	STAB1	Stabilin 1	CLEVER-1, FEEL-1, FELE-1, FEX1, KIAA0246, STAB-1
Hs.408249	NM_017564	STAB2	Stabilin 2	DKFZp434E0321, FEEL2, FELE-2, FELL2, FEX2, HARE
Hs.728838	NM_006804	STARD3	StAR-related lipid transfer (START) domain containing 3	CAB1, FLJ41370, MLN64, es64
Hs.31130	NM_003273	TM7SF2	Transmembrane 7 superfamily member 2	ANG1, DHCR14A, NET47
Hs.485392	NM_033502	TRERF1	Transcriptional regulating factor 1	BCAR2, FLJ21198, HSA277276, RAPA, RP1-139D8.5, TReP-132, dJ139D8.5
Hs.370422	NM_003383	VLDLR	Very low density lipoprotein receptor	CARMQ1, CHRMQ1, FLJ35024, VLDLRCH
Hs.47223	NM_032265	ZMYND15	Zinc finger, MYND-type containing 15	DKFZp434N127
Hs.534255	NM_004048	B2M	Beta-2-microglobulin	-
Hs.412707	NM_000194	HPRT1	Hypoxanthine phosphoribosyltransferase 1	HGPRT, HPRT
Hs.728776	NM_012423	RPL13A	Ribosomal protein L13a	L13A, TSTA1

Hs.592355	NM_002046	GAPDH	Glyceraldehyde-3-phosphate dehydrogenase	G3PD, GAPD, MGC88685
Hs.520640	NM_001101	ACTB	Actin, beta	PS1TP5BP1
N/A	SA_00105	HGDC	Human Genomic DNA Contamination	HIGX1A
N/A	SA_00104	RTC	Reverse Transcription Control	RTC
N/A	SA_00104	RTC	Reverse Transcription Control	RTC
N/A		RTC	Reverse Transcription Control	RTC
N/A	SA_00103	PPC	Positive PCR Control	PPC
N/A	SA_00103	PPC	Positive PCR Control	PPC
N/A	SA_00103	PPC	Positive PCR Control	PPC

iii) Dynamic light scattering data

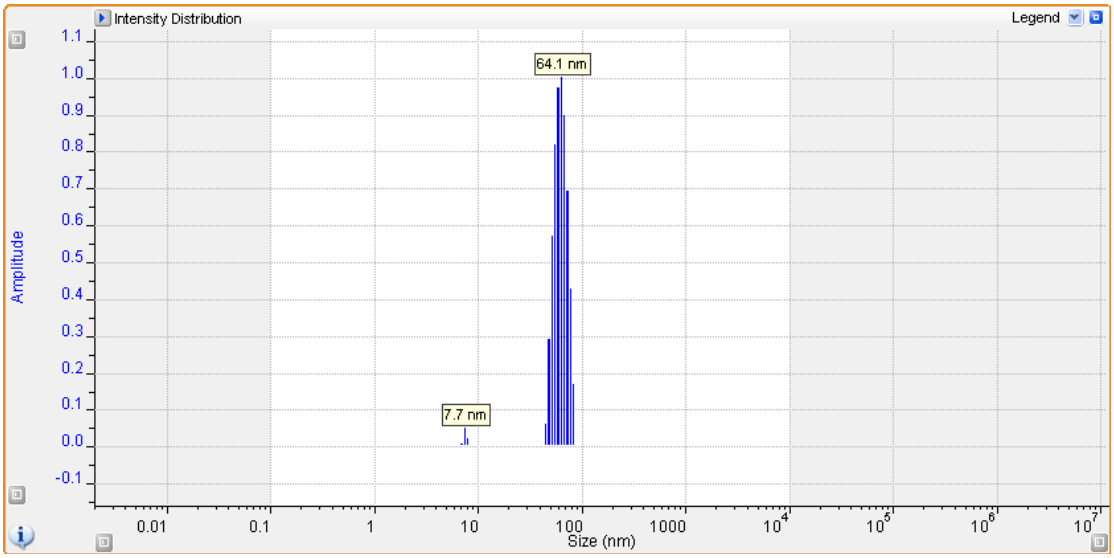

Figure 52: Dynamic light scattering. SO-PERLs were diluted 1:100 in MilliQ water and measured in a quartz cuvette on a Viscotek 802 instrument.

The laser power was set to 300 k and readings were taken 10 times for the duration of 10 seconds each. The acquired data is blotted above, representing the size distribution of prepared liposomes used for microarray and lipid droplet analyses experiments. The average radius of SO-PERLs used in these experiments was 64 nm.

iv) Gene expression in comparison to literature

	NU vs JU	NU vs JP6	NU vs JP24	Wu's HCV	Wu's HCV-CC	Blackham's JFH-1 24 h	Blackham's JFH-1 48 h
VLDLR	4.95		5.94	4.25	3.56	2.31	3.24
CYP11A1	3.36		3.68				
LCAT	2.52	3.41	4.30	-3.44	-13.50		
PRKAA2	2.45	3.31	3.61				
INSIG2	2.25		2.01				
NPC1L1	1.82	2.47	2.03	-1.98	-2.26		
APOF	1.75	2.36	1.71	-17.20	-2.90		
APOL2	1.68	2.27	2.62				
NR0B2	1.40	1.89	2.24				
SREBF2	1.17	1.58					
INSIG1	-1.54		-1.73			-4.49	-2.74
HMGCS1	-1.77	-1.31	-1.74			-2.23	-1.88
MVD	-1.78	-1.32	-1.38			-2.18	-3.45
IDI2	-1.85						
APOB	-1.94	-1.44	-1.71				
IDI1	-2.19	-1.62	-1.80			-2.08	-1.72
SNX17	-2.45	-1.81	-1.48				
DHCR24	-2.50	-1.85	-1.89				

NSDHL	-2.75					-2.1	-2.26
HMGCR	-3.04	-2.25	-2.31			-2.16	-2.07
LRPAP1	-3.27						
ABCA1	-3.37	-2.49	-3.09				
ACAA2	-2.42	-1.79	-2.09	-2.32	-5.51		
ANGPTL 3	-3.46	-2.56	-3.05				
APOA1	-3.98	-2.94	-2.73	-1.50	-1.77		
ABCG1			1.96				
AKR1D1			1.62	-4.69	-15.56		
APOA4			1.97				
CEL			-1.53				
CETP			3.22	-2.81	-22.97		
CELA3A			1.54				
CYP39A 1			-1.64	-3.17	-17.16		
CYP51A 1			-1.82			-2.58	-2.73
FDFT1			-1.23				
HMGCS2			-2.08	-1.98	-2.32	-2.65	
LDLR		1.62	2.11				-4.02
LDLRAP 1			-1.27				
SCAP			1.83				
SCARF1			5.57				
SOAT1			-1.61				
SORL1		1.90	2.83	-1.96	-4.43		
ZMYND1 5			2.04				

Table 16: Gene expression comparison of infected cells from various studies. NU vs JU describes the effect of infection in Huh7.5 cells, NU vs JP compares naïve cells with infected 6 h SO-PERL treated cells, NU vs JP24 compares naïve cells with infected 24 h SO-PERL treated cells, Wu's HCV are biopsy samples of HCV positive and cirrhotic patients, Wu's HCV-HCC are biopsy samples of HCV positive patients with hepatocellular carcinoma [331], Blackham's JFH-1 24 h describes 24 h JFH-1 infection in Huh7 cells, Blackham's JFH-1 48 h describes 48 h JFH-1 infection in Huh7 cells [331].

v) References

1. Choo, Q.L., et al., *Isolation of a cDNA clone derived from a blood-borne non-A, non-B viral hepatitis genome.* Science, 1989. **244**(4902): p. 359-62.
2. Kuo, G., et al., *An assay for circulating antibodies to a major etiologic virus of human non-A, non-B hepatitis.* Science, 1989. **244**(4902): p. 362-4.
3. WHO.
4. Health, U.D.o., 2013.
5. Chayama, K. and C.N. Hayes, *Hepatitis C virus: How genetic variability affects pathobiology of disease.* J Gastroenterol Hepatol, 2011. **26 Suppl 1**: p. 83-95.
6. Simmonds, P., *Genetic diversity and evolution of hepatitis C virus--15 years on.* J Gen Virol, 2004. **85**(Pt 11): p. 3173-88.
7. Hajarizadeh, B., J. Grebely, and G.J. Dore, *Epidemiology and natural history of HCV infection.* Nat Rev Gastroenterol Hepatol, 2013. **10**(9): p. 553-62.
8. Zaltron, S., et al., *Chronic HCV infection: epidemiological and clinical relevance.* BMC Infect Dis, 2012. **12 Suppl 2**: p. S2.
9. Hatzakis, A., et al., *The state of hepatitis B and C in Europe: report from the hepatitis B and C summit conference*.* J Viral Hepat, 2011. **18 Suppl 1**: p. 1-16.
10. Micallef, J.M., J.M. Kaldor, and G.J. Dore, *Spontaneous viral clearance following acute hepatitis C infection: a systematic review of longitudinal studies.* J Viral Hepat, 2006. **13**(1): p. 34-41.
11. Averhoff, F.M., N. Glass, and D. Holtzman, *Global burden of hepatitis C: considerations for healthcare providers in the United States.* Clin Infect Dis, 2012. **55 Suppl 1**: p. S10-5.
12. Organisation, W.H., *Hepatitis C Fact Sheet No 164* 2013.
13. Registry, E.L.T., *Liver Transplantation in Europe.* 2011.

14. Garcia-Retortillo, M., et al., *Hepatitis C virus kinetics during and immediately after liver transplantation.* Hepatology, 2002. **35**(3): p. 680-7.
15. Ly, K.N., et al., *The increasing burden of mortality from viral hepatitis in the United States between 1999 and 2007.* Ann Intern Med, 2012. **156**(4): p. 271-8.
16. Prevention, C.f.D.C.a., *Viral hepatitis populations: HIV/AIDS and viral hepatitis.* 2012.
17. Soler, M., et al., *Quasispecies heterogeneity and constraints on the evolution of the 5' noncoding region of hepatitis C virus (HCV): relationship with HCV resistance to interferon-alpha therapy.* Virology, 2002. **298**(1): p. 160-73.
18. Honda, M., et al., *Structural requirements for initiation of translation by internal ribosome entry within genome-length hepatitis C virus RNA.* Virology, 1996. **222**(1): p. 31-42.
19. Kolykhalov, A.A., et al., *Hepatitis C virus-encoded enzymatic activities and conserved RNA elements in the 3' nontranslated region are essential for virus replication in vivo.* J Virol, 2000. **74**(4): p. 2046-51.
20. You, S. and C.M. Rice, *3' RNA elements in hepatitis C virus replication: kissing partners and long poly(U).* J Virol, 2008. **82**(1): p. 184-95.
21. Griffin, S.D., et al., *The p7 protein of hepatitis C virus forms an ion channel that is blocked by the antiviral drug, Amantadine.* FEBS Lett, 2003. **535**(1-3): p. 34-8.
22. Vieyres, G., et al., *Subcellular localization and function of an epitope-tagged p7 viroporin in hepatitis C virus-producing cells.* J Virol, 2013. **87**(3): p. 1664-78.
23. Walewski, J.L., et al., *Evidence for a new hepatitis C virus antigen encoded in an overlapping reading frame.* RNA, 2001. **7**(5): p. 710-21.
24. Baril, M. and L. Brakier-Gingras, *Translation of the F protein of hepatitis C virus is initiated at a non-AUG codon in a +1 reading frame relative to the polyprotein.* Nucleic Acids Res, 2005. **33**(5): p. 1474-86.
25. Budkowska, A., et al., *Synonymous mutations in the core gene are linked to unusual serological profile in hepatitis C virus infection.* PLoS One, 2011. **6**(1): p. e15871.
26. Shao, S.W., et al., *Hepatitis C virus F protein inhibits cell apoptosis by activation of intracellular NF-kappaB pathway.* Hepatol Res, 2009. **39**(3): p. 282-9.
27. Tsao, M.L., C.H. Chao, and C.T. Yeh, *Interaction of hepatitis C virus F protein with prefoldin 2 perturbs tubulin cytoskeleton organization.* Biochem Biophys Res Commun, 2006. **348**(1): p. 271-7.
28. Boulant, S., et al., *Hepatitis C virus core protein is a dimeric alpha-helical protein exhibiting membrane protein features.* J Virol, 2005. **79**(17): p. 11353-65.
29. Chang, S.C., et al., *Nuclear localization signals in the core protein of hepatitis C virus.* Biochem Biophys Res Commun, 1994. **205**(2): p. 1284-90.
30. Fujimoto, Y., et al., *Identification of major proteins in the lipid droplet-enriched fraction isolated from the human hepatocyte cell line HuH7.* Biochim Biophys Acta, 2004. **1644**(1): p. 47-59.

31. Schwer, B., et al., *Targeting of hepatitis C virus core protein to mitochondria through a novel C-terminal localization motif.* J Virol, 2004. **78**(15): p. 7958-68.
32. Barba, G., et al., *Hepatitis C virus core protein shows a cytoplasmic localization and associates to cellular lipid storage droplets.* Proc Natl Acad Sci U S A, 1997. **94**(4): p. 1200-5.
33. Lo, S.Y., et al., *Differential subcellular localization of hepatitis C virus core gene products.* Virology, 1995. **213**(2): p. 455-61.
34. McLauchlan, J., *Properties of the hepatitis C virus core protein: a structural protein that modulates cellular processes.* J Viral Hepat, 2000. **7**(1): p. 2-14.
35. Klein, K.C., S.R. Dellos, and J.R. Lingappa, *Identification of residues in the hepatitis C virus core protein that are critical for capsid assembly in a cell-free system.* J Virol, 2005. **79**(11): p. 6814-26.
36. Mousseau, G., et al., *Dimerization-driven interaction of hepatitis C virus core protein with NS3 helicase.* J Gen Virol, 2011. **92**(Pt 1): p. 101-11.
37. Oshiumi, H., et al., *Hepatitis C virus core protein abrogates the DDX3 function that enhances IPS-1-mediated IFN-beta induction.* PLoS One, 2010. **5**(12): p. e14258.
38. Perlemuter, G., et al., *Hepatitis C virus core protein inhibits microsomal triglyceride transfer protein activity and very low density lipoprotein secretion: a model of viral-related steatosis.* Faseb J, 2002. **16**(2): p. 185-94.
39. Chung, H., et al., *Hepatitis C virus core protein induces homotolerance and cross-tolerance to Toll-like receptor ligands by activation of Toll-like receptor 2.* J Infect Dis, 2010. **202**(6): p. 853-61.
40. Gentzsch, J., et al., *hepatitis c Virus p7 is critical for capsid assembly and envelopment.* PLoS Pathog, 2013. **9**(5): p. e1003355.
41. Bartosch, B., J. Dubuisson, and F.L. Cosset, *Infectious hepatitis C virus pseudo-particles containing functional E1-E2 envelope protein complexes.* J Exp Med, 2003. **197**(5): p. 633-42.
42. Dubuisson, J., et al., *Formation and intracellular localization of hepatitis C virus envelope glycoprotein complexes expressed by recombinant vaccinia and Sindbis viruses.* J Virol, 1994. **68**(10): p. 6147-60.
43. Lavillette, D., et al., *Hepatitis C virus glycoproteins mediate low pH-dependent membrane fusion with liposomes.* J Biol Chem, 2006. **281**(7): p. 3909-17.
44. Goffard, A., et al., *Role of N-linked glycans in the functions of hepatitis C virus envelope glycoproteins.* J Virol, 2005. **79**(13): p. 8400-9.
45. Op De Beeck, A., L. Cocquerel, and J. Dubuisson, *Biogenesis of hepatitis C virus envelope glycoproteins.* J Gen Virol, 2001. **82**(Pt 11): p. 2589-95.
46. Op De Beeck, A., et al., *The transmembrane domains of hepatitis C virus envelope glycoproteins E1 and E2 play a major role in heterodimerization.* J Biol Chem, 2000. **275**(40): p. 31428-37.
47. Weiner, A.J., et al., *Sequence variation in hepatitis C viral isolates.* J Hepatol, 1991. **13 Suppl 4**: p. S6-14.
48. Zibert, A., et al., *Epitope mapping of antibodies directed against hypervariable region 1 in acute self-limiting and chronic infections due to hepatitis C virus.* J Virol, 1997. **71**(5): p. 4123-7.

49. Bankwitz, D., et al., *Hepatitis C virus hypervariable region 1 modulates receptor interactions, conceals the CD81 binding site, and protects conserved neutralizing epitopes.* J Virol, 2010. **84**(11): p. 5751-63.
50. Prentoe, J., et al., *Hypervariable region 1 differentially impacts viability of hepatitis C virus strains of genotypes 1 to 6 and impairs virus neutralization.* J Virol, 2011. **85**(5): p. 2224-34.
51. Brohm, C., et al., *Characterization of determinants important for hepatitis C virus p7 function in morphogenesis by using trans-complementation.* J Virol, 2009. **83**(22): p. 11682-93.
52. Jones, C.T., et al., *Hepatitis C virus p7 and NS2 proteins are essential for production of infectious virus.* J Virol, 2007. **81**(16): p. 8374-83.
53. Montserret, R., et al., *NMR structure and ion channel activity of the p7 protein from hepatitis C virus.* J Biol Chem, 2010. **285**(41): p. 31446-61.
54. Popescu, C.I., et al., *NS2 protein of hepatitis C virus interacts with structural and non-structural proteins towards virus assembly.* PLoS Pathog, 2011. **7**(2): p. e1001278.
55. Atoom, A.M., D.M. Jones, and R.S. Russell, *Evidence suggesting that HCV p7 protects E2 glycoprotein from premature degradation during virus production.* Virus Res, 2013. **176**(1-2): p. 199-210.
56. Murray, C.L., et al., *Alanine scanning of the hepatitis C virus core protein reveals numerous residues essential for production of infectious virus.* J Virol, 2007. **81**(19): p. 10220-31.
57. Luik, P., et al., *The 3-dimensional structure of a hepatitis C virus p7 ion channel by electron microscopy.* Proc Natl Acad Sci U S A, 2009. **106**(31): p. 12712-6.
58. Wozniak, A.L., et al., *Intracellular proton conductance of the hepatitis C virus p7 protein and its contribution to infectious virus production.* PLoS Pathog, 2010. **6**(9): p. e1001087.
59. Premkumar, A., et al., *Cation-selective ion channels formed by p7 of hepatitis C virus are blocked by hexamethylene amiloride.* FEBS Lett, 2004. **557**(1-3): p. 99-103.
60. Sakai, A., et al., *The p7 polypeptide of hepatitis C virus is critical for infectivity and contains functionally important genotype-specific sequences.* Proc Natl Acad Sci U S A, 2003. **100**(20): p. 11646-51.
61. Steinmann, E., et al., *Hepatitis C virus p7 protein is crucial for assembly and release of infectious virions.* PLoS Pathog, 2007. **3**(7): p. e103.
62. Grakoui, A., et al., *Expression and identification of hepatitis C virus polyprotein cleavage products.* J Virol, 1993. **67**(3): p. 1385-95.
63. Schregel, V., et al., *Hepatitis C virus NS2 is a protease stimulated by cofactor domains in NS3.* Proc Natl Acad Sci U S A, 2009. **106**(13): p. 5342-7.
64. Lorenz, I.C., et al., *Structure of the catalytic domain of the hepatitis C virus NS2-3 protease.* Nature, 2006. **442**(7104): p. 831-5.
65. Santolini, E., et al., *The NS2 protein of hepatitis C virus is a transmembrane polypeptide.* J Virol, 1995. **69**(12): p. 7461-71.
66. Stapleford, K.A. and B.D. Lindenbach, *Hepatitis C virus NS2 coordinates virus particle assembly through physical interactions with the E1-E2 glycoprotein and NS3-NS4A enzyme complexes.* J Virol, 2011. **85**(4): p. 1706-17.

67. Jirasko, V., et al., *Structural and functional characterization of nonstructural protein 2 for its role in hepatitis C virus assembly.* J Biol Chem, 2008. **283**(42): p. 28546-62.
68. Yang, X.J., et al., *HCV NS2 protein inhibits cell proliferation and induces cell cycle arrest in the S-phase in mammalian cells through down-regulation of cyclin A expression.* Virus Res, 2006. **121**(2): p. 134-43.
69. Bittar, C., et al., *Hepatitis C virus NS2 protein inhibits DNA damage pathway by sequestering p53 to the cytoplasm.* PLoS One, 2013. **8**(4): p. e62581.
70. Erdtmann, L., et al., *The hepatitis C virus NS2 protein is an inhibitor of CIDE-B-induced apoptosis.* J Biol Chem, 2003. **278**(20): p. 18256-64.
71. Kaukinen, P., et al., *Hepatitis C virus NS2 protease inhibits host cell antiviral response by inhibiting IKKepsilon and TBK1 functions.* J Med Virol, 2013. **85**(1): p. 71-82.
72. Kim, D.W., et al., *C-terminal domain of the hepatitis C virus NS3 protein contains an RNA helicase activity.* Biochem Biophys Res Commun, 1995. **215**(1): p. 160-6.
73. Hahm, B., et al., *NS3-4A of hepatitis C virus is a chymotrypsin-like protease.* J Virol, 1995. **69**(4): p. 2534-9.
74. Grakoui, A., et al., *Characterization of the hepatitis C virus-encoded serine proteinase: determination of proteinase-dependent polyprotein cleavage sites.* J Virol, 1993. **67**(5): p. 2832-43.
75. Bartenschlager, R., et al., *Complex formation between the NS3 serine-type proteinase of the hepatitis C virus and NS4A and its importance for polyprotein maturation.* J Virol, 1995. **69**(12): p. 7519-28.
76. Meylan, E., et al., *Cardif is an adaptor protein in the RIG-I antiviral pathway and is targeted by hepatitis C virus.* Nature, 2005. **437**(7062): p. 1167-72.
77. Li, K., et al., *Immune evasion by hepatitis C virus NS3/4A protease-mediated cleavage of the Toll-like receptor 3 adaptor protein TRIF.* Proc Natl Acad Sci U S A, 2005. **102**(8): p. 2992-7.
78. Baril, M., et al., *MAVS dimer is a crucial signaling component of innate immunity and the target of hepatitis C virus NS3/4A protease.* J Virol, 2009. **83**(3): p. 1299-311.
79. Matthews, S.J. and J.W. Lancaster, *Telaprevir: a hepatitis C NS3/4A protease inhibitor.* Clin Ther, 2012. **34**(9): p. 1857-82.
80. Venkatraman, S., *Discovery of boceprevir, a direct-acting NS3/4A protease inhibitor for treatment of chronic hepatitis C infections.* Trends Pharmacol Sci, 2012. **33**(5): p. 289-94.
81. Elazar, M., et al., *An N-terminal amphipathic helix in hepatitis C virus (HCV) NS4B mediates membrane association, correct localization of replication complex proteins, and HCV RNA replication.* J Virol, 2004. **78**(20): p. 11393-400.
82. Hugle, T., et al., *The hepatitis C virus nonstructural protein 4B is an integral endoplasmic reticulum membrane protein.* Virology, 2001. **284**(1): p. 70-81.
83. Li, S., et al., *Interaction networks of hepatitis C virus NS4B: implications for antiviral therapy.* Cell Microbiol, 2012. **14**(7): p. 994-1002.
84. Egger, D., et al., *Expression of hepatitis C virus proteins induces distinct membrane alterations including a candidate viral replication complex.* J Virol, 2002. **76**(12): p. 5974-84.

85. Kato, J., et al., *Hepatitis C virus NS4A and NS4B proteins suppress translation in vivo.* J Med Virol, 2002. **66**(2): p. 187-99.
86. Piccininni, S., et al., *Modulation of the hepatitis C virus RNA-dependent RNA polymerase activity by the non-structural (NS) 3 helicase and the NS4B membrane protein.* J Biol Chem, 2002. **277**(47): p. 45670-9.
87. Syed, G.H., Y. Amako, and A. Siddiqui, *Hepatitis C virus hijacks host lipid metabolism.* Trends Endocrinol Metab, 2010. **21**(1): p. 33-40.
88. Tanaka, T., et al., *Hepatitis C virus NS4B targets lipid droplets through hydrophobic residues in the amphipathic helices.* J Lipid Res, 2013.
89. Tai, A.W. and S. Salloum, *The role of the phosphatidylinositol 4-kinase PI4KA in hepatitis C virus-induced host membrane rearrangement.* PLoS One, 2011. **6**(10): p. e26300.
90. Reiss, S., et al., *The lipid kinase phosphatidylinositol-4 kinase III alpha regulates the phosphorylation status of hepatitis C virus NS5A.* PLoS Pathog, 2013. **9**(5): p. e1003359.
91. Evans, M.J., C.M. Rice, and S.P. Goff, *Phosphorylation of hepatitis C virus nonstructural protein 5A modulates its protein interactions and viral RNA replication.* Proc Natl Acad Sci U S A, 2004. **101**(35): p. 13038-43.
92. Brass, V., et al., *An amino-terminal amphipathic alpha-helix mediates membrane association of the hepatitis C virus nonstructural protein 5A.* J Biol Chem, 2002. **277**(10): p. 8130-9.
93. Tellinghuisen, T.L., et al., *Identification of residues required for RNA replication in domains II and III of the hepatitis C virus NS5A protein.* J Virol, 2008. **82**(3): p. 1073-83.
94. Tellinghuisen, T.L., J. Marcotrigiano, and C.M. Rice, *Structure of the zinc-binding domain of an essential component of the hepatitis C virus replicase.* Nature, 2005. **435**(7040): p. 374-9.
95. Foster, T.L., et al., *All three domains of the hepatitis C virus nonstructural NS5A protein contribute to RNA binding.* J Virol, 2010. **84**(18): p. 9267-77.
96. Shi, S.T., et al., *Hepatitis C virus NS5A colocalizes with the core protein on lipid droplets and interacts with apolipoproteins.* Virology, 2002. **292**(2): p. 198-210.
97. Warter, L., et al., *A cooperative interaction between nontranslated RNA sequences and NS5A protein promotes in vivo fitness of a chimeric hepatitis C/GB virus B.* PLoS One, 2009. **4**(2): p. e4419.
98. Shirota, Y., et al., *Hepatitis C virus (HCV) NS5A binds RNA-dependent RNA polymerase (RdRP) NS5B and modulates RNA-dependent RNA polymerase activity.* J Biol Chem, 2002. **277**(13): p. 11149-55.
99. Scheel, T.K., et al., *Analysis of functional differences between hepatitis C virus NS5A of genotypes 1-7 in infectious cell culture systems.* PLoS Pathog, 2012. **8**(5): p. e1002696.
100. Lan, K.H., et al., *HCV NS5A interacts with p53 and inhibits p53-mediated apoptosis.* Oncogene, 2002. **21**(31): p. 4801-11.
101. Chung, Y.L., M.L. Sheu, and S.H. Yen, *Hepatitis C virus NS5A as a potential viral Bcl-2 homologue interacts with Bax and inhibits apoptosis in hepatocellular carcinoma.* Int J Cancer, 2003. **107**(1): p. 65-73.
102. Macdonald, A. and M. Harris, *Hepatitis C virus NS5A: tales of a promiscuous protein.* J Gen Virol, 2004. **85**(Pt 9): p. 2485-502.

103. Tellinghuisen, T.L. and C.M. Rice, *Interaction between hepatitis C virus proteins and host cell factors.* Curr Opin Microbiol, 2002. **5**(4): p. 419-27.
104. Belda, O. and P. Targett-Adams, *Small molecule inhibitors of the hepatitis C virus-encoded NS5A protein.* Virus Res, 2012. **170**(1-2): p. 1-14.
105. Lesburg, C.A., et al., *Crystal structure of the RNA-dependent RNA polymerase from hepatitis C virus reveals a fully encircled active site.* Nat Struct Biol, 1999. **6**(10): p. 937-43.
106. Ranjith-Kumar, C.T., et al., *Requirements for de novo initiation of RNA synthesis by recombinant flaviviral RNA-dependent RNA polymerases.* J Virol, 2002. **76**(24): p. 12526-36.
107. Luo, G., et al., *De novo initiation of RNA synthesis by the RNA-dependent RNA polymerase (NS5B) of hepatitis C virus.* J Virol, 2000. **74**(2): p. 851-63.
108. Kim, S.J., et al., *Protein kinase C-related kinase 2 regulates hepatitis C virus RNA polymerase function by phosphorylation.* J Biol Chem, 2004. **279**(48): p. 50031-41.
109. Gu, M. and C.M. Rice, *Structures of hepatitis C virus nonstructural proteins required for replicase assembly and function.* Curr Opin Virol, 2013. **3**(2): p. 129-36.
110. den Boon, J.A. and P. Ahlquist, *Organelle-like membrane compartmentalization of positive-strand RNA virus replication factories.* Annu Rev Microbiol, 2010. **64**: p. 241-56.
111. Marukian, S., et al., *Cell culture-produced hepatitis C virus does not infect peripheral blood mononuclear cells.* Hepatology, 2008. **48**(6): p. 1843-50.
112. Fletcher, N.F., et al., *Hepatitis C virus infection of neuroepithelioma cell lines.* Gastroenterology, 2010. **139**(4): p. 1365-74.
113. Burgel, B., et al., *Hepatitis C virus enters human peripheral neuroblastoma cells - evidence for extra-hepatic cells sustaining hepatitis C virus penetration.* J Viral Hepat, 2011. **18**(8): p. 562-70.
114. Cormier, E.G., et al., *CD81 is an entry coreceptor for hepatitis C virus.* Proc Natl Acad Sci U S A, 2004. **101**(19): p. 7270-4.
115. Rice, C.M., *Is CD81 the key to hepatitis C virus entry?* Hepatology, 1999. **29**(3): p. 990-2.
116. Bartosch, B., et al., *Cell entry of hepatitis C virus requires a set of co-receptors that include the CD81 tetraspanin and the SR-B1 scavenger receptor.* J Biol Chem, 2003. **278**(43): p. 41624-30.
117. Scarselli, E., et al., *The human scavenger receptor class B type I is a novel candidate receptor for the hepatitis C virus.* EMBO J, 2002. **21**(19): p. 5017-25.
118. Molina, S., et al., *The low-density lipoprotein receptor plays a role in the infection of primary human hepatocytes by hepatitis C virus.* J Hepatol, 2007. **46**(3): p. 411-9.
119. Agnello, V., et al., *Hepatitis C virus and other flaviviridae viruses enter cells via low density lipoprotein receptor.* Proc Natl Acad Sci U S A, 1999. **96**(22): p. 12766-71.
120. Evans, M.J., et al., *Claudin-1 is a hepatitis C virus co-receptor required for a late step in entry.* Nature, 2007. **446**(7137): p. 801-5.
121. Meertens, L., et al., *The tight junction proteins claudin-1, -6, and -9 are entry cofactors for hepatitis C virus.* J Virol, 2008. **82**(7): p. 3555-60.

122. Zheng, A., et al., *Claudin-6 and claudin-9 function as additional coreceptors for hepatitis C virus.* J Virol, 2007. **81**(22): p. 12465-71.
123. Ploss, A., et al., *Human occludin is a hepatitis C virus entry factor required for infection of mouse cells.* Nature, 2009. **457**(7231): p. 882-6.
124. Benedicto, I., et al., *The tight junction-associated protein occludin is required for a postbinding step in hepatitis C virus entry and infection.* J Virol, 2009. **83**(16): p. 8012-20.
125. Lupberger, J., et al., *EGFR and EphA2 are host factors for hepatitis C virus entry and possible targets for antiviral therapy.* Nat Med, 2011. **17**(5): p. 589-95.
126. Sainz, B., Jr., et al., *Identification of the Niemann-Pick C1-like 1 cholesterol absorption receptor as a new hepatitis C virus entry factor.* Nat Med, 2012. **18**(2): p. 281-5.
127. Martin, D.N. and S.L. Uprichard, *Identification of transferrin receptor 1 as a hepatitis C virus entry factor.* Proc Natl Acad Sci U S A, 2013. **110**(26): p. 10777-82.
128. Basu, A., et al., *Sulfated homologues of heparin inhibit hepatitis C virus entry into mammalian cells.* J Virol, 2007. **81**(8): p. 3933-41.
129. Barth, H., et al., *Cellular binding of hepatitis C virus envelope glycoprotein E2 requires cell surface heparan sulfate.* J Biol Chem, 2003. **278**(42): p. 41003-12.
130. Koutsoudakis, G., et al., *Characterization of the early steps of hepatitis C virus infection by using luciferase reporter viruses.* J Virol, 2006. **80**(11): p. 5308-20.
131. Gardner, J.P., et al., *L-SIGN (CD 209L) is a liver-specific capture receptor for hepatitis C virus.* Proc Natl Acad Sci U S A, 2003. **100**(8): p. 4498-503.
132. Cormier, E.G., et al., *L-SIGN (CD209L) and DC-SIGN (CD209) mediate transinfection of liver cells by hepatitis C virus.* Proc Natl Acad Sci U S A, 2004. **101**(39): p. 14067-72.
133. von Hahn, T., et al., *Oxidized low-density lipoprotein inhibits hepatitis C virus cell entry in human hepatoma cells.* Hepatology, 2006. **43**(5): p. 932-42.
134. Blanchard, E., et al., *Hepatitis C virus entry depends on clathrin-mediated endocytosis.* J Virol, 2006. **80**(14): p. 6964-72.
135. Hsu, M., et al., *Hepatitis C virus glycoproteins mediate pH-dependent cell entry of pseudotyped retroviral particles.* Proc Natl Acad Sci U S A, 2003. **100**(12): p. 7271-6.
136. Timpe, J.M., et al., *Hepatitis C virus cell-cell transmission in hepatoma cells in the presence of neutralizing antibodies.* Hepatology, 2008. **47**(1): p. 17-24.
137. Witteveldt, J., et al., *CD81 is dispensable for hepatitis C virus cell-to-cell transmission in hepatoma cells.* J Gen Virol, 2009. **90**(Pt 1): p. 48-58.
138. Fofana, I., et al., *A novel monoclonal anti-CD81 antibody produced by genetic immunization efficiently inhibits Hepatitis C virus cell-cell transmission.* PLoS One, 2013. **8**(5): p. e64221.
139. Hwang, S.B., et al., *Hepatitis C virus NS5B protein is a membrane-associated phosphoprotein with a predominantly perinuclear localization.* Virology, 1997. **227**(2): p. 439-46.

140. Roohvand, F., et al., *Initiation of hepatitis C virus infection requires the dynamic microtubule network: role of the viral nucleocapsid protein.* J Biol Chem, 2009. **284**(20): p. 13778-91.
141. Tscherne, D.M., et al., *Time- and temperature-dependent activation of hepatitis C virus for low-pH-triggered entry.* J Virol, 2006. **80**(4): p. 1734-41.
142. Shi, S.T., et al., *Hepatitis C virus RNA replication occurs on a detergent-resistant membrane that cofractionates with caveolin-2.* J Virol, 2003. **77**(7): p. 4160-8.
143. Reiss, S., et al., *Recruitment and activation of a lipid kinase by hepatitis C virus NS5A is essential for integrity of the membranous replication compartment.* Cell Host Microbe, 2011. **9**(1): p. 32-45.
144. Bartenschlager, R., M. Frese, and T. Pietschmann, *Novel insights into hepatitis C virus replication and persistence.* Adv Virus Res, 2004. **63**: p. 71-180.
145. Miyanari, Y., et al., *The lipid droplet is an important organelle for hepatitis C virus production.* Nat Cell Biol, 2007. **9**(9): p. 1089-97.
146. Camus, G., et al., *Diacylglycerol glycerol acyltransferase-1 localizes hepatitis C virus NS5A protein to lipid droplets and enhances NS5A interaction with the viral capsid core.* J Biol Chem, 2013. **288**(14): p. 9915-23.
147. Boulant, S., P. Targett-Adams, and J. McLauchlan, *Disrupting the association of hepatitis C virus core protein with lipid droplets correlates with a loss in production of infectious virus.* J Gen Virol, 2007. **88**(Pt 8): p. 2204-13.
148. Shavinskaya, A., et al., *The lipid droplet binding domain of hepatitis C virus core protein is a major determinant for efficient virus assembly.* J Biol Chem, 2007. **282**(51): p. 37158-69.
149. Vogt, D.A., et al., *Lipid droplet-binding protein TIP47 regulates hepatitis C Virus RNA replication through interaction with the viral NS5A protein.* PLoS Pathog, 2013. **9**(4): p. e1003302.
150. Liu, H.M., et al., *Hepatitis C virus translation preferentially depends on active RNA replication.* PLoS One, 2012. **7**(8): p. e43600.
151. Wang, C., P. Sarnow, and A. Siddiqui, *Translation of human hepatitis C virus RNA in cultured cells is mediated by an internal ribosome-binding mechanism.* J Virol, 1993. **67**(6): p. 3338-44.
152. Kieft, J.S., et al., *Mechanism of ribosome recruitment by hepatitis C IRES RNA.* RNA, 2001. **7**(2): p. 194-206.
153. Romero-Lopez, C. and A. Berzal-Herranz, *A long-range RNA-RNA interaction between the 5′ and 3′ ends of the HCV genome.* RNA, 2009. **15**(9): p. 1740-52.
154. in *Hepatitis C Viruses: Genomes and Molecular Biology*, S.L. Tan, Editor 2006: Norfolk (UK).
155. Friebe, P. and R. Bartenschlager, *Genetic analysis of sequences in the 3′ nontranslated region of hepatitis C virus that are important for RNA replication.* J Virol, 2002. **76**(11): p. 5326-38.
156. Kim, J.H., et al., *A cellular RNA-binding protein enhances internal ribosomal entry site-dependent translation through an interaction downstream of the hepatitis C virus polyprotein initiation codon.* Mol Cell Biol, 2004. **24**(18): p. 7878-90.

157. Liu, H.M., et al., *SYNCRIP (synaptotagmin-binding, cytoplasmic RNA-interacting protein) is a host factor involved in hepatitis C virus RNA replication.* Virology, 2009. **386**(2): p. 249-56.
158. Domitrovich, A.M., et al., *Role of La autoantigen and polypyrimidine tract-binding protein in HCV replication.* Virology, 2005. **335**(1): p. 72-86.
159. Jopling, C.L., et al., *Modulation of hepatitis C virus RNA abundance by a liver-specific MicroRNA.* Science, 2005. **309**(5740): p. 1577-81.
160. Bartenschlager, R., *Hepatitis C virus molecular clones: from cDNA to infectious virus particles in cell culture.* Curr Opin Microbiol, 2006. **9**(4): p. 416-22.
161. Friebe, P., et al., *Sequences in the 5' nontranslated region of hepatitis C virus required for RNA replication.* J Virol, 2001. **75**(24): p. 12047-57.
162. Cheng, J.C., M.F. Chang, and S.C. Chang, *Specific interaction between the hepatitis C virus NS5B RNA polymerase and the 3' end of the viral RNA.* J Virol, 1999. **73**(8): p. 7044-9.
163. Kim, M., et al., *Template requirements for de novo RNA synthesis by hepatitis C virus nonstructural protein 5B polymerase on the viral X RNA.* J Virol, 2002. **76**(14): p. 6944-56.
164. Kao, C.F., S.Y. Chen, and Y.H. Lee, *Activation of RNA polymerase I transcription by hepatitis C virus core protein.* J Biomed Sci, 2004. **11**(1): p. 72-94.
165. Quinkert, D., R. Bartenschlager, and V. Lohmann, *Quantitative analysis of the hepatitis C virus replication complex.* J Virol, 2005. **79**(21): p. 13594-605.
166. Binder, M., et al., *Replication vesicles are load- and choke-points in the hepatitis C virus lifecycle.* PLoS Pathog, 2013. **9**(8): p. e1003561.
167. Wilson, J.A., et al., *Human Ago2 is required for efficient microRNA 122 regulation of hepatitis C virus RNA accumulation and translation.* J Virol, 2011. **85**(5): p. 2342-50.
168. Roberts, A.P., et al., *The P body protein LSm1 contributes to stimulation of hepatitis C virus translation, but not replication, by microRNA-122.* Nucleic Acids Res, 2013.
169. Ray, U. and S. Das, *Interplay between NS3 protease and human La protein regulates translation-replication switch of Hepatitis C virus.* Sci Rep, 2011. **1**: p. 1.
170. McLauchlan, J., et al., *Intramembrane proteolysis promotes trafficking of hepatitis C virus core protein to lipid droplets.* EMBO J, 2002. **21**(15): p. 3980-8.
171. Carrere-Kremer, S., et al., *Regulation of hepatitis C virus polyprotein processing by signal peptidase involves structural determinants at the p7 sequence junctions.* J Biol Chem, 2004. **279**(40): p. 41384-92.
172. Grakoui, A., et al., *A second hepatitis C virus-encoded proteinase.* Proc Natl Acad Sci U S A, 1993. **90**(22): p. 10583-7.
173. Hijikata, M., et al., *Two distinct proteinase activities required for the processing of a putative nonstructural precursor protein of hepatitis C virus.* J Virol, 1993. **67**(8): p. 4665-75.
174. Lin, C., et al., *Hepatitis C virus NS3 serine proteinase: trans-cleavage requirements and processing kinetics.* J Virol, 1994. **68**(12): p. 8147-57.

175. Herod, M.R., et al., *Increasing rate of cleavage at boundary between non-structural proteins 4B and 5A inhibits replication of hepatitis C virus.* J Biol Chem, 2012. **287**(1): p. 568-80.
176. Stewart, H.D., E.; White, O.; Borodavka, S.; Twarock, R.; Stockley, P.; Harris, M., *Identification of RNA aptamers specifically targeting the HCV Core protein provides evidence for packaging signals within the HCV genome*, in *International Symposium on Hepatitis C Virus and Related Viruses*2013: Melbourne, Australia.
177. Cristofari, G., et al., *The hepatitis C virus Core protein is a potent nucleic acid chaperone that directs dimerization of the viral (+) strand RNA in vitro.* Nucleic Acids Res, 2004. **32**(8): p. 2623-31.
178. Shimoike, T., et al., *Interaction of hepatitis C virus core protein with viral sense RNA and suppression of its translation.* J Virol, 1999. **73**(12): p. 9718-25.
179. Jirasko, V., et al., *Structural and functional studies of nonstructural protein 2 of the hepatitis C virus reveal its key role as organizer of virion assembly.* PLoS Pathog, 2010. **6**(12): p. e1001233.
180. Herker, E., et al., *Efficient hepatitis C virus particle formation requires diacylglycerol acyltransferase-1.* Nat Med, 2010. **16**(11): p. 1295-8.
181. Neveu, G., et al., *Identification and targeting of an interaction between a tyrosine motif within hepatitis C virus core protein and AP2M1 essential for viral assembly.* PLoS Pathog, 2012. **8**(8): p. e1002845.
182. Menzel, N., et al., *MAP-kinase regulated cytosolic phospholipase A2 activity is essential for production of infectious hepatitis C virus particles.* PLoS Pathog, 2012. **8**(7): p. e1002829.
183. Jiang, J. and G. Luo, *Apolipoprotein E but not B is required for the formation of infectious hepatitis C virus particles.* J Virol, 2009. **83**(24): p. 12680-91.
184. Huang, H., et al., *Hepatitis C virus production by human hepatocytes dependent on assembly and secretion of very low-density lipoproteins.* Proc Natl Acad Sci U S A, 2007. **104**(14): p. 5848-53.
185. Fournillier, A., et al., *A Heterologous Prime/Boost Vaccination Strategy Enhances the Immunogenicity of Therapeutic Vaccines for Hepatitis C Virus.* J Infect Dis, 2013. **208**(6): p. 1008-1019.
186. Klade, C.S., et al., *Therapeutic vaccination of chronic hepatitis C nonresponder patients with the peptide vaccine IC41.* Gastroenterology, 2008. **134**(5): p. 1385-95.
187. Barnes, E., et al., *Novel adenovirus-based vaccines induce broad and sustained T cell responses to HCV in man.* Sci Transl Med, 2012. **4**(115): p. 115ra1.
188. Sulkowski, M.S., et al., *Management of adverse effects of Peg-IFN and ribavirin therapy for hepatitis C.* Nat Rev Gastroenterol Hepatol, 2011. **8**(4): p. 212-23.
189. Foster, T.L., et al., *Resistance mutations define specific antiviral effects for inhibitors of the hepatitis C virus p7 ion channel.* Hepatology, 2011. **54**(1): p. 79-90.
190. Biotron, *BIT225 viroporin inhibitor for HCV and HIV treatment.* 2012.
191. Sherman, K.E., et al., *Response-guided telaprevir combination treatment for hepatitis C virus infection.* N Engl J Med, 2011. **365**(11): p. 1014-24.

192. Jacobson, I.M., et al., *Telaprevir for previously untreated chronic hepatitis C virus infection.* N Engl J Med, 2011. **364**(25): p. 2405-16.
193. Gentile, I., et al., *A Novel Promising Therapeutic Option Against Hepatitis C Virus: an Oral Nucleotide NS5B Polymerase Inhibitor Sofosbuvir.* Curr Med Chem, 2013. **20**(30): p. 3733-42.
194. Chae, H.B., S.M. Park, and S.J. Youn, *Direct-acting antivirals for the treatment of chronic hepatitis C: open issues and future perspectives.* ScientificWorldJournal, 2013. **2013**: p. 704912.
195. Meuleman, P., et al., *Anti-CD81 antibodies can prevent a hepatitis C virus infection in vivo.* Hepatology, 2008. **48**(6): p. 1761-8.
196. Meuleman, P., et al., *A human monoclonal antibody targeting scavenger receptor class B type I precludes hepatitis C virus infection and viral spread in vitro and in vivo.* Hepatology, 2012. **55**(2): p. 364-72.
197. Syder, A.J., et al., *Small molecule scavenger receptor BI antagonists are potent HCV entry inhibitors.* J Hepatol, 2011. **54**(1): p. 48-55.
198. Del Campo, J.A., A. Rojas, and M. Romero-Gomez, *Entry of hepatitis C virus into the cell: a therapeutic target.* World J Gastroenterol, 2012. **18**(33): p. 4481-5.
199. Janssen, H.L., et al., *Treatment of HCV infection by targeting microRNA.* N Engl J Med, 2013. **368**(18): p. 1685-94.
200. Hopkins, S., et al., *The cyclophilin inhibitor SCY-635 suppresses viral replication and induces endogenous interferons in patients with chronic HCV genotype 1 infection.* J Hepatol, 2012. **57**(1): p. 47-54.
201. Vaillancourt, F.H., et al., *Evaluation of phosphatidylinositol-4-kinase IIIalpha as a hepatitis C virus drug target.* J Virol, 2012. **86**(21): p. 11595-607.
202. Qu, X., et al., *Inhibitors of endoplasmic reticulum alpha-glucosidases potently suppress hepatitis C virus virion assembly and release.* Antimicrob Agents Chemother, 2011. **55**(3): p. 1036-44.
203. Iacovacci, S., et al., *Molecular characterization and dynamics of hepatitis C virus replication in human fetal hepatocytes infected in vitro.* Hepatology, 1997. **26**(5): p. 1328-37.
204. Lazaro, C.A., et al., *Hepatitis C virus replication in transfected and serum-infected cultured human fetal hepatocytes.* Am J Pathol, 2007. **170**(2): p. 478-89.
205. Lohmann, V., et al., *Replication of subgenomic hepatitis C virus RNAs in a hepatoma cell line.* Science, 1999. **285**(5424): p. 110-3.
206. Blight, K.J., A.A. Kolykhalov, and C.M. Rice, *Efficient initiation of HCV RNA replication in cell culture.* Science, 2000. **290**(5498): p. 1972-4.
207. Pietschmann, T., et al., *Persistent and transient replication of full-length hepatitis C virus genomes in cell culture.* J Virol, 2002. **76**(8): p. 4008-21.
208. Wakita, T., et al., *Production of infectious hepatitis C virus in tissue culture from a cloned viral genome.* Nat Med, 2005. **11**(7): p. 791-6.
209. Lindenbach, B.D., et al., *Complete replication of hepatitis C virus in cell culture.* Science, 2005. **309**(5734): p. 623-6.
210. Lindenbach, B.D., et al., *Cell culture-grown hepatitis C virus is infectious in vivo and can be recultured in vitro.* Proc Natl Acad Sci U S A, 2006. **103**(10): p. 3805-9.

211. Zhong, J., et al., *Robust hepatitis C virus infection in vitro.* Proc Natl Acad Sci U S A, 2005. **102**(26): p. 9294-9.
212. Blight, K.J., J.A. McKeating, and C.M. Rice, *Highly permissive cell lines for subgenomic and genomic hepatitis C virus RNA replication.* J Virol, 2002. **76**(24): p. 13001-14.
213. Saito, T., et al., *Regulation of innate antiviral defenses through a shared repressor domain in RIG-I and LGP2.* Proc Natl Acad Sci U S A, 2007. **104**(2): p. 582-7.
214. Meex, S.J., et al., *Huh-7 or HepG2 cells: which is the better model for studying human apolipoprotein-B100 assembly and secretion?* J Lipid Res, 2011. **52**(1): p. 152-8.
215. Ploss, A., et al., *Persistent hepatitis C virus infection in microscale primary human hepatocyte cultures.* Proc Natl Acad Sci U S A, 2010. **107**(7): p. 3141-5.
216. Andrus, L., et al., *Expression of paramyxovirus V proteins promotes replication and spread of hepatitis C virus in cultures of primary human fetal liver cells.* Hepatology, 2011. **54**(6): p. 1901-12.
217. Schwartz, R.E., et al., *Modeling hepatitis C virus infection using human induced pluripotent stem cells.* Proc Natl Acad Sci U S A, 2012. **109**(7): p. 2544-8.
218. Houghton, M., *Prospects for prophylactic and therapeutic vaccines against the hepatitis C viruses.* Immunol Rev, 2011. **239**(1): p. 99-108.
219. Mercer, D.F., et al., *Hepatitis C virus replication in mice with chimeric human livers.* Nat Med, 2001. **7**(8): p. 927-33.
220. Moriya, K., et al., *Hepatitis C virus core protein induces hepatic steatosis in transgenic mice.* J Gen Virol, 1997. **78 (Pt 7)**: p. 1527-31.
221. Lerat, H., M. Higgs, and J.M. Pawlotsky, *Animal models in the study of hepatitis C virus-associated liver pathologies.* Expert Rev Gastroenterol Hepatol, 2011. **5**(3): p. 341-52.
222. Dorner, M., et al., *Completion of the entire hepatitis C virus life cycle in genetically humanized mice.* Nature, 2013.
223. Seok, J., et al., *Genomic responses in mouse models poorly mimic human inflammatory diseases.* Proc Natl Acad Sci U S A, 2013. **110**(9): p. 3507-12.
224. Sandmann, L. and A. Ploss, *Barriers of hepatitis C virus interspecies transmission.* Virology, 2013. **435**(1): p. 70-80.
225. Bukh, J., *Animal models for the study of hepatitis C virus infection and related liver disease.* Gastroenterology, 2012. **142**(6): p. 1279-1287 e3.
226. Burbelo, P.D., et al., *Serology-enabled discovery of genetically diverse hepaciviruses in a new host.* J Virol, 2012. **86**(11): p. 6171-8.
227. Kapoor, A., et al., *Identification of rodent homologs of hepatitis C virus and pegiviruses.* MBio, 2013. **4**(2): p. e00216-13.
228. Bukh, J., C.L. Apgar, and M. Yanagi, *Toward a surrogate model for hepatitis C virus: An infectious molecular clone of the GB virus-B hepatitis agent.* Virology, 1999. **262**(2): p. 470-8.
229. Pollock, S., et al., *Uptake and trafficking of liposomes to the endoplasmic reticulum.* Faseb J.
230. Pollock, S., et al., *Polyunsaturated liposomes are antiviral against hepatitis B and C viruses and HIV by decreasing cholesterol levels in infected cells.* Proc Natl Acad Sci U S A, 2010. **107**(40): p. 17176-81.

231. Gibellini, F. and T.K. Smith, *The Kennedy pathway--De novo synthesis of phosphatidylethanolamine and phosphatidylcholine.* IUBMB Life, 2010. **62**(6): p. 414-28.
232. Vance, D.E., Z. Li, and R.L. Jacobs, *Hepatic phosphatidylethanolamine N-methyltransferase, unexpected roles in animal biochemistry and physiology.* J Biol Chem, 2007. **282**(46): p. 33237-41.
233. Vance, D.E., C.J. Walkey, and Z. Cui, *Phosphatidylethanolamine N-methyltransferase from liver.* Biochim Biophys Acta, 1997. **1348**(1-2): p. 142-50.
234. McIntosh, T.J. and S.A. Simon, *Area per molecule and distribution of water in fully hydrated dilauroylphosphatidylethanolamine bilayers.* Biochemistry, 1986. **25**(17): p. 4948-52.
235. Berdel, W.E., et al., *Ether lipid derivatives: antineoplastic activity in vitro and the structure-activity relationship.* Lipids, 1986. **21**(4): p. 301-4.
236. Sekas, G., et al., *Origin of plasma lysophosphatidylcholine: evidence for direct hepatic secretion in the rat.* J Lab Clin Med, 1985. **105**(2): p. 190-4.
237. Shin, L., et al., *Lysophosphatidylcholine inhibits membrane-associated SNARE complex disassembly.* J Cell Mol Med, 2012. **16**(8): p. 1701-8.
238. Mehta, D., *Lysophosphatidylcholine: an enigmatic lysolipid.* Am J Physiol Lung Cell Mol Physiol, 2005. **289**(2): p. L174-5.
239. Yuan, C., et al., *The size of lipid rafts: an atomic force microscopy study of ganglioside GM1 domains in sphingomyelin/DOPC/cholesterol membranes.* Biophys J, 2002. **82**(5): p. 2526-35.
240. Simons, K. and E. Ikonen, *Functional rafts in cell membranes.* Nature, 1997. **387**(6633): p. 569-72.
241. Brown, D.A. and E. London, *Functions of lipid rafts in biological membranes.* Annu Rev Cell Dev Biol, 1998. **14**: p. 111-36.
242. Kolesnick, R.N., F.M. Goni, and A. Alonso, *Compartmentalization of ceramide signaling: physical foundations and biological effects.* J Cell Physiol, 2000. **184**(3): p. 285-300.
243. Bijl, N., et al., *Modulation of glycosphingolipid metabolism significantly improves hepatic insulin sensitivity and reverses hepatic steatosis in mice.* Hepatology, 2009. **50**(5): p. 1431-41.
244. Calhoun, W.I. and G.G. Shipley, *Fatty acid composition and thermal behavior of natural sphingomyelins.* Biochim Biophys Acta, 1979. **555**(3): p. 436-41.
245. Huitema, K., et al., *Identification of a family of animal sphingomyelin synthases.* EMBO J, 2004. **23**(1): p. 33-44.
246. Simons, K. and D. Toomre, *Lipid rafts and signal transduction.* Nat Rev Mol Cell Biol, 2000. **1**(1): p. 31-9.
247. Leventhal, A.R., et al., *Acid sphingomyelinase-deficient macrophages have defective cholesterol trafficking and efflux.* J Biol Chem, 2001. **276**(48): p. 44976-83.
248. Milhas, D., C.J. Clarke, and Y.A. Hannun, *Sphingomyelin metabolism at the plasma membrane: implications for bioactive sphingolipids.* FEBS Lett, 2010. **584**(9): p. 1887-94.
249. Yeagle, P.L., *Modulation of membrane function by cholesterol.* Biochimie, 1991. **73**(10): p. 1303-10.

250. Brown, M.S. and J.L. Goldstein, *The SREBP pathway: regulation of cholesterol metabolism by proteolysis of a membrane-bound transcription factor.* Cell, 1997. **89**(3): p. 331-40.
251. Zelcer, N. and P. Tontonoz, *Liver X receptors as integrators of metabolic and inflammatory signaling.* J Clin Invest, 2006. **116**(3): p. 607-14.
252. Rayner, K.J., et al., *MiR-33 contributes to the regulation of cholesterol homeostasis.* Science, 2010. **328**(5985): p. 1570-3.
253. Marquart, T.J., et al., *miR-33 links SREBP-2 induction to repression of sterol transporters.* Proc Natl Acad Sci U S A, 2010. **107**(27): p. 12228-32.
254. Icard, V., et al., *Secretion of hepatitis C virus envelope glycoproteins depends on assembly of apolipoprotein B positive lipoproteins.* PLoS One, 2009. **4**(1): p. e4233.
255. Heinecke, J.W., *The HDL proteome: a marker--and perhaps mediator--of coronary artery disease.* J Lipid Res, 2009. **50 Suppl**: p. S167-71.
256. Robenek, H., et al., *Adipophilin-enriched domains in the ER membrane are sites of lipid droplet biogenesis.* J Cell Sci, 2006. **119**(Pt 20): p. 4215-24.
257. Kleinig, H., *Nuclear membranes from mammalian liver. II. Lipid composition.* J Cell Biol, 1970. **46**(2): p. 396-402.
258. Penno, A., G. Hackenbroich, and C. Thiele, *Phospholipids and lipid droplets.* Biochim Biophys Acta, 2013. **1831**(3): p. 589-94.
259. Arisawa, K., et al., *Changes in the phospholipid fatty acid composition of the lipid droplet during the differentiation of 3T3-L1 adipocytes.* J Biochem, 2013. **154**(3): p. 281-9.
260. Wilfling, F., et al., *Triacylglycerol synthesis enzymes mediate lipid droplet growth by relocalizing from the ER to lipid droplets.* Dev Cell, 2013. **24**(4): p. 384-99.
261. Herms, A., et al., *Cell-to-Cell Heterogeneity in Lipid Droplets Suggests a Mechanism to Reduce Lipotoxicity.* Curr Biol, 2013. **23**(15): p. 1489-96.
262. Wolins, N.E., et al., *Adipocyte protein S3-12 coats nascent lipid droplets.* J Biol Chem, 2003. **278**(39): p. 37713-21.
263. Wolins, N.E., et al., *OXPAT/PAT-1 is a PPAR-induced lipid droplet protein that promotes fatty acid utilization.* Diabetes, 2006. **55**(12): p. 3418-28.
264. Miura, S., et al., *Functional conservation for lipid storage droplet association among Perilipin, ADRP, and TIP47 (PAT)-related proteins in mammals, Drosophila, and Dictyostelium.* J Biol Chem, 2002. **277**(35): p. 32253-7.
265. Bulankina, A.V., et al., *TIP47 functions in the biogenesis of lipid droplets.* J Cell Biol, 2009. **185**(4): p. 641-55.
266. Listenberger, L.L., et al., *Adipocyte differentiation-related protein reduces the lipid droplet association of adipose triglyceride lipase and slows triacylglycerol turnover.* J Lipid Res, 2007. **48**(12): p. 2751-61.
267. Krahmer, N., et al., *Protein correlation profiles identify lipid droplet proteins with high confidence.* Mol Cell Proteomics, 2013. **12**(5): p. 1115-26.
268. Pu, J., et al., *Interactomic study on interaction between lipid droplets and mitochondria.* Protein Cell, 2011. **2**(6): p. 487-96.
269. Bostrom, P., et al., *Cytosolic lipid droplets increase in size by microtubule-dependent complex formation.* Arterioscler Thromb Vasc Biol, 2005. **25**(9): p. 1945-51.

270. Cabodevilla, A.G., et al., *Cell survival during complete nutrient deprivation depends on lipid droplet-fueled beta-oxidation of fatty acids.* J Biol Chem, 2013. **288**(39): p. 27777-88.
271. Welte, M.A., *Proteins under new management: lipid droplets deliver.* Trends Cell Biol, 2007. **17**(8): p. 363-9.
272. Samsa, M.M., et al., *Dengue virus capsid protein usurps lipid droplets for viral particle formation.* PLoS Pathog, 2009. **5**(10): p. e1000632.
273. Cocchiaro, J.L. and R.H. Valdivia, *New insights into Chlamydia intracellular survival mechanisms.* Cell Microbiol, 2009. **11**(11): p. 1571-8.
274. Herker, E. and M. Ott, *Emerging role of lipid droplets in host/pathogen interactions.* J Biol Chem, 2012. **287**(4): p. 2280-7.
275. Cheung, W., et al., *Rotaviruses associate with cellular lipid droplet components to replicate in viroplasms, and compounds disrupting or blocking lipid droplets inhibit viroplasm formation and viral replication.* J Virol, 2010. **84**(13): p. 6782-98.
276. Bozza, P.T. and J.P. Viola, *Lipid droplets in inflammation and cancer.* Prostaglandins Leukot Essent Fatty Acids, 2010. **82**(4-6): p. 243-50.
277. Boren, J. and K.M. Brindle, *Apoptosis-induced mitochondrial dysfunction causes cytoplasmic lipid droplet formation.* Cell Death Differ, 2012. **19**(9): p. 1561-70.
278. Zietkowski, D., et al., *Comparison of NMR lipid profiles in mitotic arrest and apoptosis as indicators of paclitaxel resistance in cervical cell lines.* Magn Reson Med, 2012. **68**(2): p. 369-77.
279. Herker, E. and M. Ott, *Unique ties between hepatitis C virus replication and intracellular lipids.* Trends Endocrinol Metab, 2011. **22**(6): p. 241-8.
280. Thomssen, R., et al., *Association of hepatitis C virus in human sera with beta-lipoprotein.* Med Microbiol Immunol, 1992. **181**(5): p. 293-300.
281. Hijikata, M., et al., *Equilibrium centrifugation studies of hepatitis C virus: evidence for circulating immune complexes.* J Virol, 1993. **67**(4): p. 1953-8.
282. Paola Manzini, G.M.D., David J.C Brown, Salim I Khakoo, James S Owen, *Hepatitis C virus (HCV) tends to associate preferentially with high-density lipoproteins by standard ultracentrifugal fractionation of plasma from patients with chronic HCV infection.* Hepatology Research, 1998. **11**(3).
283. Yamamoto, M., et al., *Structural requirements of virion-associated cholesterol for infectivity, buoyant density and apolipoprotein association of hepatitis C virus.* J Gen Virol, 2011. **92**(Pt 9): p. 2082-7.
284. Scholtes, C., et al., *High plasma level of nucleocapsid-free envelope glycoprotein-positive lipoproteins in hepatitis C patients.* Hepatology, 2012. **56**(1): p. 39-48.
285. Kaito, M., et al., *Hepatitis C virus particle detected by immunoelectron microscopic study.* J Gen Virol, 1994. **75 (Pt 7)**: p. 1755-60.
286. Catanese, M.T., et al., *Ultrastructural analysis of hepatitis C virus particles.* Proc Natl Acad Sci U S A, 2013.
287. Meunier, J.C., et al., *Apolipoprotein c1 association with hepatitis C virus.* J Virol, 2008. **82**(19): p. 9647-56.
288. Nielsen, S.U., et al., *Association between hepatitis C virus and very-low-density lipoprotein (VLDL)/LDL analyzed in iodixanol density gradients.* J Virol, 2006. **80**(5): p. 2418-28.

289. Brown, M.S. and J.L. Goldstein, *A receptor-mediated pathway for cholesterol homeostasis.* Science, 1986. **232**(4746): p. 34-47.
290. Jiang, J., et al., *Hepatitis C virus attachment mediated by apolipoprotein E binding to cell surface heparan sulfate.* J Virol, 2012. **86**(13): p. 7256-67.
291. Boren, J., et al., *Identification of the low density lipoprotein receptor-binding site in apolipoprotein B100 and the modulation of its binding activity by the carboxyl terminus in familial defective apo-B100.* J Clin Invest, 1998. **101**(5): p. 1084-93.
292. Williams, D.L., et al., *Binding and cross-linking studies show that scavenger receptor BI interacts with multiple sites in apolipoprotein A-I and identify the class A amphipathic alpha-helix as a recognition motif.* J Biol Chem, 2000. **275**(25): p. 18897-904.
293. Zahid, M.N., et al., *The postbinding activity of scavenger receptor class B type I mediates initiation of hepatitis C virus infection and viral dissemination.* Hepatology, 2013. **57**(2): p. 492-504.
294. Betters, J.L. and L. Yu, *NPC1L1 and cholesterol transport.* FEBS Lett, 2010. **584**(13): p. 2740-7.
295. Kapadia, S.B., et al., *Initiation of hepatitis C virus infection is dependent on cholesterol and cooperativity between CD81 and scavenger receptor B type I.* J Virol, 2007. **81**(1): p. 374-83.
296. Camus, G., et al., *Diacylglycerol acyltransferase-1 localizes hepatitis C virus NS5A protein to lipid droplets and enhances NS5A interaction with the viral capsid core.* J Biol Chem, 2013. **288**(14): p. 9915-23.
297. Salloum, S., et al., *Rab18 Binds to Hepatitis C Virus NS5A and Promotes Interaction between Sites of Viral Replication and Lipid Droplets.* PLoS Pathog, 2013. **9**(8): p. e1003513.
298. Tanaka, T., et al., *Hepatitis C virus NS4B targets lipid droplets through hydrophobic residues in the amphipathic helices.* J Lipid Res, 2013. **54**(4): p. 881-92.
299. Saxena, V., et al., *Annexin A2 is involved in the formation of hepatitis C virus replication complex on the lipid raft.* J Virol, 2012. **86**(8): p. 4139-50.
300. Shirasaki, T., et al., *MicroRNA-27a regulates lipid metabolism and inhibits hepatitis C virus replication in human hepatoma cells.* J Virol, 2013. **87**(9): p. 5270-86.
301. Gastaminza, P., et al., *Cellular determinants of hepatitis C virus assembly, maturation, degradation, and secretion.* J Virol, 2008. **82**(5): p. 2120-9.
302. Chang, K.S., et al., *Human apolipoprotein e is required for infectivity and production of hepatitis C virus in cell culture.* J Virol, 2007. **81**(24): p. 13783-93.
303. Rubbia-Brandt, L., et al., *Hepatocyte steatosis is a cytopathic effect of hepatitis C virus genotype 3.* J Hepatol, 2000. **33**(1): p. 106-15.
304. Serfaty, L., et al., *Hepatitis C virus induced hypobetalipoproteinemia: a possible mechanism for steatosis in chronic hepatitis C.* J Hepatol, 2001. **34**(3): p. 428-34.
305. Hofer, H., et al., *Hepatocellular fat accumulation and low serum cholesterol in patients infected with HCV-3a.* Am J Gastroenterol, 2002. **97**(11): p. 2880-5.
306. Simo, R., et al., *High prevalence of hepatitis C virus infection in diabetic patients.* Diabetes Care, 1996. **19**(9): p. 998-1000.

307. Mason, A.L., et al., *Association of diabetes mellitus and chronic hepatitis C virus infection.* Hepatology, 1999. **29**(2): p. 328-33.
308. Dienes, H.P., et al., *Histologic observations in human hepatitis non-A, non-B.* Hepatology, 1982. **2**(5): p. 562-71.
309. Chang, M.L., et al., *Altered expression patterns of lipid metabolism genes in an animal model of HCV core-related, nonobese, modest hepatic steatosis.* BMC Genomics, 2008. **9**: p. 109.
310. Lerat, H., et al., *Hepatitis C virus proteins induce lipogenesis and defective triglyceride secretion in transgenic mice.* J Biol Chem, 2009. **284**(48): p. 33466-74.
311. Su, A.I., et al., *Genomic analysis of the host response to hepatitis C virus infection.* Proc Natl Acad Sci U S A, 2002. **99**(24): p. 15669-74.
312. Roingeard, P., *Hepatitis C virus diversity and hepatic steatosis.* J Viral Hepat, 2013. **20**(2): p. 77-84.
313. Harris, C., et al., *Hepatitis C virus core protein decreases lipid droplet turnover: a mechanism for core-induced steatosis.* J Biol Chem, 2011. **286**(49): p. 42615-25.
314. Castera, L., et al., *Effect of antiviral treatment on evolution of liver steatosis in patients with chronic hepatitis C: indirect evidence of a role of hepatitis C virus genotype 3 in steatosis.* Gut, 2004. **53**(3): p. 420-4.
315. Woodhouse, S.D., et al., *Transcriptome sequencing, microarray, and proteomic analyses reveal cellular and metabolic impact of hepatitis C virus infection in vitro.* Hepatology, 2010. **52**(2): p. 443-53.
316. Walters, K.A., et al., *Genomic analysis reveals a potential role for cell cycle perturbation in HCV-mediated apoptosis of cultured hepatocytes.* PLoS Pathog, 2009. **5**(1): p. e1000269.
317. Kasai, D., et al., *HCV replication suppresses cellular glucose uptake through down-regulation of cell surface expression of glucose transporters.* J Hepatol, 2009. **50**(5): p. 883-94.
318. Shintani, Y., et al., *Hepatitis C virus infection and diabetes: direct involvement of the virus in the development of insulin resistance.* Gastroenterology, 2004. **126**(3): p. 840-8.
319. Shaheen, M., et al., *Hepatitis C, metabolic syndrome, and inflammatory markers: results from the Third National Health and Nutrition Examination Survey [NHANES III].* Diabetes Res Clin Pract, 2007. **75**(3): p. 320-6.
320. Yoneda, M., et al., *Hepatitis C virus directly associates with insulin resistance independent of the visceral fat area in nonobese and nondiabetic patients.* J Viral Hepat, 2007. **14**(9): p. 600-7.
321. Banerjee, S., et al., *Hepatitis C virus core protein upregulates serine phosphorylation of insulin receptor substrate-1 and impairs the downstream akt/protein kinase B signaling pathway for insulin resistance.* J Virol, 2008. **82**(6): p. 2606-12.
322. Bose, S.K., et al., *Hepatitis C virus activates the mTOR/S6K1 signaling pathway in inhibiting IRS-1 function for insulin resistance.* J Virol, 2012. **86**(11): p. 6315-22.
323. Patel, H.M., *Serum opsonins and liposomes: their interaction and opsonophagocytosis.* Crit Rev Ther Drug Carrier Syst, 1992. **9**(1): p. 39-90.

324. Allen, C., et al., *Controlling the physical behavior and biological performance of liposome formulations through use of surface grafted poly(ethylene glycol).* Biosci Rep, 2002. **22**(2): p. 225-50.
325. Sapra, P., P. Tyagi, and T.M. Allen, *Ligand-targeted liposomes for cancer treatment.* Curr Drug Deliv, 2005. **2**(4): p. 369-81.
326. Felnerova, D., et al., *Liposomes and virosomes as delivery systems for antigens, nucleic acids and drugs.* Curr Opin Biotechnol, 2004. **15**(6): p. 518-29.
327. Konig, S., et al., *Empty liposomes induce antitumoral effects associated with macrophage responses distinct from those of the TLR1/2 agonist Pam3CSK 4 (BLP).* Cancer Immunol Immunother, 2013. **62**(10): p. 1587-97.
328. Lewis, R.E., et al., *Pretreatment with empty liposomes attenuates the immunopathology of invasive pulmonary aspergillosis in corticosteroid-immunosuppressed mice.* Antimicrob Agents Chemother, 2007. **51**(3): p. 1078-81.
329. McDonald, J.G. and D.W. Russell, *Editorial: 25-Hydroxycholesterol: a new life in immunology.* J Leukoc Biol, 2010. **88**(6): p. 1071-2.
330. Liu, S.Y., et al., *Interferon-inducible cholesterol-25-hydroxylase broadly inhibits viral entry by production of 25-hydroxycholesterol.* Immunity, 2013. **38**(1): p. 92-105.
331. Wu, J.M., N.J. Skill, and M.A. Maluccio, *Evidence of aberrant lipid metabolism in hepatitis C and hepatocellular carcinoma.* HPB (Oxford), 2010. **12**(9): p. 625-36.
332. Barger, J.F., et al., *S6K1 determines the metabolic requirements for BCR-ABL survival.* Oncogene, 2013. **32**(4): p. 453-61.
333. Clark, P.J., et al., *Hepatitis C virus selectively perturbs the distal cholesterol synthesis pathway in a genotype-specific manner.* Hepatology, 2012. **56**(1): p. 49-56.
334. Ciccaglione, A.R., et al., *Microarray analysis identifies a common set of cellular genes modulated by different HCV replicon clones.* BMC Genomics, 2008. **9**: p. 309.
335. Aizaki, H., et al., *Expression profiling of liver cell lines expressing entire or parts of hepatitis C virus open reading frame.* Hepatology, 2002. **36**(6): p. 1431-8.
336. Basu, A., et al., *Microarray analyses and molecular profiling of Stat3 signaling pathway induced by hepatitis C virus core protein in human hepatocytes.* Virology, 2006. **349**(2): p. 347-58.
337. Aizaki, H., et al., *Critical role of virion-associated cholesterol and sphingolipid in hepatitis C virus infection.* J Virol, 2008. **82**(12): p. 5715-24.
338. Lambert, J.E., et al., *Elevated lipogenesis and diminished cholesterol synthesis in patients with hepatitis C viral infection compared to healthy humans.* Hepatology, 2013. **57**(5): p. 1697-704.
339. Abd-Eldaem, A.A., et al., *Role of statins in the treatment of chronic hepatitis c virus infection.* J Egypt Soc Parasitol, 2012. **42**(3): p. 535-40.
340. Forde, K.A., et al., *Do statins reduce hepatitis C RNA titers during routine clinical use?* World J Gastroenterol, 2009. **15**(40): p. 5020-7.
341. Chong, P.H., J.D. Seeger, and C. Franklin, *Clinically relevant differences between the statins: implications for therapeutic selection.* Am J Med, 2001. **111**(5): p. 390-400.

342. Chhatwal, P., et al., *Bile acids specifically increase hepatitis C virus RNA-replication.* PLoS One, 2012. **7**(4): p. e36029.
343. Murakami, Y., et al., *Selective estrogen receptor modulators inhibit hepatitis C virus infection at multiple steps of the virus life cycle.* Microbes Infect, 2013. **15**(1): p. 45-55.
344. Pelazas-Gonzalez, R., et al., *Bone alterations in hepatitis C virus infected patients.* Eur J Intern Med, 2013. **24**(1): p. 92-6.
345. Pitteloud, N., et al., *Relationship between testosterone levels, insulin sensitivity, and mitochondrial function in men.* Diabetes Care, 2005. **28**(7): p. 1636-42.
346. Mekky, R.Y. and A.I. Abdelaziz, *Sex hormones and HCV: an unresolved mystery.* Expert Rev Gastroenterol Hepatol, 2013. **7**(1): p. 69-75.
347. Volle, D.H., et al., *The small heterodimer partner is a gonadal gatekeeper of sexual maturation in male mice.* Genes Dev, 2007. **21**(3): p. 303-15.
348. Kruit, J.K., et al., *Islet cholesterol accumulation due to loss of ABCA1 leads to impaired exocytosis of insulin granules.* Diabetes, 2011. **60**(12): p. 3186-96.
349. Davalos, A., et al., *miR-33a/b contribute to the regulation of fatty acid metabolism and insulin signaling.* Proc Natl Acad Sci U S A, 2011. **108**(22): p. 9232-7.
350. Wijesekara, N., et al., *miR-33a modulates ABCA1 expression, cholesterol accumulation, and insulin secretion in pancreatic islets.* Diabetes, 2012. **61**(3): p. 653-8.
351. Ng, D.S. and N.M. Saw, *The role of HDL and its modulators in the development of diabetes.* Curr Opin Lipidol, 2012. **23**(2): p. 167-8.
352. Blackham, S., et al., *Gene expression profiling indicates the roles of host oxidative stress, apoptosis, lipid metabolism, and intracellular transport genes in the replication of hepatitis C virus.* J Virol, 2010. **84**(10): p. 5404-14.
353. Foka, P., et al., *Hepatitis C virus modulates lipid regulatory factor Angiopoietin-like 3 gene expression by repressing HNF-1alpha activity.* J Hepatol, 2013.
354. Pollock, S., *LIPOSOME-BASED ANTIVIRAL STRATEGIES*, in *Department of Biochemistry*2008, University of Oxford: Oxford, UK.
355. Kato, T., et al., *Cell culture and infection system for hepatitis C virus.* Nat Protoc, 2006. **1**(5): p. 2334-9.
356. Bligh, E.G. and W.J. Dyer, *A rapid method of total lipid extraction and purification.* Can J Biochem Physiol, 1959. **37**(8): p. 911-7.
357. Lamaziere, A., et al., *Lipidomics of hepatic lipogenesis inhibition by omega 3 fatty acids.* Prostaglandins Leukot Essent Fatty Acids, 2013. **88**(2): p. 149-54.
358. Nestel, P.J. and E.A. Couzens, *Turnover of individual cholesterol esters in human liver and plasma.* J Clin Invest, 1966. **45**(7): p. 1234-40.
359. Lamaziere, A., et al., *The deficit of lipid in cultured cells contrasted with clinical lipidomics.* Mol Nutr Food Res, 2013. **57**(8): p. 1401-9.
360. Nishimura, M., et al., *Decreases in the serum VLDL-TG/non-VLDL-TG ratio from early stages of chronic hepatitis C: alterations in TG-rich lipoprotein levels.* PLoS One, 2011. **6**(2): p. e17309.

361. von dem Bussche, A., et al., *Hepatitis C virus NS2 protein triggers endoplasmic reticulum stress and suppresses its own viral replication.* J Hepatol, 2010. **53**(5): p. 797-804.
362. Asselah, T., et al., *In vivo hepatic endoplasmic reticulum stress in patients with chronic hepatitis C.* J Pathol, 2010. **221**(3): p. 264-74.
363. Kannan, R.P., et al., *Hepatitis C virus infection causes cell cycle arrest at the level of initiation of mitosis.* J Virol, 2011. **85**(16): p. 7989-8001.
364. Garcia-Mediavilla, M.V., et al., *Liver X receptor alpha-mediated regulation of lipogenesis by core and NS5A proteins contributes to HCV-induced liver steatosis and HCV replication.* Lab Invest, 2012. **92**(8): p. 1191-202.
365. Ricchi, M., et al., *Differential effect of oleic and palmitic acid on lipid accumulation and apoptosis in cultured hepatocytes.* J Gastroenterol Hepatol, 2009. **24**(5): p. 830-40.
366. Solinas, G., et al., *Saturated fatty acids inhibit induction of insulin gene transcription by JNK-mediated phosphorylation of insulin-receptor substrates.* Proc Natl Acad Sci U S A, 2006. **103**(44): p. 16454-9.
367. Rhead, M.M., et al., *Conversion of oleic acid to saturated fatty acids in severn estuary sediments.* Nature, 1971. **232**(5309): p. 327-30.
368. Munday, A.D. and J.A. Lopez, *Posttranslational protein palmitoylation: promoting platelet purpose.* Arterioscler Thromb Vasc Biol, 2007. **27**(7): p. 1496-9.
369. Charollais, J. and F.G. Van Der Goot, *Palmitoylation of membrane proteins (Review).* Mol Membr Biol, 2009. **26**(1): p. 55-66.
370. Majeau, N., et al., *Palmitoylation of hepatitis C virus core protein is important for virion production.* J Biol Chem, 2009. **284**(49): p. 33915-25.
371. Sato, C., et al., *Impaired mitochondrial beta-oxidation in patients with chronic hepatitis C: relation with viral load and insulin resistance.* BMC Gastroenterol, 2013. **13**: p. 112.
372. Roe, B., et al., *Metabolomic profile of hepatitis C virus-infected hepatocytes.* PLoS One, 2011. **6**(8): p. e23641.
373. Lyn, R.K., et al., *Dynamics of lipid droplets induced by the hepatitis C virus core protein.* Biochem Biophys Res Commun, 2010. **399**(4): p. 518-24.
374. Dawidowicz, E.A., *Dynamics of membrane lipid metabolism and turnover.* Annu Rev Biochem, 1987. **56**: p. 43-61.
375. Weil, T.T., R.M. Parton, and I. Davis, *Making the message clear: visualizing mRNA localization.* Trends Cell Biol, 2010. **20**(7): p. 380-90.
376. Schifferer, M. and O. Griesbeck, *Application of aptamers and autofluorescent proteins for RNA visualization.* Integr Biol (Camb), 2009. **1**(8-9): p. 499-505.
377. Haukenes, G., et al., *Labeling of RNA transcripts of eukaryotic cells in culture with BrUTP using a liposome transfection reagent (DOTAP).* Biotechniques, 1997. **22**(2): p. 308-12.
378. Milev, M.P., C.M. Brown, and A.J. Mouland, *Live cell visualization of the interactions between HIV-1 Gag and the cellular RNA-binding protein Staufen1.* Retrovirology, 2010. **7**: p. 41.
379. Grunwald, D. and R.H. Singer, *In vivo imaging of labelled endogenous beta-actin mRNA during nucleocytoplasmic transport.* Nature, 2010. **467**(7315): p. 604-7.

380. Peters, R., *Translocation through the nuclear pore complex: selectivity and speed by reduction-of-dimensionality.* Traffic, 2005. **6**(5): p. 421-7.
381. Beach, D.L., E.D. Salmon, and K. Bloom, *Localization and anchoring of mRNA in budding yeast.* Curr Biol, 1999. **9**(11): p. 569-78.
382. Bertrand, E., et al., *Localization of ASH1 mRNA particles in living yeast.* Mol Cell, 1998. **2**(4): p. 437-45.
383. Haim, L., et al., *A genomic integration method to visualize localization of endogenous mRNAs in living yeast.* Nat Methods, 2007. **4**(5): p. 409-12.
384. Belaya, K. and D. St Johnston, *Using the mRNA-MS2/MS2CP-FP system to study mRNA transport during Drosophila oogenesis.* Methods Mol Biol, 2011. **714**: p. 265-83.
385. Dynes, J.L. and O. Steward, *Dynamics of bidirectional transport of Arc mRNA in neuronal dendrites.* J Comp Neurol, 2007. **500**(3): p. 433-47.
386. Mor, A., et al., *Dynamics of single mRNP nucleocytoplasmic transport and export through the nuclear pore in living cells.* Nat Cell Biol, 2010. **12**(6): p. 543-52.
387. Boireau, S., et al., *The transcriptional cycle of HIV-1 in real-time and live cells.* J Cell Biol, 2007. **179**(2): p. 291-304.
388. Lee, N., G. Pimienta, and J.A. Steitz, *AUF1/hnRNP D is a novel protein partner of the EBER1 noncoding RNA of Epstein-Barr virus.* RNA, 2012. **18**(11): p. 2073-82.
389. Zhang, F. and A.E. Simon, *A novel procedure for the localization of viral RNAs in protoplasts and whole plants.* Plant J, 2003. **35**(5): p. 665-73.
390. McKinney, S.A., et al., *A bright and photostable photoconvertible fluorescent protein.* Nat Methods, 2009. **6**(2): p. 131-3.
391. Komurian-Pradel, F., et al., *Quantitation of HCV RNA using real-time PCR and fluorimetry.* J Virol Methods, 2001. **95**(1-2): p. 111-9.
392. Fraser, C.S. and J.A. Doudna, *Structural and mechanistic insights into hepatitis C viral translation initiation.* Nat Rev Microbiol, 2007. **5**(1): p. 29-38.
393. Moradpour, D., V. Brass, and F. Penin, *Function follows form: the structure of the N-terminal domain of HCV NS5A.* Hepatology, 2005. **42**(3): p. 732-5.
394. Palomares-Jerez, M.F., H. Nemesio, and J. Villalain, *Interaction with membranes of the full C-terminal domain of protein NS4B from hepatitis C virus.* Biochim Biophys Acta, 2012. **1818**(11): p. 2536-49.
395. Moradpour, D., et al., *Insertion of green fluorescent protein into nonstructural protein 5A allows direct visualization of functional hepatitis C virus replication complexes.* J Virol, 2004. **78**(14): p. 7400-9.
396. Nagai, M., A. Yoshida, and N. Sato, *Additive effects of bovine serum albumin, dithiothreitol, and glycerol on PCR.* Biochem Mol Biol Int, 1998. **44**(1): p. 157-63.
397. Heinrich, B.S., et al., *Protein expression redirects vesicular stomatitis virus RNA synthesis to cytoplasmic inclusions.* PLoS Pathog, 2010. **6**(6): p. e1000958.